2018-01-01

Geant4 Study Of A Gamma Ray Collimator For Proton Therapy

Selim Romero
University of Texas at El Paso, selimiles@live.com

GEANT4 STUDY OF A GAMMA RAY COLLIMATOR FOR PROTON THERAPY

SELIM SABAG ROMERO GONZALEZ

Master's Program in Physics

APPROVED:

Jorge A. López, Ph.D., Chair

Rajendra Zope, Ph.D.

Wei Qian, Ph.D.

Charles Ambler, Ph.D.
Dean of the Graduate School

DEDICATION

I dedicate this writing to a person who guided me since childhood and woke up my interest in science.

GEANT4 STUDY OF A GAMMA RAY COLLIMATOR FOR PROTON THERAPY

by

SELIM SABAG ROMERO GONZALEZ, B.S.

THESIS

Presented to the Faculty of the Graduate School of

The University of Texas at El Paso

in Partial Fulfillment

of the Requirements

for the Degree of

MASTER OF SCIENCE

Department of Physics

THE UNIVERSITY OF TEXAS AT EL PASO

May 2018

ACKNOWLEDGEMENTS

In this project participated Ph.D. candidate Jason Holmes from the Arizona State University, UTEP M.S. student Omar Hernández Rodríguez, and my mentor Dr. Jorge A. López Gallardo, I thank all of them for the opportunity of collaborating with them.

Likewise, I thank UTEP's Physics Department for supporting my M.S. studies with a teaching assistantship, as well as my presentation of this work at the 2017 meeting of the Texas Section of the American Physical Society in Dallas, Texas.

Finally, I thank the members of my thesis committee, Dr. Rajendra Zope, and Dr. Wei Qian, for their time and comments, my professors for these two years of academic preparation, and the staff of the Physics Department for their continuous support.

ABSTRACT

This thesis presents the results of an investigation of the use of collimators in proton therapy. The problem to solve is that in the proton therapy, we do not have the certainty if the target-tumor is receiving all the energy to destroy it or if we are really shooting at this one, so the remaining question is: where the beam is hitting? How to know it? to answer those questions our work has the propose of study proton therapy to determine where the proton interactions occur, these kinds of interactions usually produce gamma rays, and we simulated in GEANT4 the gamma production of a radial source interacting with a collimator made of lead, so our study focused on getting characteristic of the detected gammas and relate those characteristics to a location of the gamma source. The detector was placed behind the collimator, as shown in chapter 4.

Each simulation of GEANT4 captured the signal in the detector and this information was analyzed with the program ROOT CERN, providing us the signal in regions of the detector to suggest some characteristics of a detector device.

The results obtained are simulations for the number of gammas obtained as a function of the position along the detector, the previous was repeated for different configurations of the detector and different positions of the gamma source, as shown in chapter 5.

TABLE OF CONTENTS

LIST OF TABLES

LIST OF FIGURES

CHAPTER 1: INTRODUCTION

Medical physics is the application of physics to medicine and it is commonly focused on the use of nuclear and atomic physics for diagnostics and treatment, especially of cancer. An important part of the mission statement for medical physicists (see e.g. European Federation of Medical Physicists, [Guibelalde, 2012]) is to use devices to measure and limit patient risks and protection from associated x-rays, electromagnetic fields, and other beams. A particular activity connected to this is dosimetry measurements, that is, the measurement of doses administered to patients.

A newer treatment in radiation oncology physics is proton therapy which uses a beam of protons to irradiate diseased tissue in the treatment of cancer. The main advantage of proton therapy is that protons tend to deposit their energy in a narrow range by minimizing the irradiation to other parts of the body. Proton therapy uses an accelerator to target a tumor with a beam of protons damaging the DNA of cells and killing them.

Proton therapy started in 1946 at the Harvard Cyclotron Laboratory [Wilson, 1946], and continued at the Berkeley Radiation Laboratory in 1954. The treatment was refined and implemented in hospitals at the Clatterbridge Centre for Oncology in the UK in 1989 [PTCOG, 2013] to be followed by many hospitals worldwide, including the Mayo Clinic Cancer Center in Scottsdale, AZ [Mayo, 2018]; the present project is a collaboration between Dr. Jorge A. Lopez's group with Dr. Ricardo Alarcon's group from the Arizona State University and the Mayo Clinic.

Protons present several advantages over other types of radiation. As protons are more massive than electrons, for instance, they tend to have little lateral side scatter in the tissue keeping

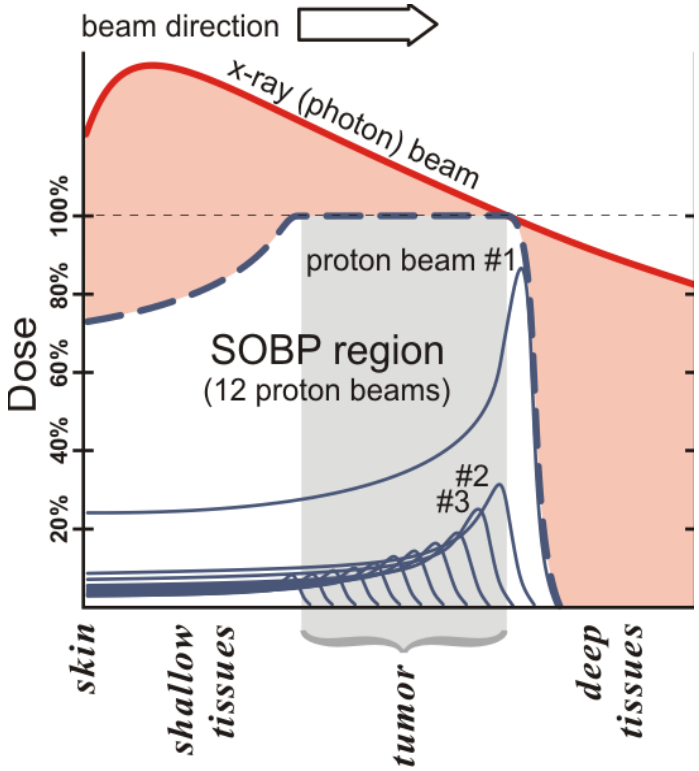

FIGURE 1.1 SPREAD OF X-RAY RADIATION COMPARED TO PROTON RADIATION.

Figure 1.1 Spread of x-ray radiation compared to proton radiation. The spread-out Bragg peak (SOBP) is actually produced by several Bragg peaks (blue lines) at different energies [Levin, 2005].

the beam narrow and focused on the tumor. Calibrating the proton energy allows the beam to deliver its energy in a certain range, mainly on the last few millimeters of the particle's range, i.e. in the Bragg peak [Camphausen, 2008]. A typical spread-out Bragg peak (SOBP) is illustrated in Figure 1.1 where it is compared to the radiation produced by an x-ray beam.

Typical energies of the proton beams are in the range of 70 to 250 MeV. Adjusting the proton energy can focus the damage within the tumor, delivering reduced radiation to tissue closer to the surface of the body and an immeasurably small radiation to cells beyond the Bragg peak [Metz, 2006]. In practice protons of different energies are used to add Bragg peaks at different

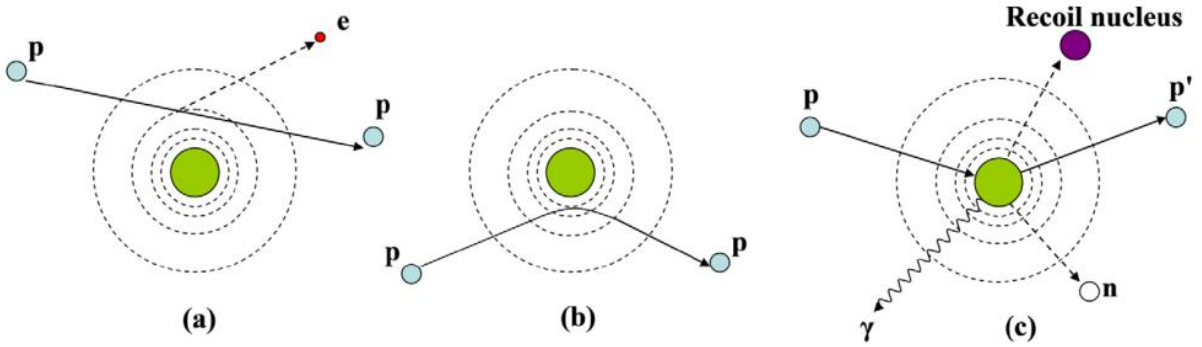

FIGURE 2. PROTON INTERACTION MECHANISMS: (A) PROTON-ELECTRON INTERACTIONS, (B) DEFLECTION OF PROTON BY THE NUCLEUS COULOMB FIELD, (C) PROTON-NUCLEUS

Figure 1.2. Proton interaction mechanisms: (a) proton-electron interactions, (b) deflection of proton by the nucleus Coulomb field, (c) proton-nucleus collision [Newhauser, 2015].

depths to treat an entire tumor. Notice that the tissue in front of the tumor receives smaller doses and those beyond the SOBP almost none.

In spite of the theoretical knowledge about the energy deposition of the proton beam on the human tissue, a lingering question is, where exactly is the energy being deposited? This is especially needed to be able to adjust the beam energy (and the SOBP) during real-time irradiations. As it is impossible to perform in situ inspections during the irradiation, it is necessary to rely on indirect observations. This is the ultimate goal of this thesis, namely, to determine the location of the area irradiated.

As it will be seen in detail in the next Chapter, protons interact with the tissue through the mechanisms illustrated in Figure 1.2, namely by inelastic Coulombic interaction with an atomic nucleus, deflection of proton trajectory by repulsive Coulomb elastic scattering with a nucleus, or by a direct collision with a nucleus removing a proton or neutron while creating a gamma ray.

Since all these processes happen in any irradiation, one can focus on, e.g. the production of gamma rays to study the location of the energy deposition.

Gamma rays are high-energy photons which interact with matter in a variety of ways, namely Mössbauer Effect, Coherent Scattering, Pair Production, Photoelectric Effect and Compton Effect (see e. g. [PhysMed,2018]). The first three have no relevance to nuclear medicine while the other two are more important for medical imaging. In our case, luckily, we only need to determine the location of where the gamma rays have been produced and, for that, no interaction is needed. That is, by detecting gammas (their direction and energy) it is possible to determine the location of the source and, thus, the area where the irradiation is taking place. This thesis will focus on relating the detection of gammas and their point of origin.

Thus, the need for detecting the gamma rays being produced in proton irradiation. At a difference with optical light, gamma rays (and x-rays) cannot be focused to produce images and, at best, one can only filter the beams with collimators to produce parallel rays which can be used to determine the main direction of a burst, and use it to determine the possible location of the source. A collimator is a device that filters a shower of gamma rays allowing only those parallel to a specified direction to go through. In this thesis gamma-ray collimators will be studied for an optimal location of the source of the rays.

In particular, in this thesis, we study the design of collimators needed to determine the directionality of gamma rays produced in proton therapy. In the next section, we will talk about the physics related, to be followed in chapter 3 by GENAT4 program and the last chapters are from analysis, data process and its interpretation.

CHAPTER 2: PHYSICS OF PROTON THERAPY

Medical physics is an applied branch of physics in charge of the application of theoretical concepts, diagnostic methods, and treatment of human diseases. It goes hand in hand with medical electronics, bioengineering and health physics. In general, a medical physicist contributes to three main areas: applications in clinical service and consultation, research and development, and teaching. The applications essentially focus on radiological imaging and radiation treatment. Most of the development is on therapeutic technics, monitor equipment and design of treatment plans with radio-oncologists [AAPM, 2018].

2.1 BASICS OF PARTICLE-MATTER INTERACTIONS

The main players in medical physics are the basic particles (electrons, protons, and neutrons), and electromagnetic radiation (x rays and gamma rays). Other participants are the neutrinos, positrons, and lower electromagnetic radiation (microwave and radio waves). Although complex theories exist to understand the interaction among these particles and radiations, for medical physics it suffices to take the existence of these particles as granted, and their interactions as Coulombic, i.e. through their electric charges. All of these participants are generically known as ionizing radiation, for their ability to "ionize" (i.e. to remove electrons) from matter through which they propagate.

X rays are produced, like any other electromagnetic radiation, through the acceleration or deceleration of electric charges. For an electromagnetic radiation to be considered as soft X rays, their energy must be in the range between 5 to 10 keV (or wavelength between 0.2 to 0.1 nm), and

as hard X rays if they have higher energies. Hard X rays are useful in medical radiography because their wavelengths are comparable to the size of atoms and can penetrate soft matter (tissue), while soft X-rays are not as useful as they are rapidly absorbed in air.

X rays are produced when atomic electrons jump from a high energy level to a low energy one releasing the difference in energy as a photon. X rays of specific energies can be produced by selectively exciting atomic electrons of certain atoms to particular orbits to produce a large number of photons with similar wavelengths; these X rays are known as K-shell or M-shell X rays. Conversely, when atomic electrons are excited at a wide range of energies, the X rays produced have a large range of wavelengths; because these rays are usually produced when a beam of electrons is stopped by a metallic target (usually tungsten, aluminum, etc.) exciting the target's electrons and producing X rays with varying wavelengths, such radiation is known as bremsstrahlung (braking radiation).

Gamma rays are also electromagnetic radiation but with more energy than the values that can be achieved by transitions of atomic electrons. Gamma rays are produced by collisions between particles and the atomic nucleus, and are in the order of MeVs with very small wavelengths (such as 10^{-11} m). Due to their small wavelength tissue is transparent to gamma rays.

There are many different types of interactions between particles and radiation, but the ones involving proton of interest for this thesis are those illustrated in Figure 1.2. Collisions between protons and atoms can result in proton-electron collisions (a), proton-Coulomb field interaction (b), and proton-nucleus collisions (c). The focus of this thesis is to locate the point of interaction between protons and tissue, although in any proton irradiation all three types of proton-atoms interactions occur, only the third one provides a signal that can be used to determine the location of the interaction: gamma-ray emission.

Protons can interact with atomic nuclei and produce gamma rays in several manners. Identifying nuclei as A, B, C, etc. excited nuclei as A*, B*, etc., protons as p, and gamma rays as γ, these interactions are:

A) Radiative capture: $p + A \rightarrow B^* \rightarrow B + \gamma$, such as $p + {}^{27}Al \rightarrow {}^{28}Si + \gamma$.

B) Inelastic scattering: $p + A \rightarrow A^* \rightarrow A + \gamma$, such as $p + {}^{27}Al \rightarrow p + {}^{27}Al + \gamma$.

C) Rearrangement collisions: $p + A \rightarrow C^* \rightarrow C + \gamma$, such as $p + {}^{27}Al \rightarrow {}^{4}He + {}^{24}Mg + \gamma$.

The gamma rays from these reactions are emitted with a wide range of energies, but usually in the few MeVs. The proton-nucleus interaction is a quantum process that involves the nucleus' proton and neutron energy levels, specifically, the incident proton loses energy exciting the charges of the nucleus producing gamma rays in a process similar to the emission of x rays by bremsstrahlung. At some energies, however, the energy transferred from the incident proton to the nucleus is exactly what is needed to make the nucleons change levels exciting the nucleus which de-excites by emitting gamma rays of a specific energy; these energies are known as resonance energies (E_R) and the gamma yield peak is known as "Lewis Peak".

Figure 2.1 shows a characteristic gamma-ray spectra produced in proton-induced reactions with the resonant peaks clearly visible; those peaks are used in the technique known as PIGE (proton induced gamma-ray emission) to identify the gamma-emitting nucleus. Table 2.1 lists a few characteristic gamma-producing proton-induced reactions and the energies involved.

Gamma rays can ionize atoms they encounter in their trajectory, but most gamma rays will simply exit the body without any interaction. Gamma radiation is the most penetrating of the radiation known, it penetrates easily body tissue, and it can only be stopped by a few centimeters of lead or about 1 meter of concrete. Since tissue and bone are practically transparent to gamma

rays, once produced inside a human body, the gammas will exit in straight lines, and thus it is feasible to use this type of radiation to determine the point of creation of the gamma rays, i.e. the region being affected by the proton beam.

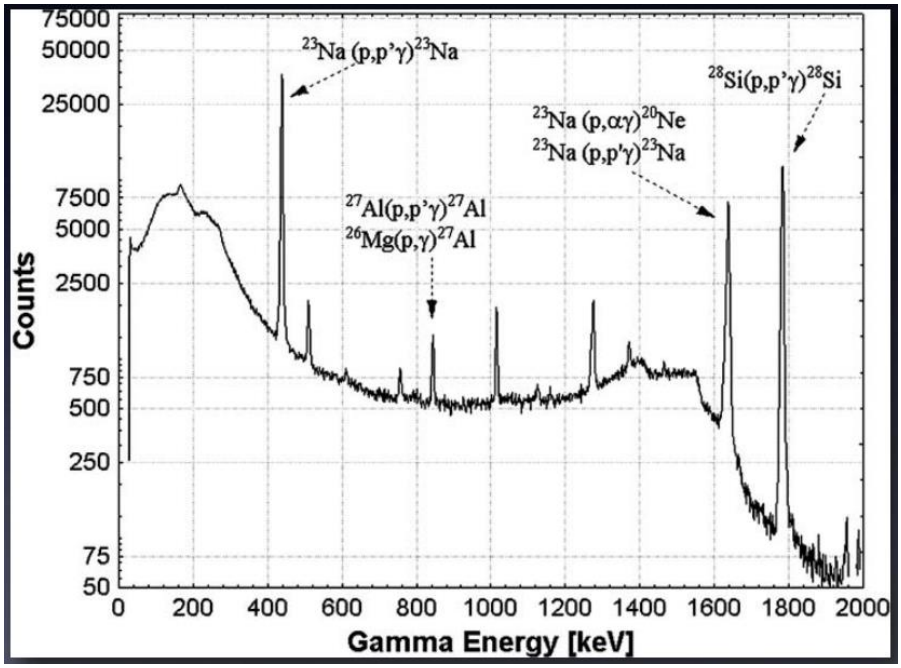

FIGURE 2.1. CHARACTERISTIC GAMMA RAY SPECTRA IN PROTON-INDUCED REACTIONS [CHIARI, 2013]. CLEARLY VISIBLE ARE THE RESONANT PEAKS.

TABLE 2.1. CHARACTERISTIC GAMMA RAY ENERGIES IN PROTON-INDUCED REACTIONS [CHIARI, 2013].

Element	Reaction	Er (keV)	Gamma ray energy (MeV)
Li	$^{7}Li(p,\gamma)^{8}Be$	441.4	17.7, 14.7
B	$^{11}B(p, \gamma)^{12}C$	163	4.43
C	$^{13}C(p, \gamma)^{14}N$	1748	9.17
N	$^{14}N(p, \gamma)^{15}O$ $^{15}N(p, \gamma)^{12}C$	1059 429	8.3, 5.2, 3.0 17.7, 14.7
O	$^{18}O(p, \gamma)^{19}F$	1167	6.3, 2.6
F	$^{19}F(p, \gamma)^{16}O$	340.5	6.1
Na	$^{23}Na(p, \gamma)^{20}Ne$	1011	1.63

2.2 FUNDAMENTALS OF PROTON THERAPY

There are many ways to treat cancer, and proton therapy is one of the newer approaches. The main advantage of using protons is that high-energy protons have a well-defined range (due to its pronounced Bragg peak). In this subsection, a brief review of the use of protons in cancer therapy is presented.

2.2.1 HISTORY OF PROTON BEAM THERAPY

In 1946 Robert R. Wilson was the first person that suggested using protons in a medical treatment. The application took place in the 1950s in nuclear physics research facilities and limited

to few parts of the body. It was not until the late 1970s that the advancement in imaging, computers, accelerators, and beam delivery technology made proton therapy more practical for cancer treatment [MDACC, 2018].

2.2.2 PROTON THERAPY PHYSICS

The idea behind any radiologic cancer treatment is the elimination of cancerous cells by a direct exposition of the cells to a beam of particles or electromagnetic radiation. For the case of proton therapy, it is the interaction between protons and the atomic electrons of cancerous cells what deposits energy in such cells killing them. This proton-electron interaction is electromagnetic in nature and, due to its long range, it continuously transfers energy from the protons to the electrons (and slowing down the proton). The rate of energy loss increases with smaller speeds and, thus, in proportion to the depth penetrated; this is what makes protons especially appealing.

The stopping power of a medium is proportional to the rate of energy loss according to:

$$S(E) = \frac{1}{\rho}\frac{\partial E}{\partial z}. \tag{2.1}$$

Where ρ is the density of the medium, $S(E)$ is the stopping power of charged particles with energy E, and z is the direction of motion. For charged particles that have masses much larger than the electron mass m_e (such as the proton, $m_p \approx 2000\ m_e$), expression 2.1 becomes the Bethe equation:

$$S(E) = 0.307\frac{Z}{A}\left(\frac{1}{\beta^2}\right)\left(\frac{1}{2}\ln\frac{2m_e c^2\gamma^2\beta^2 T_{max}}{I^2} - \beta^2\right). \tag{2.2}$$

Where $\beta = \frac{v}{c}$, $\gamma = \frac{1}{\sqrt{1-\beta^2}}$, T_{max} is the maximum transferable energy to an electron, I is the mean ionization potential of the media, A is the mass number, and Z the atomic number. In recent applications, I has been replaced by actual measurements which can be extracted from tables.

The stopping power of a material decreases as the beam speed v increases, i.e. $S(E)\ \alpha\ \frac{1}{v^2}$. This combination of the Bethe equation with a statistical Coulomb interaction leads the curves shown in Figure 2.2 of the absorbed dose deposited by as a function of depth along the axis of the beam [Knopf, 2013]; the pronounced peak at a certain location is known as the Bragg peak. Figure 2.2 shows the great difference between the curve of photons and protons (cf. Figure 1.1). Noticing that the area under each curve is proportional to the energy delivered indicates that different beams cause a different amount of damage lengthwise along the trajectory of the beam. The advantage of protons over other types of beams in depositing energy in a specific region is clearly observable in Figure 2.2: by combining (pristine) beams at different energies it is possible to produce a spread-out Bragg peak (SOBP) that irradiates a larger but specific area, not damaging healthy tissue nearby.

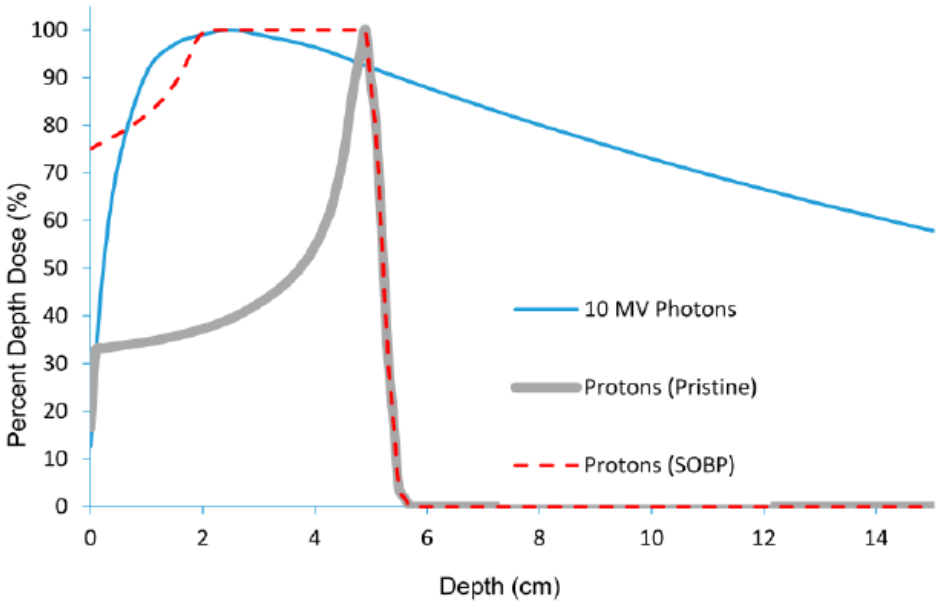

FIGURE 2.2. PERCENT DEPTH DOSE AS A FUNCTION OF DEPTH [BERNAM, 2015].

2.2.3 DELIVERY OF PROTONS

Protons are delivered in cancer treatments in a beam produced by an accelerator. The beam, which is usually very thin, is widened through scattering with a foil generating a broad beam suitable for therapy. The beam is then shaped to the geometry of the target, using an aperture (for lateral dose), a range compensator (for distal conformation) and proton energy range modulation to spread the dose along the beam direction forming the spread-out Bragg peak.

Additionally, depending on the geometry of the target, it is possible to have the beam subjected to an active scanning across the target. This scanning is usually used with a narrow pencil thick proton beam which scans through the objective combined with energy changes to produce the SOBP.

2.3 THIS THESIS

The perennial risk of radiotherapy is the inherent uncertainty of the method. Is the beam depositing energy where is needed? Is any healthy tissue being damaged? Although these questions can be answered by analyzing a biopsy, it would be better to be able to answer them during the irradiation, i.e. *in vivo*; this can be done by capturing and studying the gamma rays produced during the irradiation.

The purpose of this thesis tries to study gamma rays *in vivo* to determine their point of origin. The study is done by simulating a source of gammas rays emitted by a patient, and a device to capture the gammas. The simulations are performed using the platform GEANT4 (GEometry ANd Tracking) which mimics the generation of particles and their passage through matter using Monte Carlo methods; GEANT4 will be described in Chapter 3. The detection system will be described in Chapter 4.

CHAPTER 3: GEANT4

Geant4 is a powerful platform designed by the European Organization for Nuclear Research known as CERN (Conseil Européen pour la Recherche Nucléaire) to do accurate simulations of complex particle interactions based on the Monte Carlo method. GEANT4 is routinely used to study nuclear and particle reactions, develop particle detectors, medical physics processes, and a plethora of other physical mechanisms. This chapter presents a brief overview of Geant4.

3.1 GEANT4 HISTORY

The original code GEANT was written in 1974 in Fortran with the purpose of tracking particles produced in nuclear reactions at CERN. As more detectors and information about reactions were added, GEANT evolved into a more complex simulation package [12]. The evolution of GEANT was possible thanks to the voluntary collaboration of physicists around the world who use, debug and improve the program.

There have been major upgrades to the package named, respectively, GEANT2, GEANT3, and Geant4 (in lower case). GEANT2 maintained the skeleton of the original version while adding many new features. GEANT3 differs from the previous version by the introduction of electromagnetic processes and the FLUKA interface and other additions. A more revolutionary upgrade happened with the release of Geant4 which was a complete rewrite in C++ with a modern object-oriented design; versions exist for most operating systems, although it is Linux native.

Nowadays Geant4 is maintained and improved by the Geant4 international collaboration, and the latest version is 10.4 released in 2017 [Geant4, 2018].

3.2 GEANT4 FUNCTIONALITY

A Geant4 simulation consists of a source of particles or electromagnetic radiation, a medium with a target, a detection system, and extra software for the analysis of the data produced. In crafting a simulation, it is necessary to specify the type of particles that will be used as projectiles in the simulation, their directions, and energies. It is also necessary to identify the composition of the medium through which the beam will travel (gas, solid, liquid, type of particles, temperature, density), and the target (a type of particles, shape, structured materials, etc.). And finally –and more cumbersome— a detection system must be designed in accordance with the specifications of the experiment to be simulated. Luckily Geant4 has all the proper ingredients to facilitate these tasks.

Geant4 has a vast library of particles with all the pertinent information such as mass, charge, spin, etc.; beams can be created with different energies and in any initial directions. Likewise, medium materials (such as vacuum, air, specific gases, etc.) can be selected from the Geant4 libraries at any densities or pressures. Similarly, targets can be crafted with any geometry needed and of any material which, again, can be specified from a library; targets can be gaseous, liquids or solids and at any temperature. Detectors must be designed according to the specifications of the experimental equipment, but Geant4 also includes most types of general detection materials, such as silicon and the like, and drafting tools to design required shapes.

The simulation operates by creating one particle at a time and sending it towards the physical chamber in a given direction and at some energy. The particle then travels through the medium filling the chamber and interacts according to the physical laws selected for the simulation. It is possible to simulate all of the possible physical processes, such as scatterings, particle production, annihilation, electromagnetic radiation, or energy loss, etc., simply by selecting the wanted interactions from a Geant4 table; simulations focusing on specific effects (e.g. energy loss) usually avoid all non-wanted interactions to save on computer time.

The final step of the simulation is the collection of information produced and its analysis. These two steps are normally done through a graphical interface such as ROOT or another one of the specialized software packages; ROOT will be briefly described below.

In summary, each Geant4 simulation contains the following steps each of which are implemented as C++ class categories (cf. Figure 3.1):

- Description of the geometry of the system
- Description of the materials involved
- Description of the fundamental particles of interest
- The generation of primary events
- The tracking of particles through materials and electromagnetic fields
- Description of the physical processes governing particle interactions
- The response of sensitive detector components
- The generation of event data

- The storage of events and tracks

- The visualization of the detector and particle trajectories

- The capture and analysis of simulation data at different levels of detail and refinement

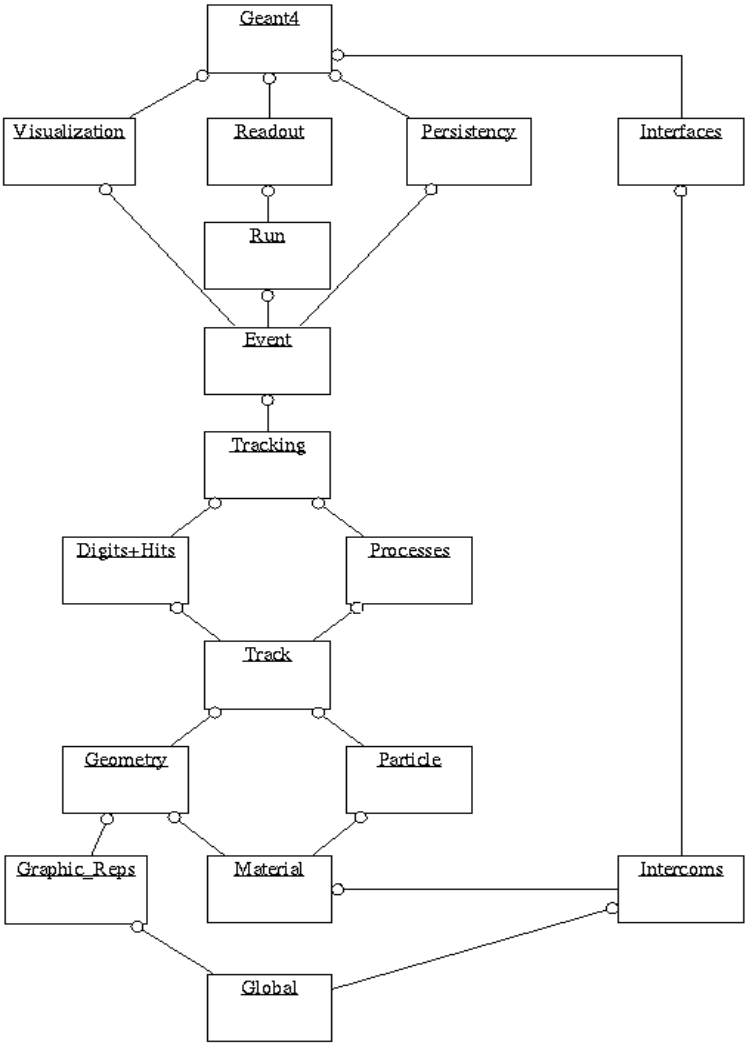

FIGURE 3.1 GEANT4 CLASS CATEGORIES [GEANT4, 2018]

In particular, these class categories are:

- Global: Category to set the constants, random number handling, and system units.

- Materials and particles: Category to set up the physical properties of materials and particles for the simulation of particle interactions.
- Geometry: Category to set the geometry of the detector or target, the particle-matter interaction, and the tracking of particles.
- Track: category required to advance (steps) and track particles through the medium.
- Processes: category that controls the physical interactions such as electromagnetic interactions of photons, leptons hadrons, and ions, also containing hadronic interactions. All those processes are invoked by tracking.
- Tracking: Category to manages the track's state evolution and provides information about processes and particle-matter interactions.
- Event: Category that manages the tracks.
- Run: Category that manages a collection of events in a given implementation.
- Readout: Category that allows the handling of pile-up or cumulative information.

Finally, all those categories, classes and libraries provide information outside of the toolkit to a user interface which provides visualization or data manager.

3.3 COMPARISION OF GEANT4 WITH OTHER TOOLS

GEANT4 is not the only platform that simulates the passing of particles through matter, other programs used in medical physics are MCNP, EGS4, EGSnrc, etc. Comparison between these programs shows that, for heterogeneous media, there are relative deviations around 5% between the Monte Carlo codes. For monoenergetic electrons in homogeneous media, Geant4 and EGSnrc are as close to one another as they are too experimental measurements. For depth-dose curves, the difference it is just a small fraction of the peak dose smaller than 4%. In conclusion, Geant4 is as promising simulation toolkit for low-energy medical physics as any other one [Carrier, 2004].

3.4 ROOT CERN

Root is a scientific software framework that is retrofitted to Geant4 to provide the necessary functionalities to deal with big data processing, statistical, visualization and storage. Its programming language contains mainly C++, but also it has other languages integrated such as python and R [ROOT, 2018]. Geant4 generates ROOT files to process and manage the data.

Root was developed in the mid-1990's after previous successful platforms, such as PAW, and PIAF had reached their limits to handle the vast amounts of data produced by the Large Hadron Collider, which were orders of magnitude larger than anything seen before. Parallel to that, computer science had progressed especially in the Object-Oriented Design, which took advantage in the design of ROOT; physicists developed ROOT in the "Bazaar-style", i.e. an informal style

producing a package specific, appropriate and very powerful for storing and mining big data in the order of Terabytes [ROOTUG, 2018].

CHAPTER 4: SIMULATION

The overall goal of the project is to determine the location of proton-tissue interactions during irradiation. As explained before, out of the several interactions between a proton beam and tissue, only those producing gamma rays can help us with this goal; the study focuses on the produced gammas, so our simulation doesn't start with a proton beam impinging on tissue, leading us to a gamma source inside of a target. The goal of the simulation is to determine in what ways the detection of gammas can be used to find the source location. Reiterating the importance of this study, it is to introduce an *in vivo* method to relate the acquisition of data with the irradiated signal of the target (e.g. tissue, tumor, bone, etc.) at that precise moment of therapy.

The gamma rays produced within the patient are assumed to exit freely toward the detection system. The gammas are produced in all directions (radial source) and collimated toward the detector with parallel collimating plates. The collimator will align the gamma rays in a preferential direction, leading to a reduction of width and intensity of the gamma rays.

In optics, a collimator is made of mirrors and lenses to focus a beam on a point(s), for high energy particles-waves (e.g. x rays and gamma rays) is quite demanding, due to a small wavelength. Therefore, that approach is not easily possible since an optical device cannot filtrate at high frequencies, because a relatively long spacing parameter in a collimator; to achieve a gamma-ray filter, it is needed a hard material (e.g. lead or tungsten) and one of the study cases of this thesis is to analyze the spacing in the collimator.

In x-ray and gamma-ray collimation is used to simply block the rays that are not of our interest.

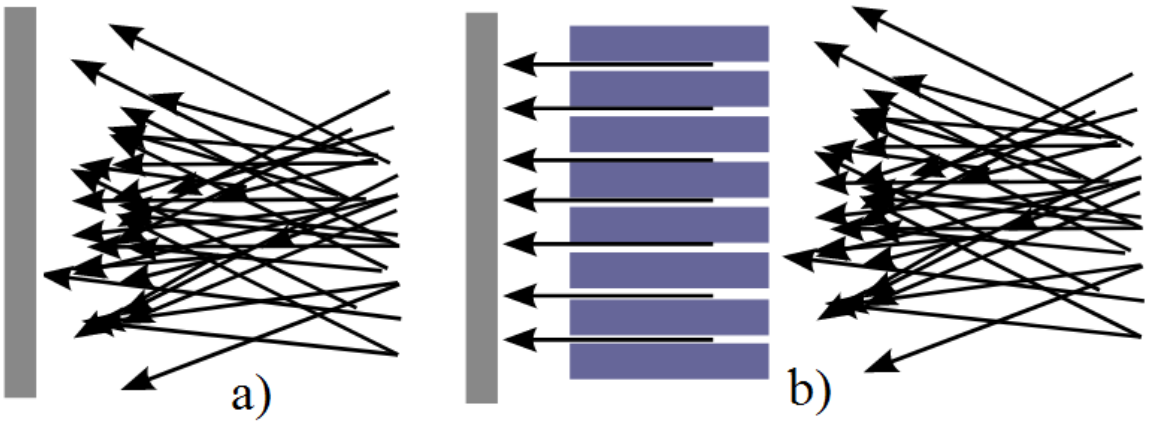

FIGURE 4.1. BEAM OF GAMMA RAYS WITH AND WITHOUT A COLLIMATOR. THE GAMMAS ARE RECORDED ON THE LEFT PLATES [FON, 2018].

Figure 4.1 illustrates a beam of gamma rays a) without and b) with a collimator. In panel a), without a collimator the imprint on the plate will record rays from all directions losing the original direction of travel of the ray; for example, rays traveling downwards may be recorded at the bottom of the plate, and vice versa, resulting in a blurred pattern with no significance. On the other hand, in figure 4.1.b the collimator (made of sheets of metal, such a lead) will be opaque to the incoming radiation, allowing only those rays parallel to the openings of the sandwich arrangement shown.

This type of collimators are used for x rays, gamma rays, and neutron beams. In industry, they are used to reduce the exposure of radiation on films to create radiographs, for instance. In radiotherapy treatments, collimators are used to shape the beam of radiation (electrons or photons) and limit its size.

4.1 COLLIMATOR-DETECTOR GEOMETRY

In the present simulation, the collimator is made of parallel lead plates with dimensions of 20 cm (Y component) by 20 cm (Z component), 2.2 mm of thickness and 4 mm of pitch (spacing) initially. Behind the collimator is a sensitive detector of 40 cm long (X component) by 20 cm (Y component) by 20 cm (Z component) and filled with water (water phantom). Figure 4.2 illustrates the collimator-detector arrangement.

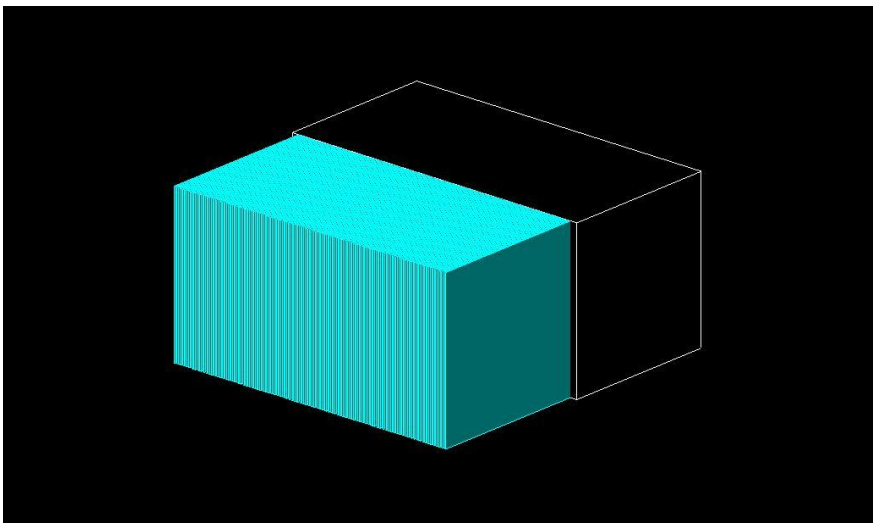

FIGURE 4.2. GEOMETRICAL ARRANGEMENT OF THE COLLIMATOR (BLUE BLADES) AND THE WATER PHANTOM DETECTOR (TRANSPARENT BOX).

Figure 4.3 illustrates the geometry of the collimation of gamma-rays produced by a single radial source. The black bars represent the collimator, the black dot at the bottom is the gamma-ray source, and the thin lines are gamma-ray trajectories. The radial source is located at (0,0, Z).

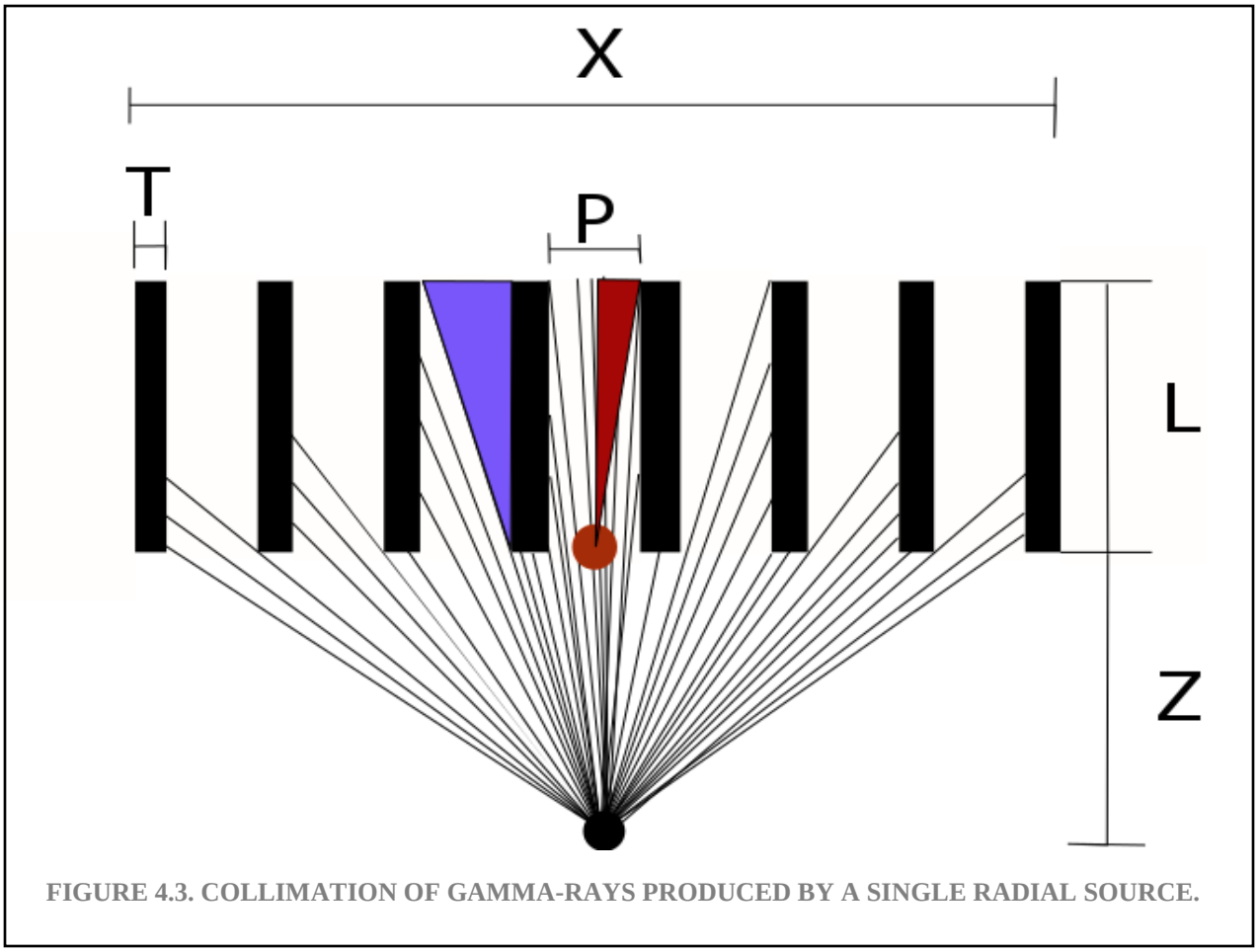

FIGURE 4.3. COLLIMATION OF GAMMA-RAYS PRODUCED BY A SINGLE RADIAL SOURCE.

In Figure 4.3 the red triangle represents the maximum angle of capture, obtained in the case where the source is just outside the collimator (next to the human body). In this case

$$\theta_{max} = \tan^{-1}\left(\frac{P}{2L}\right) \tag{4.1}$$

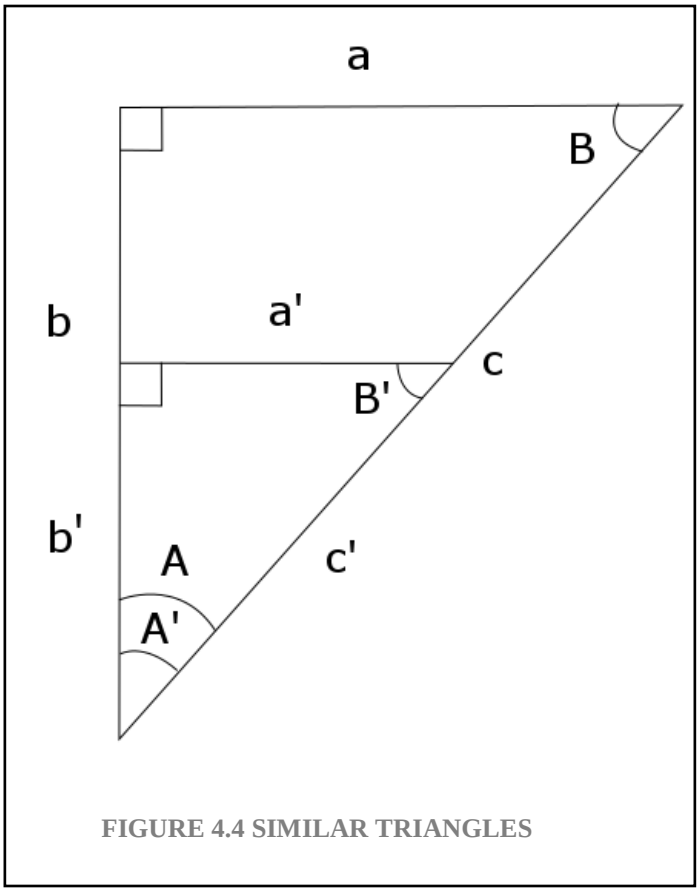

FIGURE 4.4 SIMILAR TRIANGLES

Where θ_{max} is related to the maximum capture of the signal for the first pitch (first complete zone). Given the geometry and using the similarity of triangles (see Figure 4.4), it can be seen that $A = \theta$ and $B = \psi$, and then get.

$$\theta_{max} = \tan^{-1}\left(\frac{P}{2L}\right) = \tan^{-1}\left(\frac{\frac{P}{2}+P+T}{L+Z}\right) \tag{4.2}$$

In general, for both, the nth pitch and thickness, the next relationship comes out:

Naturally, from both relations, the following relationship comes out:

$$\theta_{max} = \tan^{-1}\left(\frac{\frac{P}{2}+n(P+T)}{L+Z}\right) \tag{4.3}$$

We are interested in only whole numbers of n for a full measure in a pitch or just not have a signal there.

A property that shows the previous relationship is:

$$\lim_{z\to 0}\frac{\frac{P}{2}+n(P+T)}{L+Z}=\frac{P}{2L} \tag{4.3}$$

It is clear that Z depends on the n number (number of layers) and vice versa, so we should notice that the blue area from the figure 4.5 contains signal loss in the x-projection that is between $\frac{p}{2}<b_1(x)\leq\frac{3p}{3}$, where b_1 is the first signal loss of the second pitch zone.

The next statements can have the following relationship of Figure 4.4.

$$\tan B=\frac{b(z)}{L} \qquad\qquad \tan B'=\frac{\frac{P}{2}+T+b(z)}{z+L}$$

The previous quantities are equal, consequently, after solving for $b(z)$ and using some properties, there comes out:

$$b(z)=\frac{L}{z}\left(\frac{p}{2}+T\right)$$

$$\lim_{z\to\infty} b(z)=0$$

Looking for a general description for the nth spacing, it can be obtained by the following expression: (or 2n+1)

$$b_n(z)=\frac{L}{z}\left(\frac{2n+1}{2}P+nT\right) \tag{4.4}$$

There is a periodicity condition given by $0\leq b_n(x)\leq P$.

$$\lim_{n\to 0}(\tan B_n) = \tan B_0 = \frac{P}{2\,z}$$

Which looks like our expression for the maximum angle $\tan\theta_{max} = \frac{P}{2\,L}$ but z is greater than L, then it makes a minor angle and a lower signal capture in the first zone.

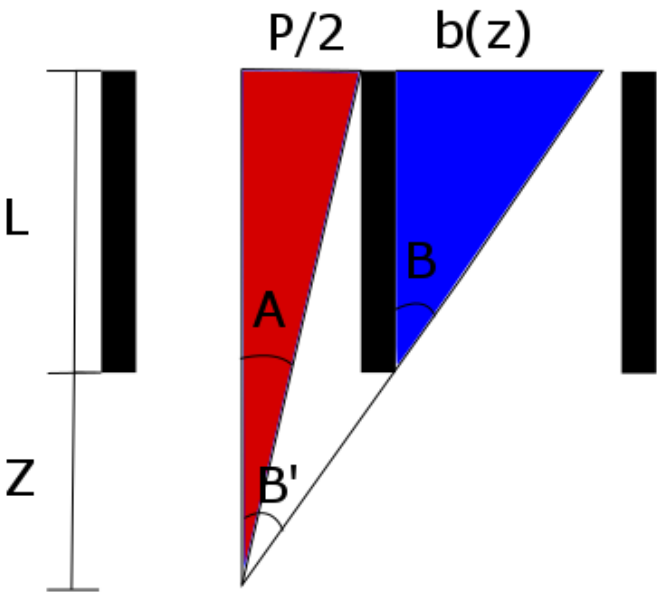

FIGURE 4.5. SIMILARITY OF SIGNAL LOSS.

4.2 SIMULATION SPECIFICATIONS

The source will be placed at a variable distance in the Z direction, with the objective of optimizing the capture of gamma-rays and filtering the desired signal. The simulated source, for simplicity, will be a random radial source in the XZ plane at (0,0, Z). Now a sketch of the device-source interaction will be shown.

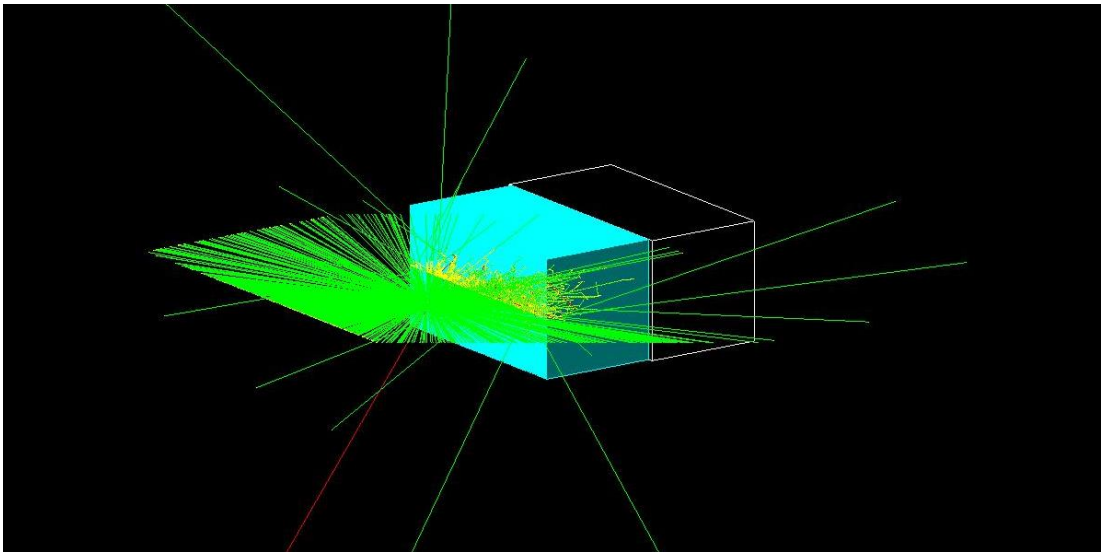

FIGURE 4.6 DEVICE-SOURCE INTERACTION 1

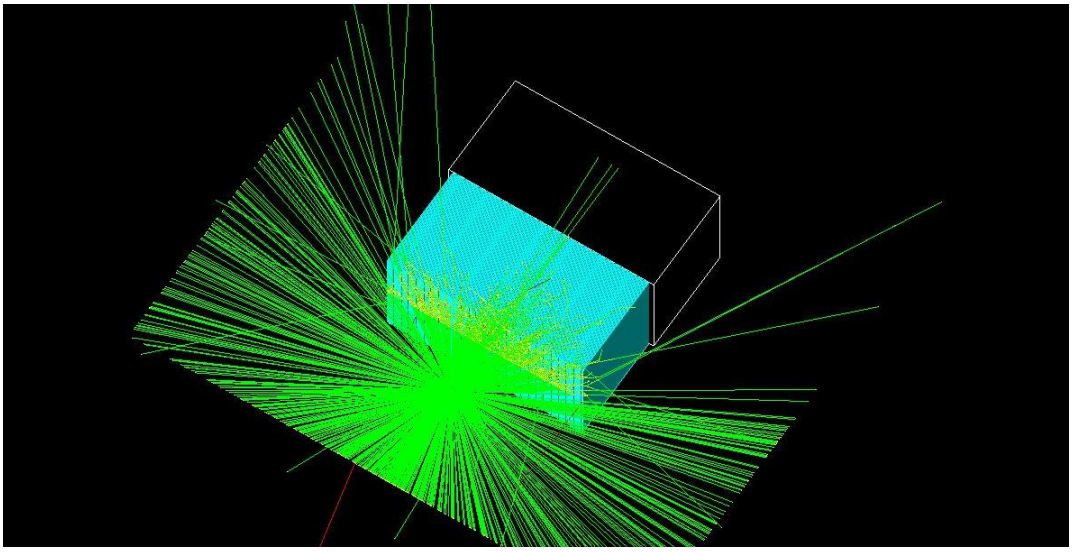

FIGURE 4.7 DEVICE-SOURCE INTERACTION 2

The above images are different views for the mentioned parameters, although the source was placed at 10 cm away from the center of the collimator, it can be clearly observed the filtering effect. The energy used for the previous tests was 2 MeV.

4.3 DATA PROCESSING

After running the program with the aforementioned parameters, with a source of one thousand events (1000 radial random gamma-rays) being filtered by the defined collimator, and each run will produce a .root file that which has the information to do the analysis with CERN ROOT program.

Our predefined load file will integrate over all the measured signal that has been captured by the sensitive detector, simultaneously it will do a partial integration as needed and also will show the gamma counts along the x-axis.

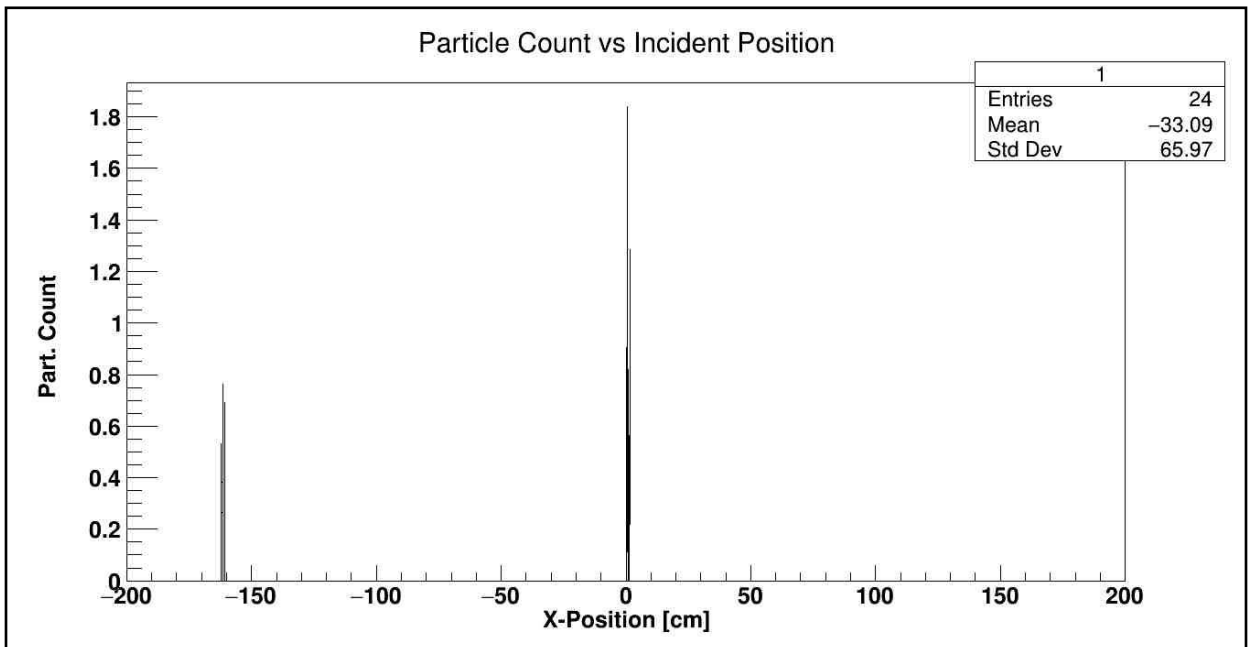

FIGURE 4.8 PARTICLE COUNT ON THE X DIRECTION OF THE DETECTOR

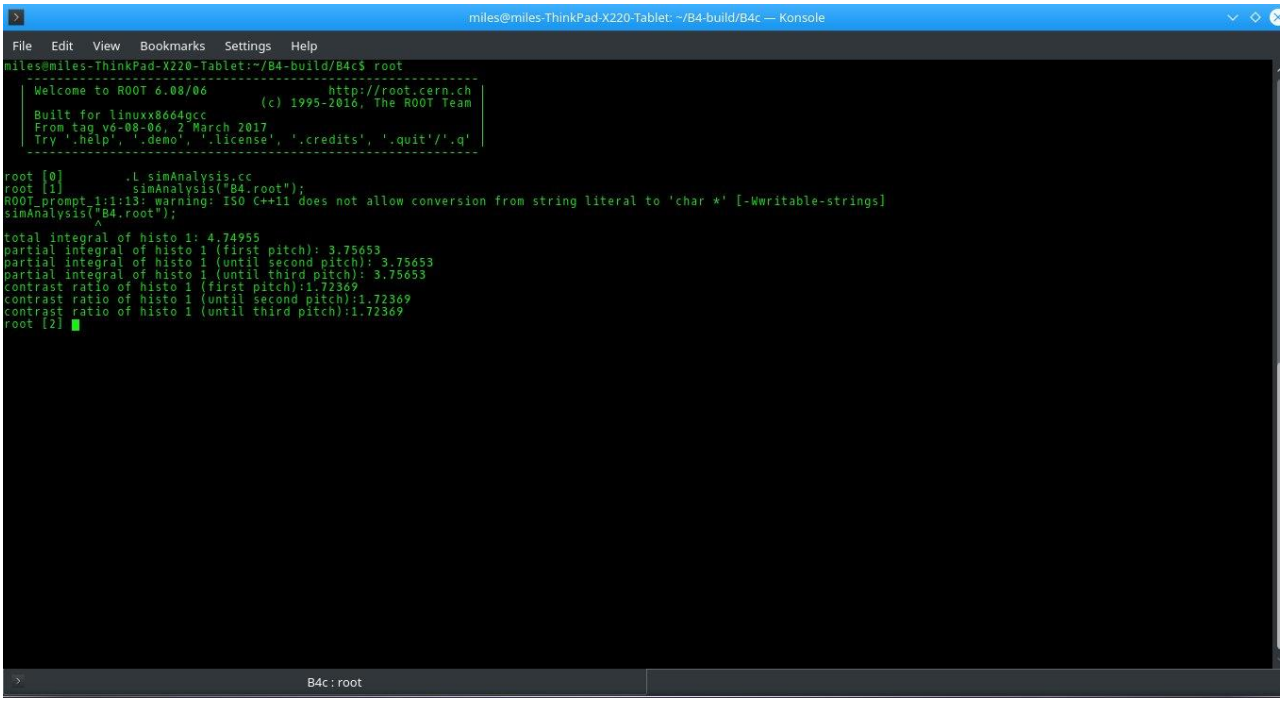

FIGURE 4.9 PROCESSING WITH ROOT.

The information generated is the integration of the signal over first zone (first pitch), second zone (second pitches) and the third zone (third pitches), and it tells us the number of counts made into those regions.

total integral of histo1:4.74955
partial integral of histo 1 (first pitch): 3.75653
partial integral of histo 1 (until second pitch): 3.75653
partial integral of histo 1 (until third pitch): 3.75653
contrast ratio of histo 1 (first pitch):1.72369
contrast ratio of histo 1 (until second pitch):1.72369
contrast ratio of histo 1 (until third pitch):1.72369

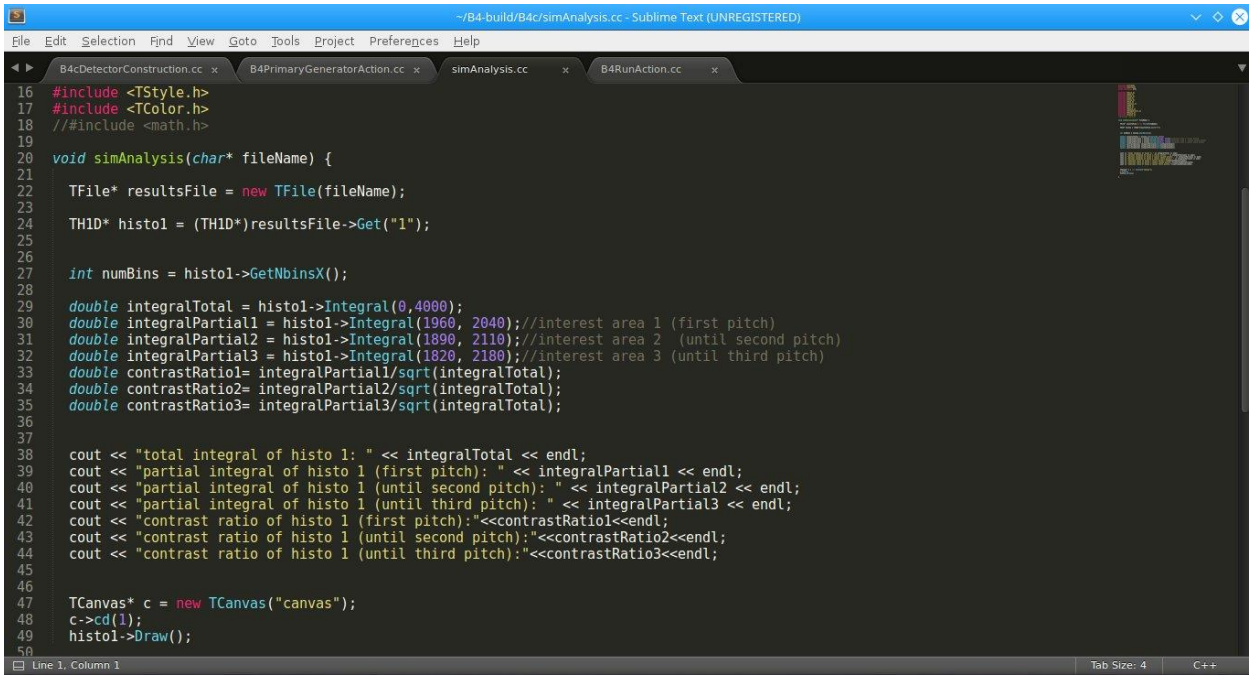

FIGURE 4.10 LOAD FILE TO ANALYZE WITH ROOT.

The number of bins will be 4000 that will be the partitioning of the length x, for the sensitive detector is 40 cm long over 4000 bins, thus giving us the minimum step of 0.01cm/bin.

An important quantity is the signal measured and its numerical integration, and the mathematical expression is the following.

$$TotalSignal = \int_{-\frac{l}{2}}^{\frac{l}{2}} Count\ dx$$

Where l is the total length of the collimator and count is the total number of gamma rays that interacted with the sensitive detector.

There is also a new quantity to recall, this being the contrast ratio, which measures the signal obtained. The definition of the contrast ratio is as follows.

$$CNR = \frac{\int_{-\frac{x_0}{2}}^{\frac{x_0}{2}} Count\ dx}{\sqrt{\int_{-\frac{l}{2}}^{\frac{l}{2}} Count\ dx}}$$

It is also known as signal-to-noise ratio (S/N), that compares the level of the desired signal to the level of the noise ($\sqrt{\sigma}$) in the measurement, this is commonly used in science and engineering to clean up the signal [Wilkins, 2006].

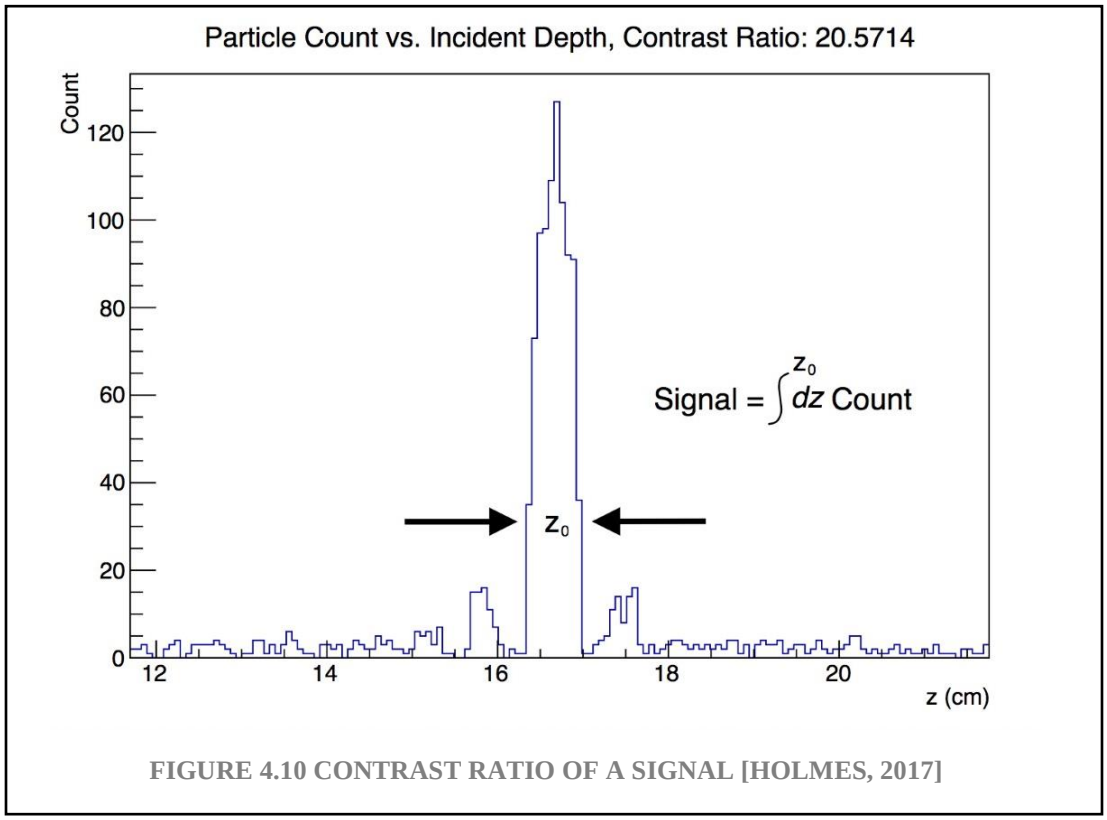

FIGURE 4.10 CONTRAST RATIO OF A SIGNAL [HOLMES, 2017]

CHAPTER 5: RESULTS AND ANALYSIS

The objective of this chapter is to study a set of variables, namely pitch, thickness, and energy, for a set of established distances between the collimator and the source.

The following abbreviations will be used:

- total integral of histo1 → T.I.
- partial integral of histo 1 (first pitch) → P.I.1A (first area)
- partial integral of histo 1 (until second pitch) → P.I.2A (second area)
- partial integral of histo 1 (until third pitch)→P.I.3A (third area)
- contrast ratio of histo 1 (first pitch) → CNR.1A
- contrast ratio of histo 1 (until second pitch)→ CNR.2A
- contrast ratio of histo 1 (until third pitch)→CNR.3A

The default values for the simulation are: initial position at 0 cm (between the collimator and the source), the layers of the collimator are made of lead with geometry of 20 cm long by 20 cm height with 2 mm of thickness, and the spacing (pitch) between each lead plate is measured from center to center of each plate.

5.1 RESULTS CHANGING PITCH WITH 2 MEV ENERGY

5.1.1 SIMULATION FOR 2 MM THICKNESS AND 4 MM PITCH

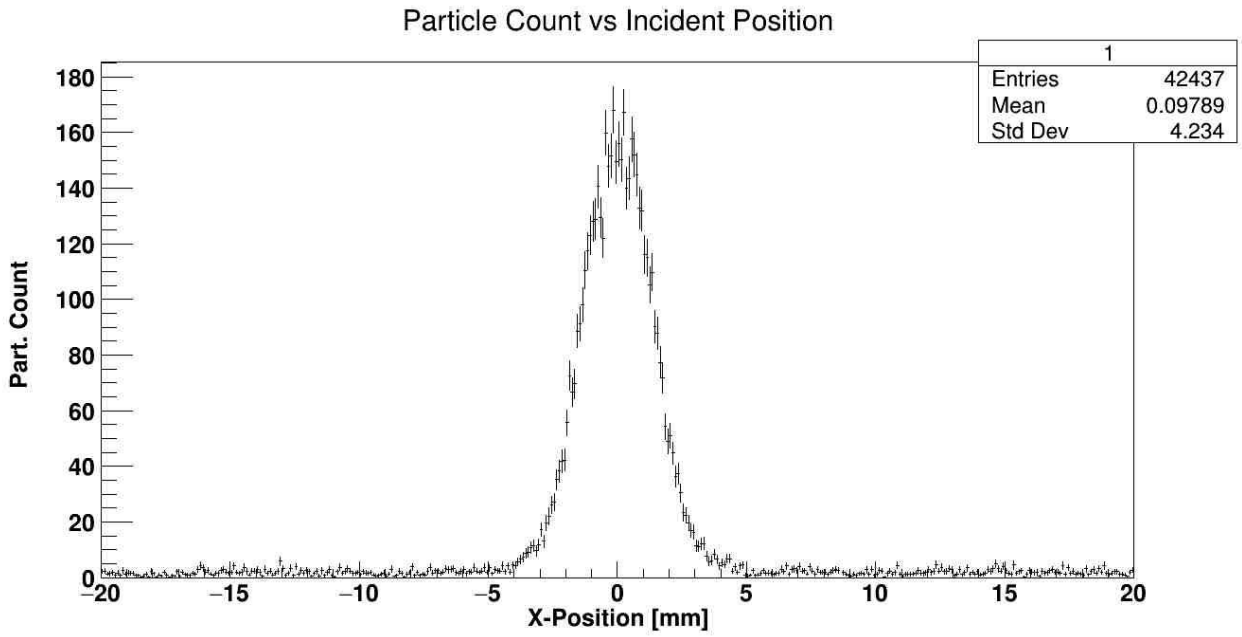

FIGURE 5.1 INCIDENT PARTICLE COUNT VS POSITION (ALONG X DIRECTION) SOURCE AT $Z = 0\ cm$ FROM THE COLLIMATOR WITH T=2 MM AND P= 4MM, E=2MEV.

total integral of histo 1: 8070.44

partial integral of histo 1 (first pitch): 4715.53

partial integral of histo 1 (until second pitch): 5629.77

partial integral of histo 1 (until third pitch): 5848.61

contrast ratio of histo 1 (first pitch):52.4907

contrast ratio of histo 1 (until second pitch):62.6675

contrast ratio of histo 1 (until third pitch):65.1034

As expected, it's a well-located peak in figure 5.1, where the y component of the graph is the gamma count and the x-axis is the length of the collimator (with the special zoom at the center).

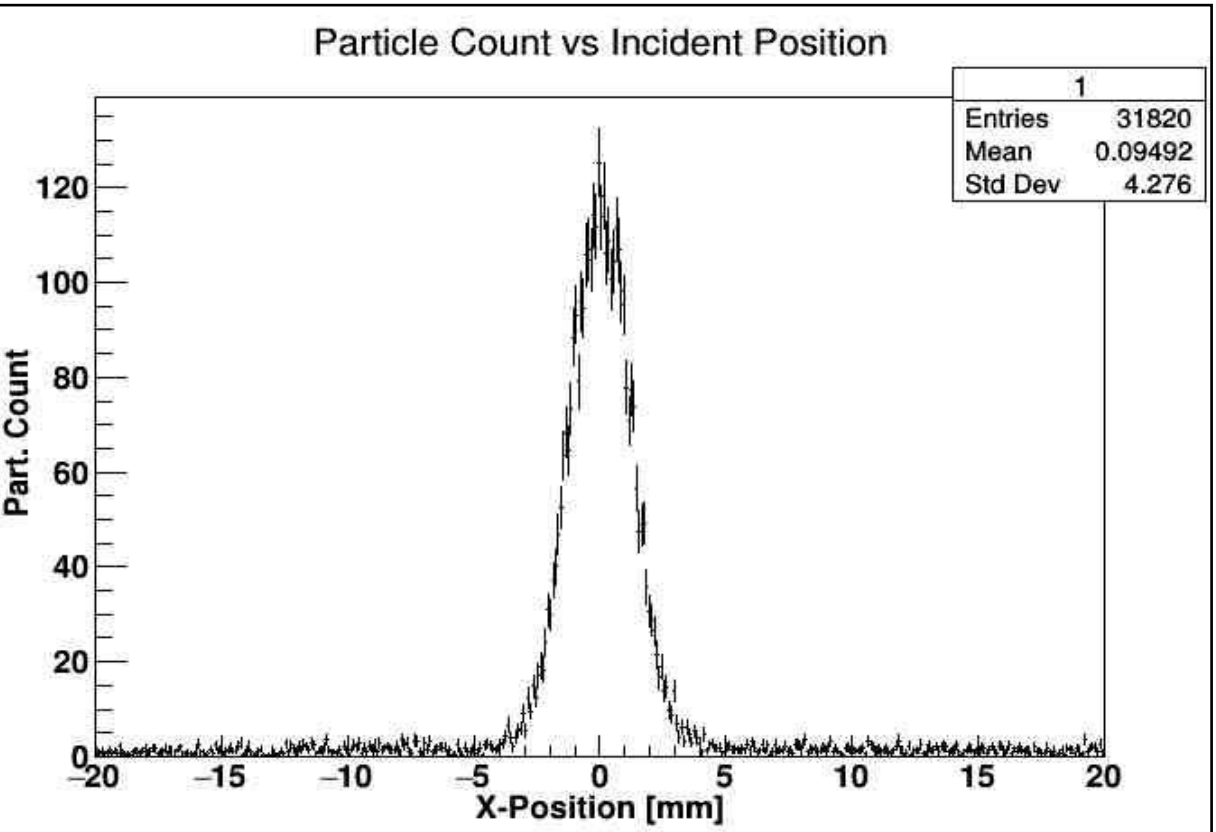

FIGURE 5.2 INCIDENT PARTICLE COUNT VS POSITION (ALONG X DIRECTION) SOURCE AT $Z = 10\ cm$ FROM THE COLLIMATOR WITH T=2 MM AND P= 4MM, , E=2MEV.

total integral of histo 1: 5973.37

partial integral of histo 1 (first pitch): 3259.76

partial integral of histo 1 (until second pitch): 3800.89

partial integral of histo 1 (until third pitch): 3982.29

contrast ratio of histo 1 (first pitch):42.177

contrast ratio of histo 1 (until second pitch):49.1785

contrast ratio of histo 1 (until third pitch):51.5256

In the figure 5.2 can be observed that there is a little bit more noise around 5 to 20 millimeters.

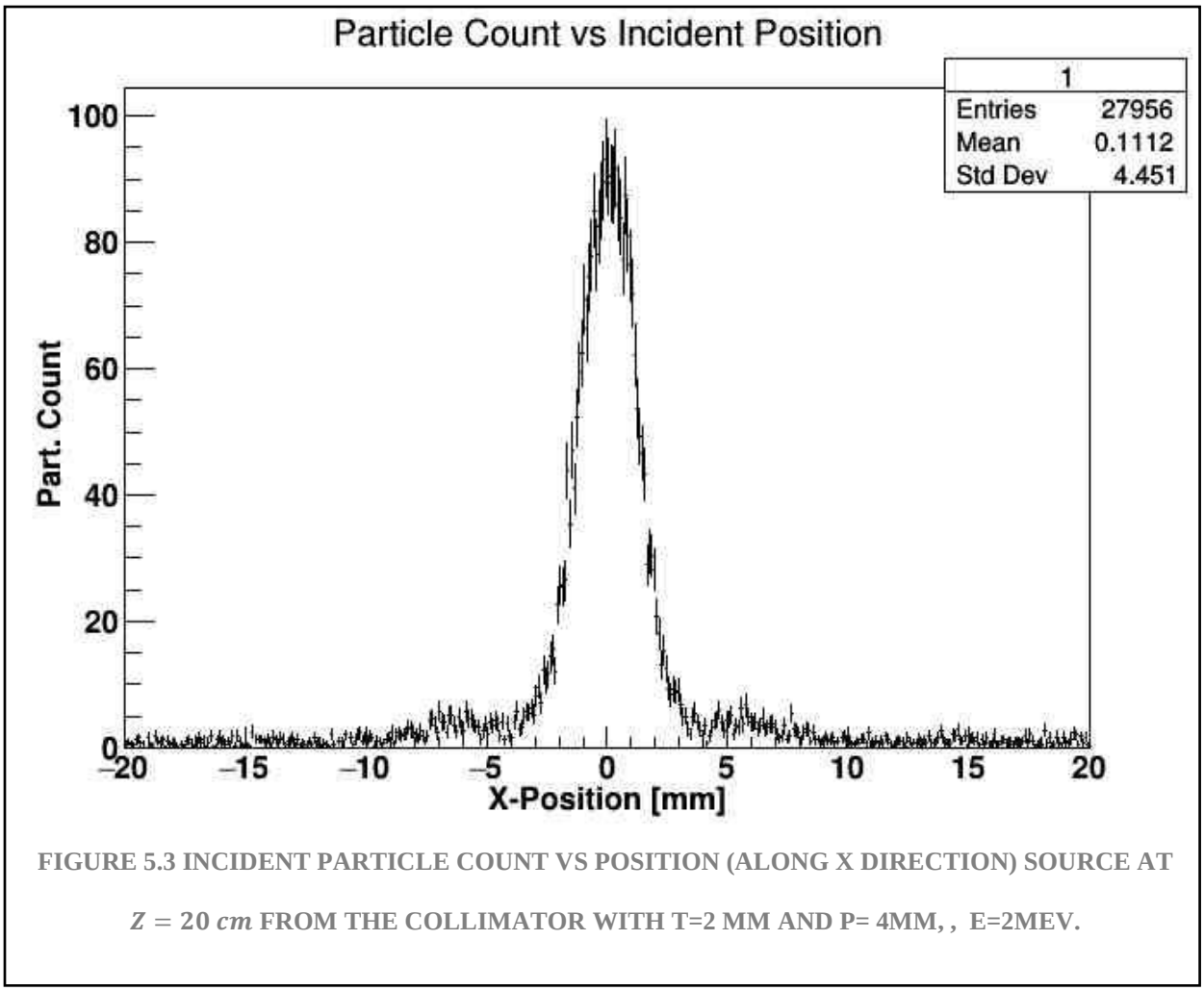

FIGURE 5.3 INCIDENT PARTICLE COUNT VS POSITION (ALONG X DIRECTION) SOURCE AT $Z = 20\ cm$ FROM THE COLLIMATOR WITH T=2 MM AND P= 4MM, , E=2MEV.

total integral of histo 1: 5190.26

partial integral of histo 1 (first pitch): 2545.4

partial integral of histo 1 (until second pitch): 3138.29

partial integral of histo 1 (until third pitch): 3283.05

contrast ratio of histo 1 (first pitch):35.3314

contrast ratio of histo 1 (until second pitch):43.561

contrast ratio of histo 1 (until third pitch):45.5705

In Figure 5.3, it can now be observed the increase of the new signal captured in the next cavities from the center.

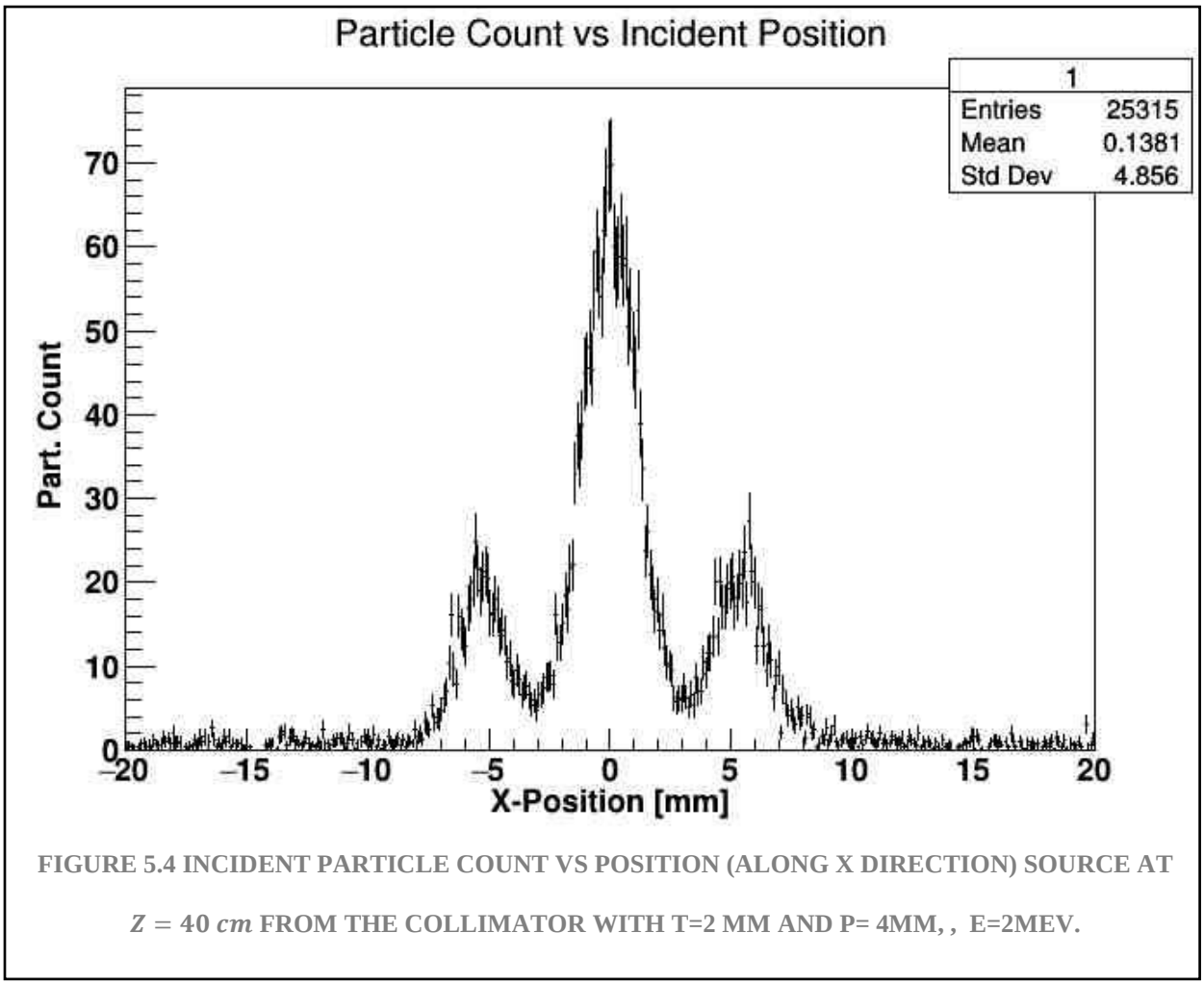

FIGURE 5.4 INCIDENT PARTICLE COUNT VS POSITION (ALONG X DIRECTION) SOURCE AT $Z = 40\ cm$ FROM THE COLLIMATOR WITH T=2 MM AND P= 4MM, , E=2MEV.

total integral of histo 1: 4756.81

partial integral of histo 1 (first pitch): 1727.19

partial integral of histo 1 (until second pitch): 3053.7

partial integral of histo 1 (until third pitch): 3187.17

contrast ratio of histo 1 (first pitch):25.0427

contrast ratio of histo 1 (until second pitch):44.276

contrast ratio of histo 1 (until third pitch):46.2112

Now the peaks in figure 5.4, are the increase in the signal measurement at the second areas and its analysis will be left for later.

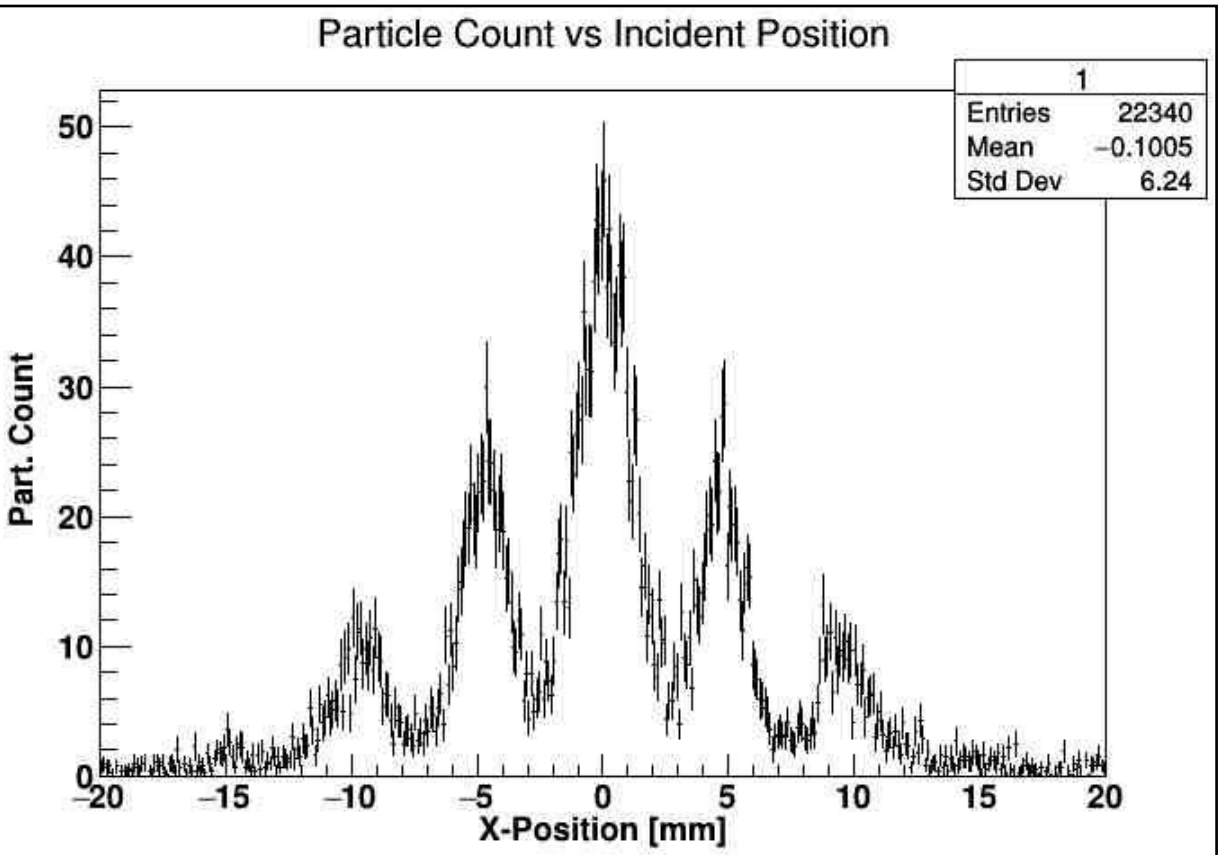

FIGURE 5.5 INCIDENT PARTICLE COUNT VS POSITION (ALONG X DIRECTION) SOURCE AT $Z = 80\ cm$ FROM THE COLLIMATOR WITH T=2 MM AND P= 4MM, , E=2MEV.

total integral of histo 1: 4272.83

partial integral of histo 1 (first pitch): 1096.22

partial integral of histo 1 (until second pitch): 2416.54

partial integral of histo 1 (until third pitch): 2973.11

contrast ratio of histo 1 (first pitch):16.7702

contrast ratio of histo 1 (until second pitch):36.9689

contrast ratio of histo 1 (until third pitch):45.4834

This is the most interesting pattern (figure 5.5), which will usually remain for the distance of the source at 80 cm from the collimator.

5.1.2 SIMULATION FOR 2 MM THICKNESS AND 5 MM PITCH

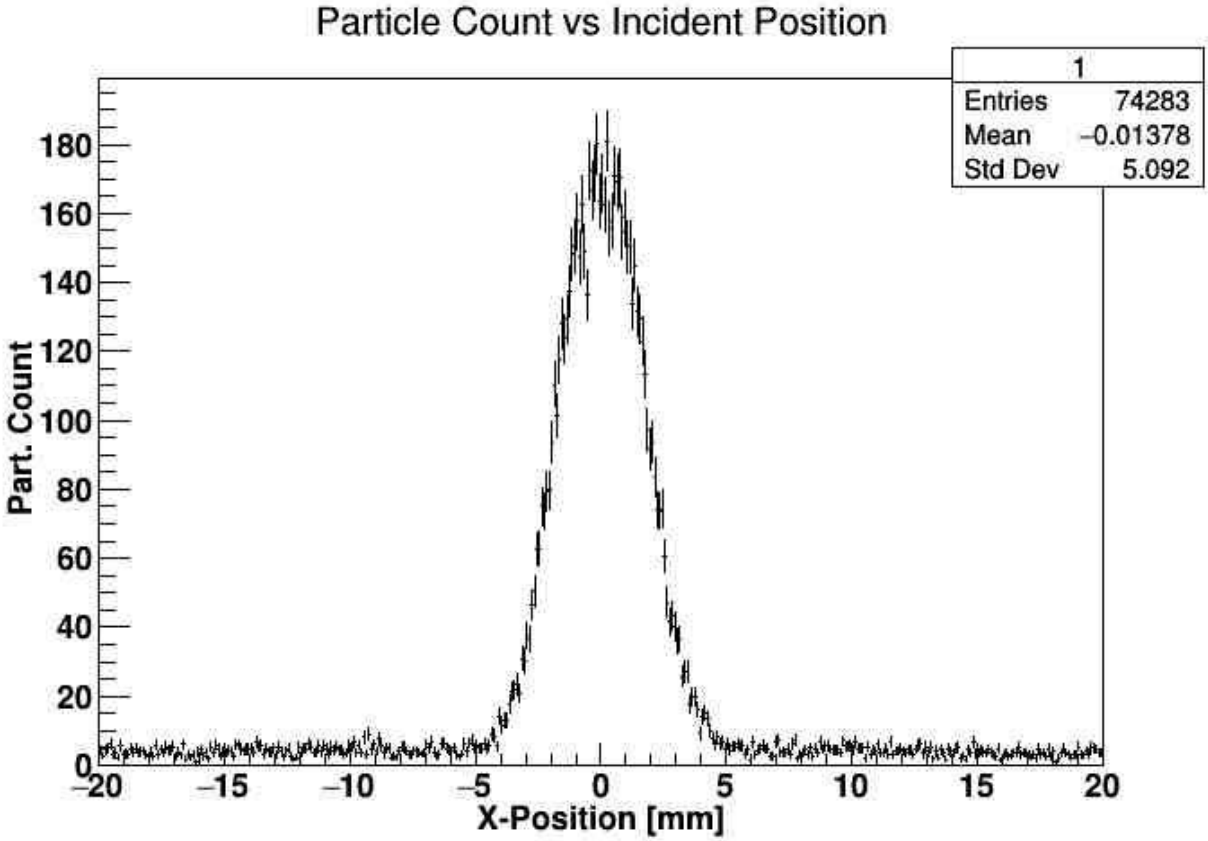

FIGURE 5.6 INCIDENT PARTICLE COUNT VS POSITION (ALONG X DIRECTION) SOURCE AT $Z = 0\ cm$ FROM THE COLLIMATOR WITH $T = 2\ mm$ AND $P = 5mm,$ E=2MEV.

total integral of histo 1: 13777.8

partial integral of histo 1 (first pitch): 6595.67

partial integral of histo 1 (until second pitch): 8019.16

partial integral of histo 1 (until third pitch): 8599.58

contrast ratio of histo 1 (first pitch):56.1913

contrast ratio of histo 1 (until second pitch):68.3186

contrast ratio of histo 1 (until third pitch):73.2635

Again, there is initial patter already seen but now in figure 5.6, it will only be mentioned that it is for a different pitch.

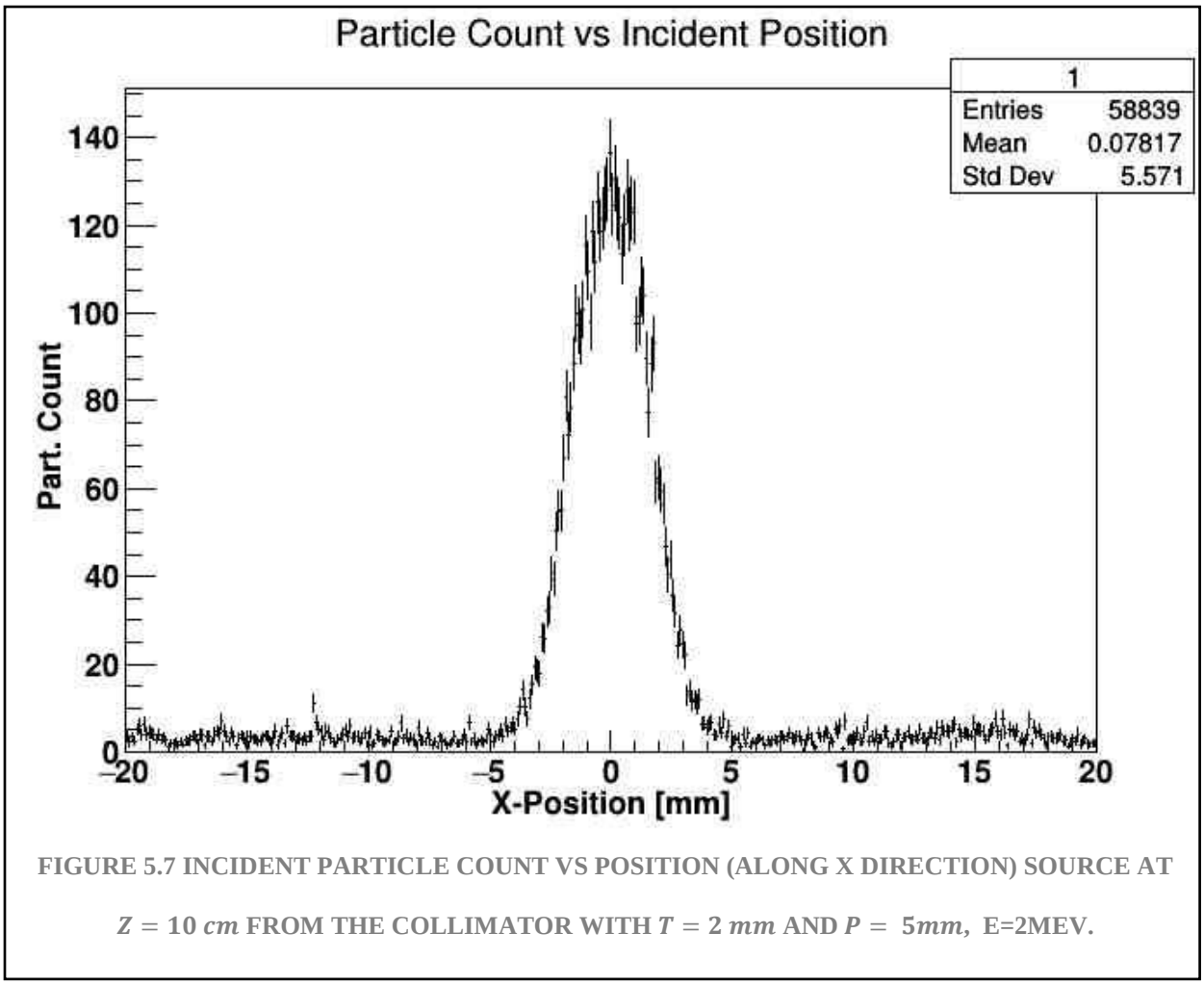

FIGURE 5.7 INCIDENT PARTICLE COUNT VS POSITION (ALONG X DIRECTION) SOURCE AT $Z = 10\ cm$ FROM THE COLLIMATOR WITH $T = 2\ mm$ AND $P = 5mm$, E=2MEV.

total integral of histo 1: 10797.7

partial integral of histo 1 (first pitch): 4718.81

partial integral of histo 1 (until second pitch): 5562.68

partial integral of histo 1 (until third pitch): 6088.26

contrast ratio of histo 1 (first pitch):45.4115

contrast ratio of histo 1 (until second pitch):53.5325

contrast ratio of histo 1 (until third pitch):58.5905

In the graph above (figure 5.7), can be seen again the noise of the second areas.

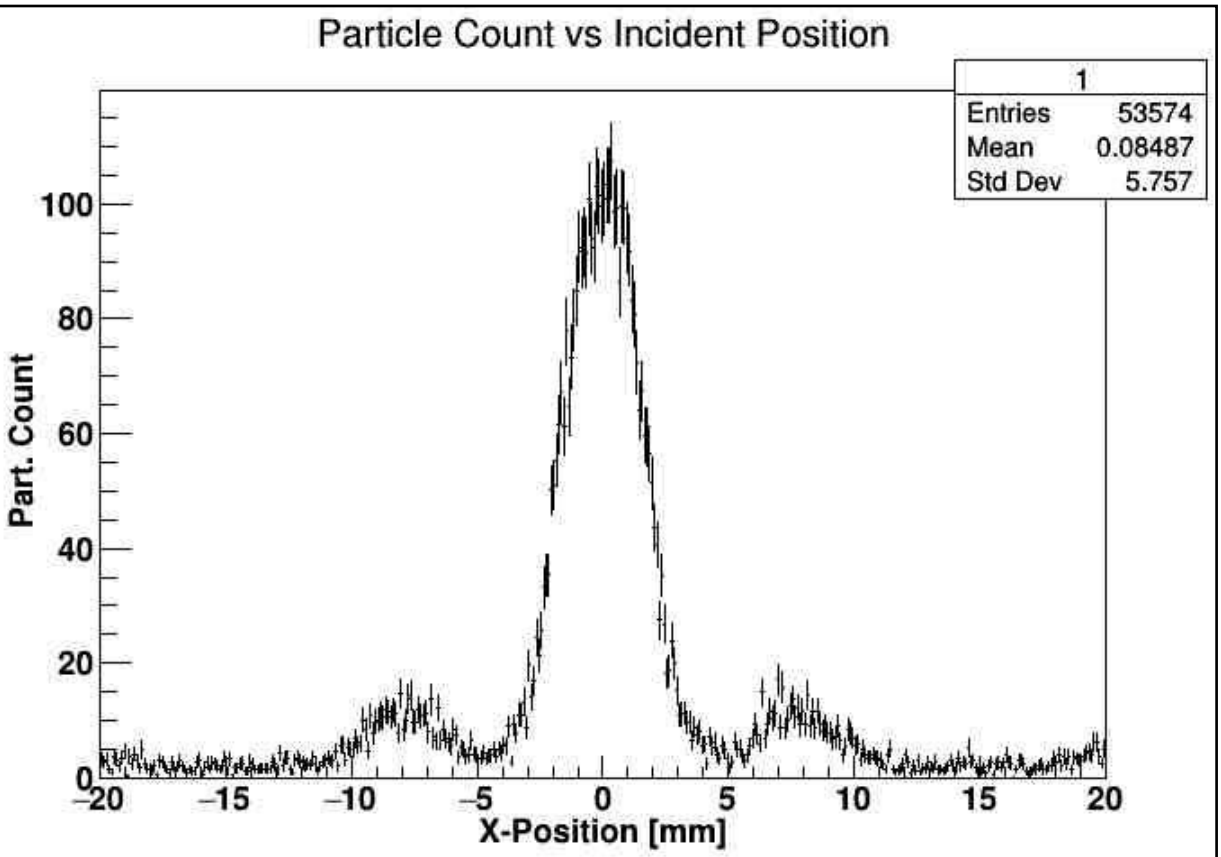

FIGURE 5.8 INCIDENT PARTICLE COUNT VS POSITION (ALONG X DIRECTION) SOURCE AT $Z = 20\ cm$ FROM THE COLLIMATOR WITH $T = 2\ mm$ AND $P = 5mm$, E=2MEV.

total integral of histo 1: 9843.17

partial integral of histo 1 (first pitch): 3691.91

partial integral of histo 1 (until second pitch): 4934.95

partial integral of histo 1 (until third pitch): 5320.98

contrast ratio of histo 1 (first pitch):37.2121

contrast ratio of histo 1 (until second pitch):49.7411

contrast ratio of histo 1 (until third pitch):53.632

Now in Figure 5.8, the signal of the second areas is defined again.

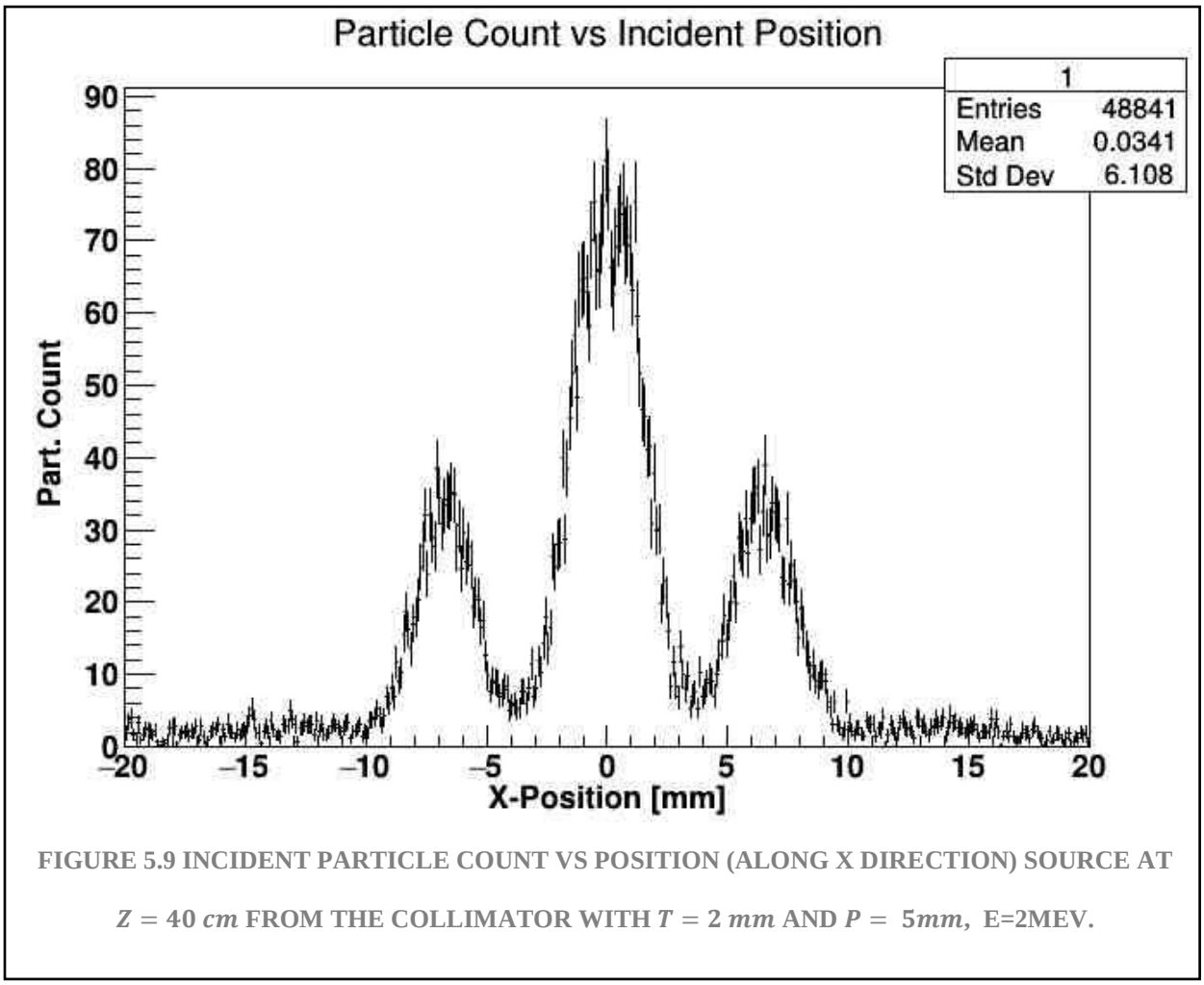

FIGURE 5.9 INCIDENT PARTICLE COUNT VS POSITION (ALONG X DIRECTION) SOURCE AT $Z = 40\ cm$ FROM THE COLLIMATOR WITH $T = 2\ mm$ AND $P = 5mm$, E=2MEV.

total integral of histo 1: 9059.54

partial integral of histo 1 (first pitch): 2604.17

partial integral of histo 1 (until second pitch): 4991.73

partial integral of histo 1 (until third pitch): 5351.68

contrast ratio of histo 1 (first pitch):27.36

contrast ratio of histo 1 (until second pitch):52.4443

contrast ratio of histo 1 (until third pitch):56.226

Figure 5.9 shows again a great signal capture in the second areas of the collimator, but with little more noise on the sides.

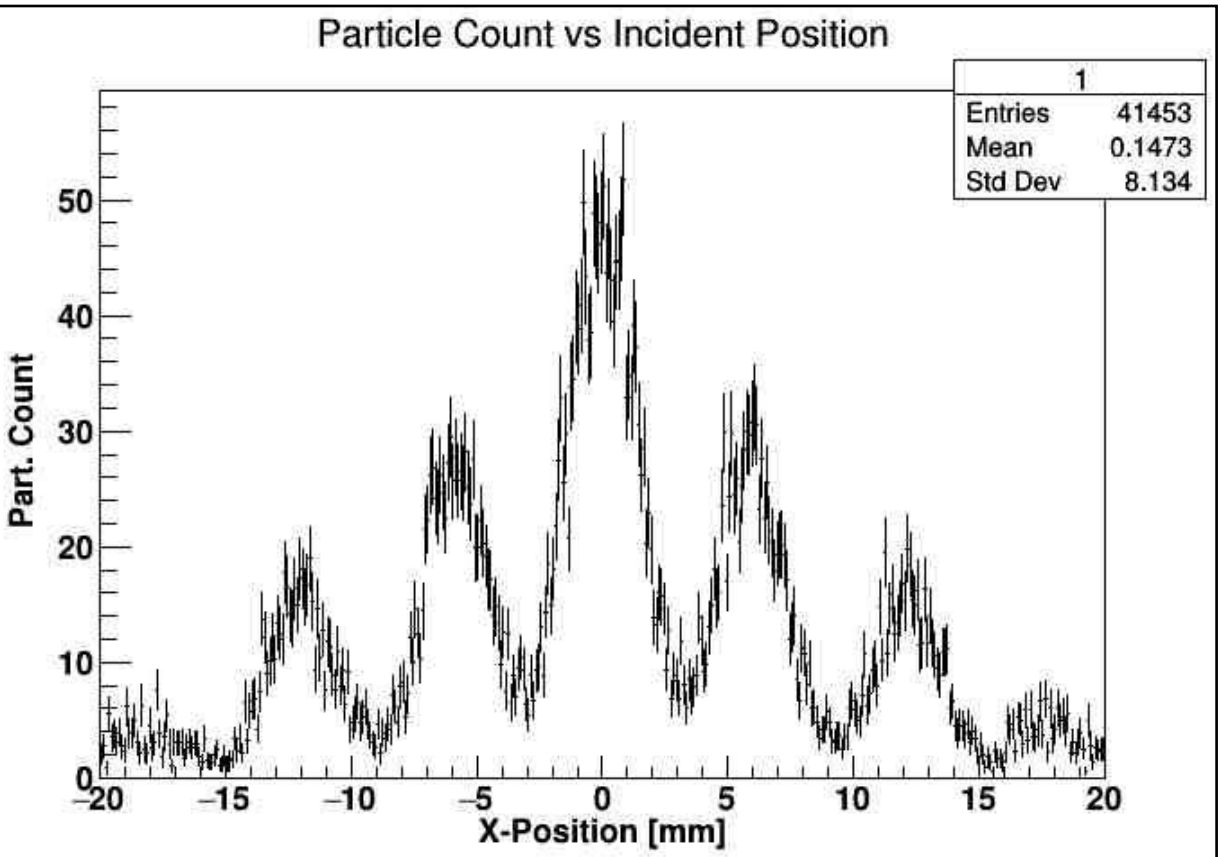

FIGURE 5.10 INCIDENT PARTICLE COUNT VS POSITION (ALONG X DIRECTION) SOURCE AT $Z = 80\ cm$ FROM THE COLLIMATOR WITH $T = 2\ mm$ AND $P = 5mm$, E=2MEV

total integral of histo 1: 7844.37

partial integral of histo 1 (first pitch): 1616.67

partial integral of histo 1 (until second pitch): 3644.25

partial integral of histo 1 (until third pitch): 4766.07

contrast ratio of histo 1 (first pitch):18.2533

contrast ratio of histo 1 (until second pitch):41.1461

contrast ratio of histo 1 (until third pitch):53.8122

As we can see, the third areas are very well defined and the increase of the fourth areas is also observed, but in our study, it will not be included.

5.1.3 SIMULATION FOR 2 MM THICKNESS AND 6 MM PITCH

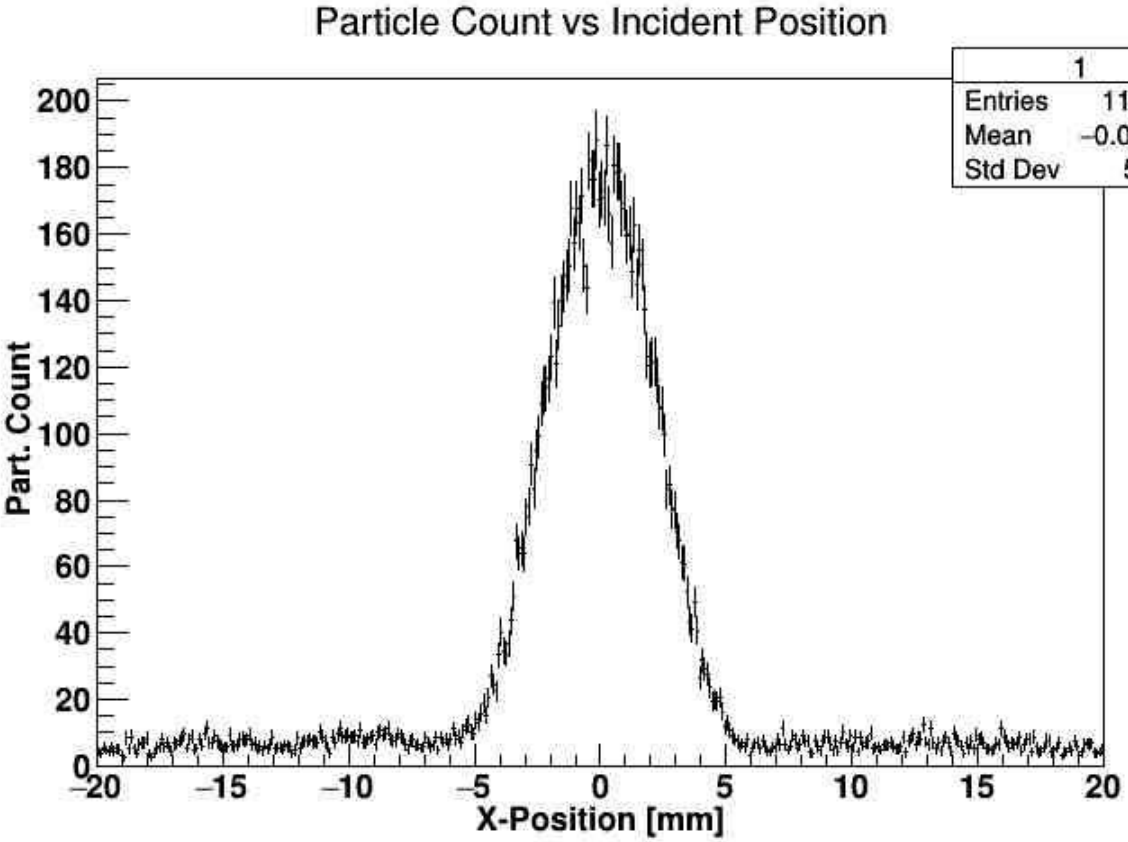

FIGURE 5.11 INCIDENT PARTICLE COUNT VS POSITION (ALONG X DIRECTION) SOURCE AT $Z = 0\ cm$ FROM THE COLLIMATOR WITH $T = 2\ mm$ AND $P = 6mm$, E=2MEV.

total integral of histo 1: 20607.5

partial integral of histo 1 (first pitch): 8341.5

partial integral of histo 1 (until second pitch): 10634.4

partial integral of histo 1 (until third pitch): 11692.3

contrast ratio of histo 1 (first pitch):58.1074

contrast ratio of histo 1 (until second pitch):74.0795

contrast ratio of histo 1 (until third pitch):81.4493

In Figure 5.11, it is again the well-defined peak at the center, which seems slightly wider.

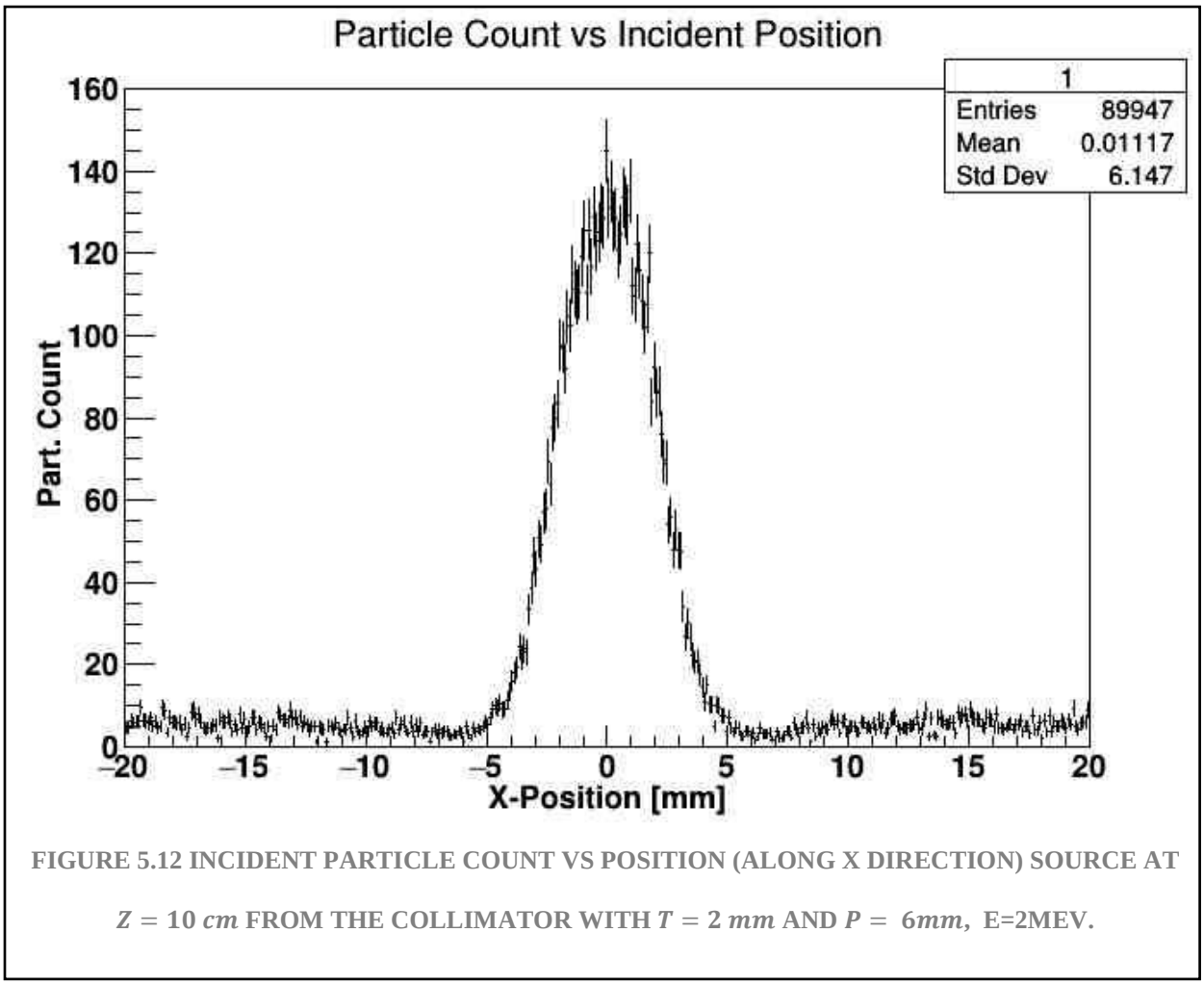

FIGURE 5.12 INCIDENT PARTICLE COUNT VS POSITION (ALONG X DIRECTION) SOURCE AT $Z = 10\ cm$ FROM THE COLLIMATOR WITH $T = 2\ mm$ AND $P = 6mm$, E=2MEV.

total integral of histo 1: 16328.1

partial integral of histo 1 (first pitch): 6015.68

partial integral of histo 1 (until second pitch): 7178.03

partial integral of histo 1 (until third pitch): 8059.87

contrast ratio of histo 1 (first pitch):47.0779

contrast ratio of histo 1 (until second pitch):56.1743

contrast ratio of histo 1 (until third pitch):63.0754

In Figure 5.12, it is seen again that the second areas increase but at a lower rate of change.

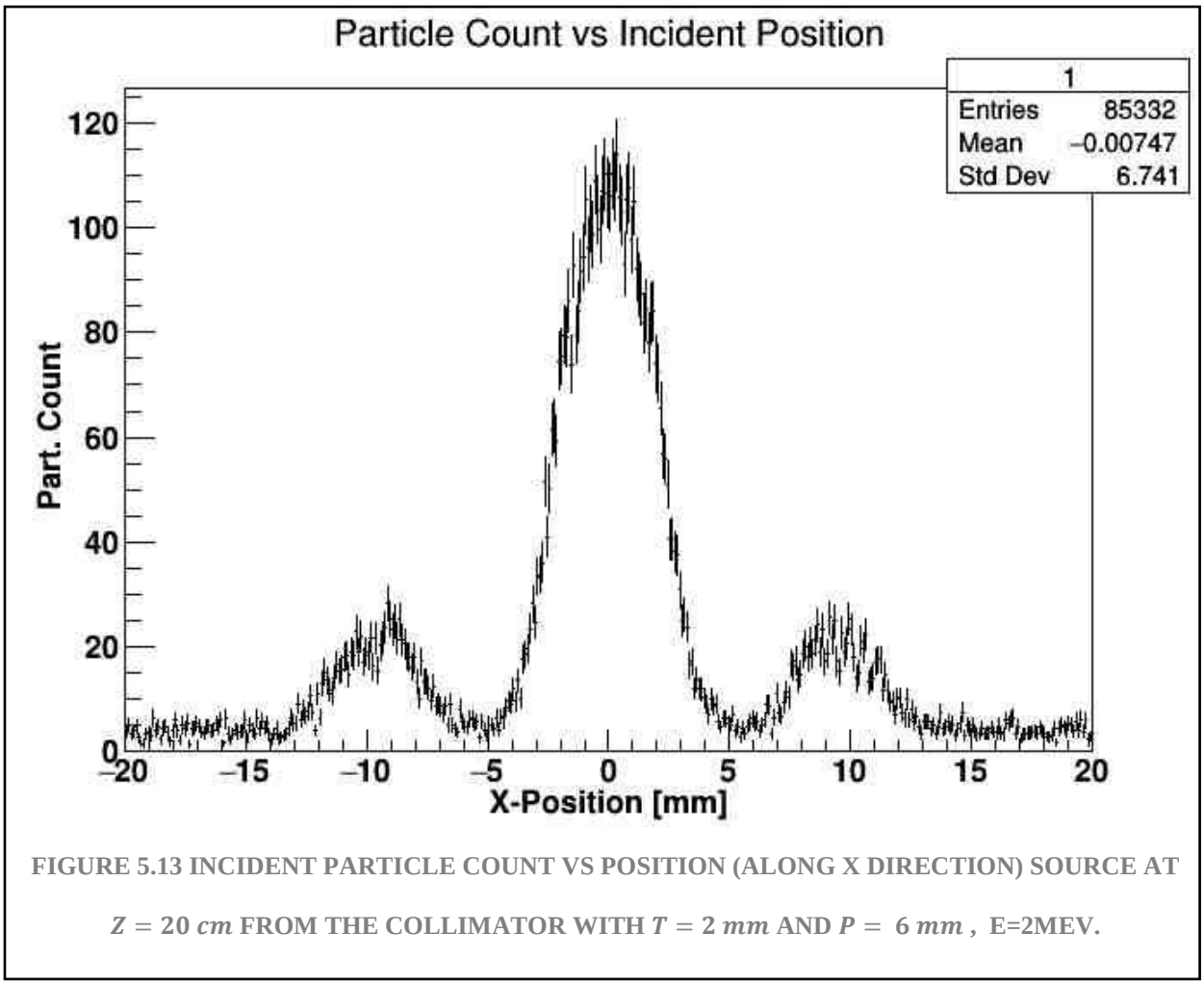

FIGURE 5.13 INCIDENT PARTICLE COUNT VS POSITION (ALONG X DIRECTION) SOURCE AT $Z = 20\ cm$ FROM THE COLLIMATOR WITH $T = 2\ mm$ AND $P = 6\ mm$, E=2MEV.

total integral of histo 1: 15517.1

partial integral of histo 1 (first pitch): 4803.65

partial integral of histo 1 (until second pitch): 6929.35

partial integral of histo 1 (until third pitch): 7812.47

contrast ratio of histo 1 (first pitch):38.5626

contrast ratio of histo 1 (until second pitch):55.6272

contrast ratio of histo 1 (until third pitch):62.7167

In Figure 5.13 shows the same pattern that we have seen, but with noise at the sides.

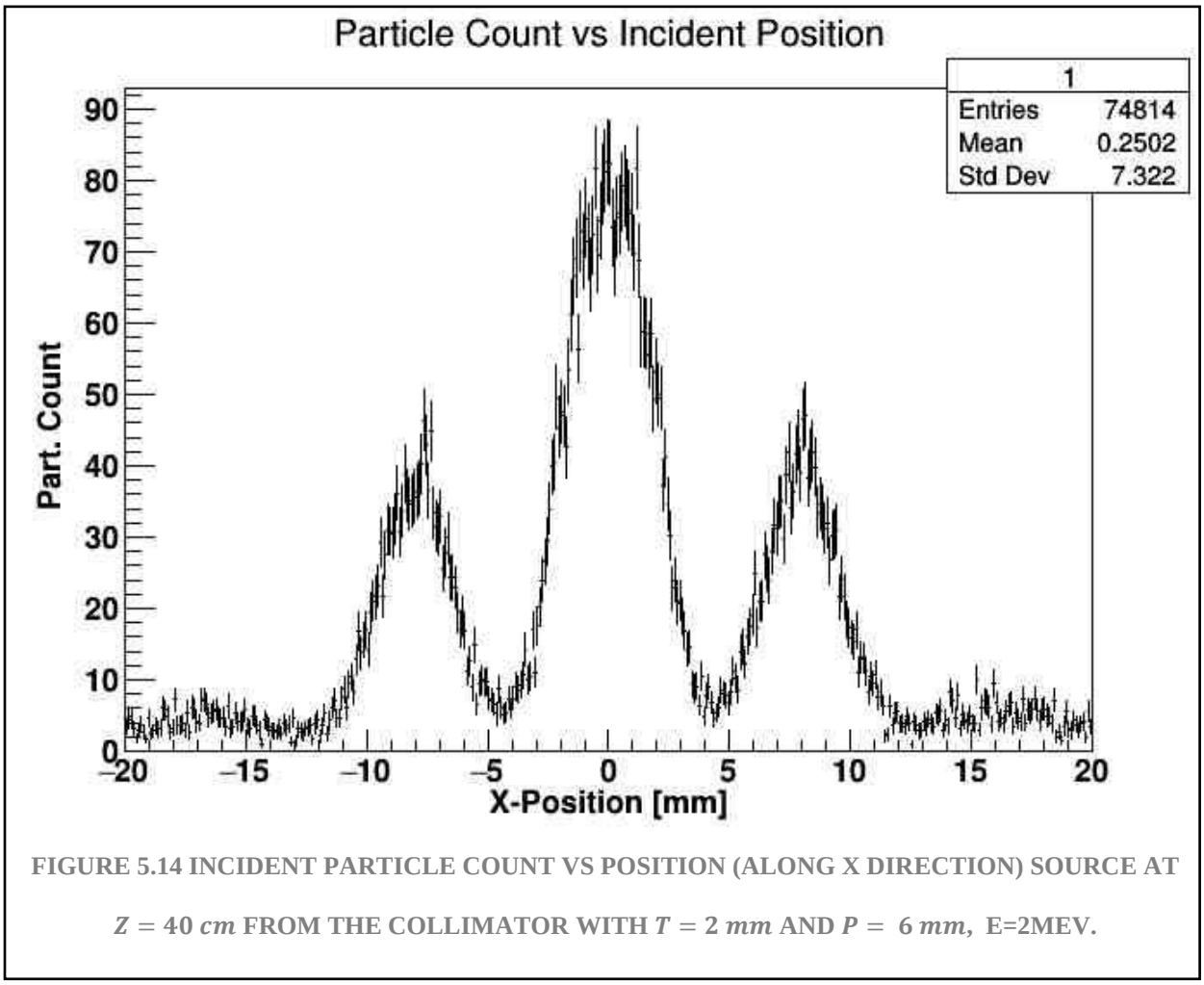

FIGURE 5.14 INCIDENT PARTICLE COUNT VS POSITION (ALONG X DIRECTION) SOURCE AT $Z = 40\ cm$ FROM THE COLLIMATOR WITH $T = 2\ mm$ AND $P = 6\ mm$, E=2MEV.

total integral of histo 1: 13839.1

partial integral of histo 1 (first pitch): 3385.21

partial integral of histo 1 (until second pitch): 6699.22

partial integral of histo 1 (until third pitch): 7420.65

contrast ratio of histo 1 (first pitch):28.7761

contrast ratio of histo 1 (until second pitch):56.9469

contrast ratio of histo 1 (until third pitch):63.0794

In Figure 5.14, same pattern and with noise at the sides, apparently also looks slightly wider than the previous graphs for the distance of 40 cm.

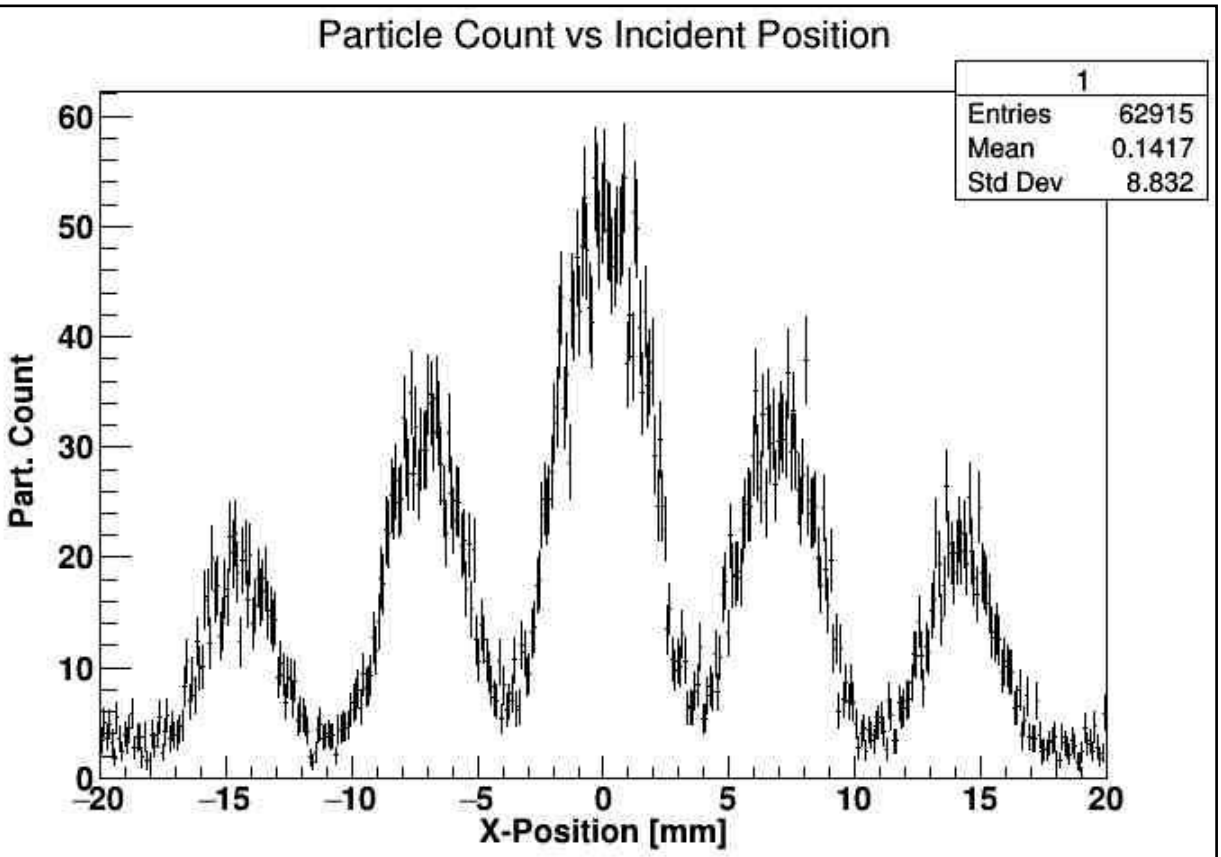

FIGURE 5.15 INCIDENT PARTICLE COUNT VS POSITION (ALONG X DIRECTION) SOURCE AT $Z = 80\ cm$ FROM THE COLLIMATOR WITH $T = 2\ mm$ AND $P = 6\ mm$, E=2MEV.

total integral of histo 1: 11750.6

partial integral of histo 1 (first pitch): 2158.84

partial integral of histo 1 (until second pitch): 4878.09

partial integral of histo 1 (until third pitch): 6475.51

contrast ratio of histo 1 (first pitch):19.9155

contrast ratio of histo 1 (until second pitch):45.0007

contrast ratio of histo 1 (until third pitch):59.7371

In Figure 5.15, same pattern but now it is definitely wider compared to the last graphs of 40 cm, compared to the pitch graph of 5 mm at least.

5.1.4 SIMULATION FOR 2 MM THICKNESS AND 3 MM PITCH

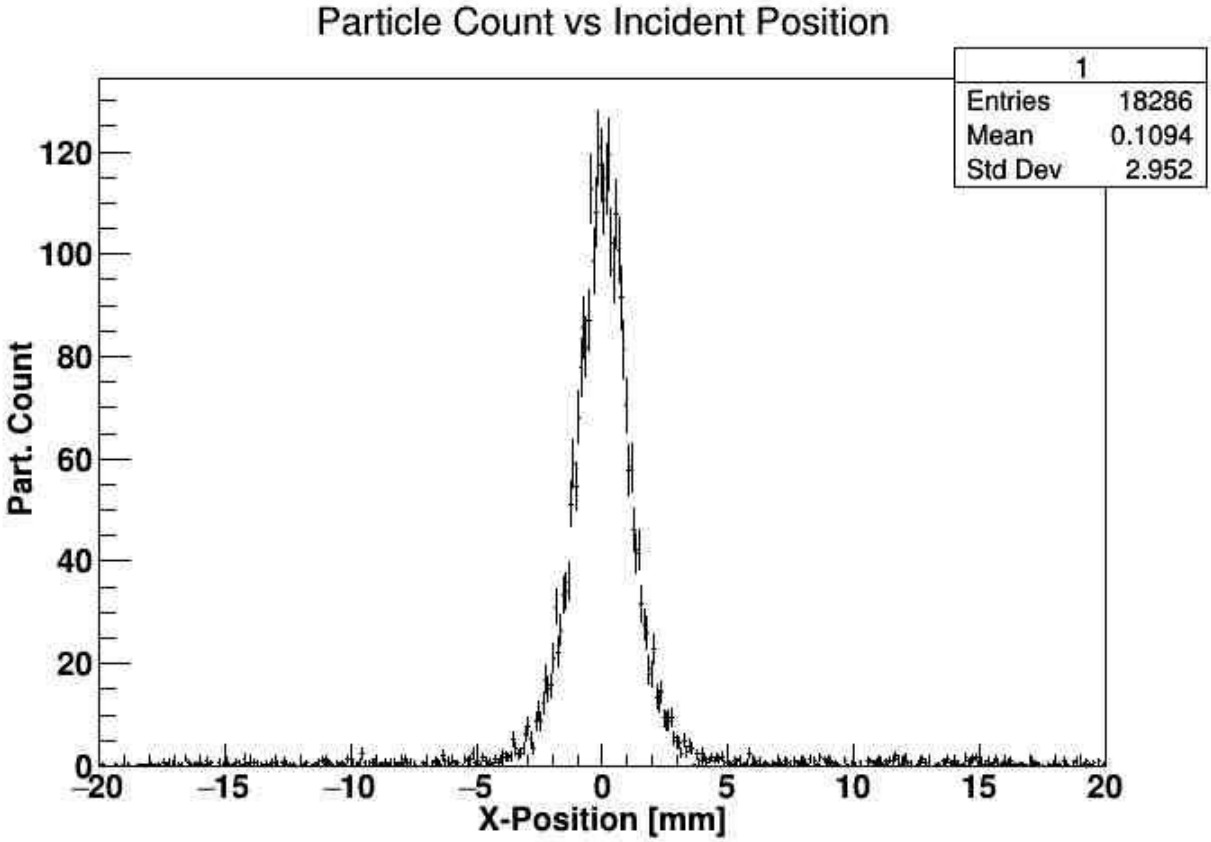

FIGURE 5.16 INCIDENT PARTICLE COUNT VS POSITION (ALONG X DIRECTION) SOURCE AT $Z = 0\ cm$ FROM THE COLLIMATOR WITH $T = 2\ mm$ AND $P = 3\ mm$, E=2MEV.

total integral of histo 1: 3597.91

partial integral of histo 1 (first pitch): 2470.18

partial integral of histo 1 (until second pitch): 3016.41

partial integral of histo 1 (until third pitch): 3073.62

contrast ratio of histo 1 (first pitch):41.1817

contrast ratio of histo 1 (until second pitch):50.2882

contrast ratio of histo 1 (until third pitch):51.2419

In Figure 5.16, a thin peak was obtained, given the pitch of 3 mm.

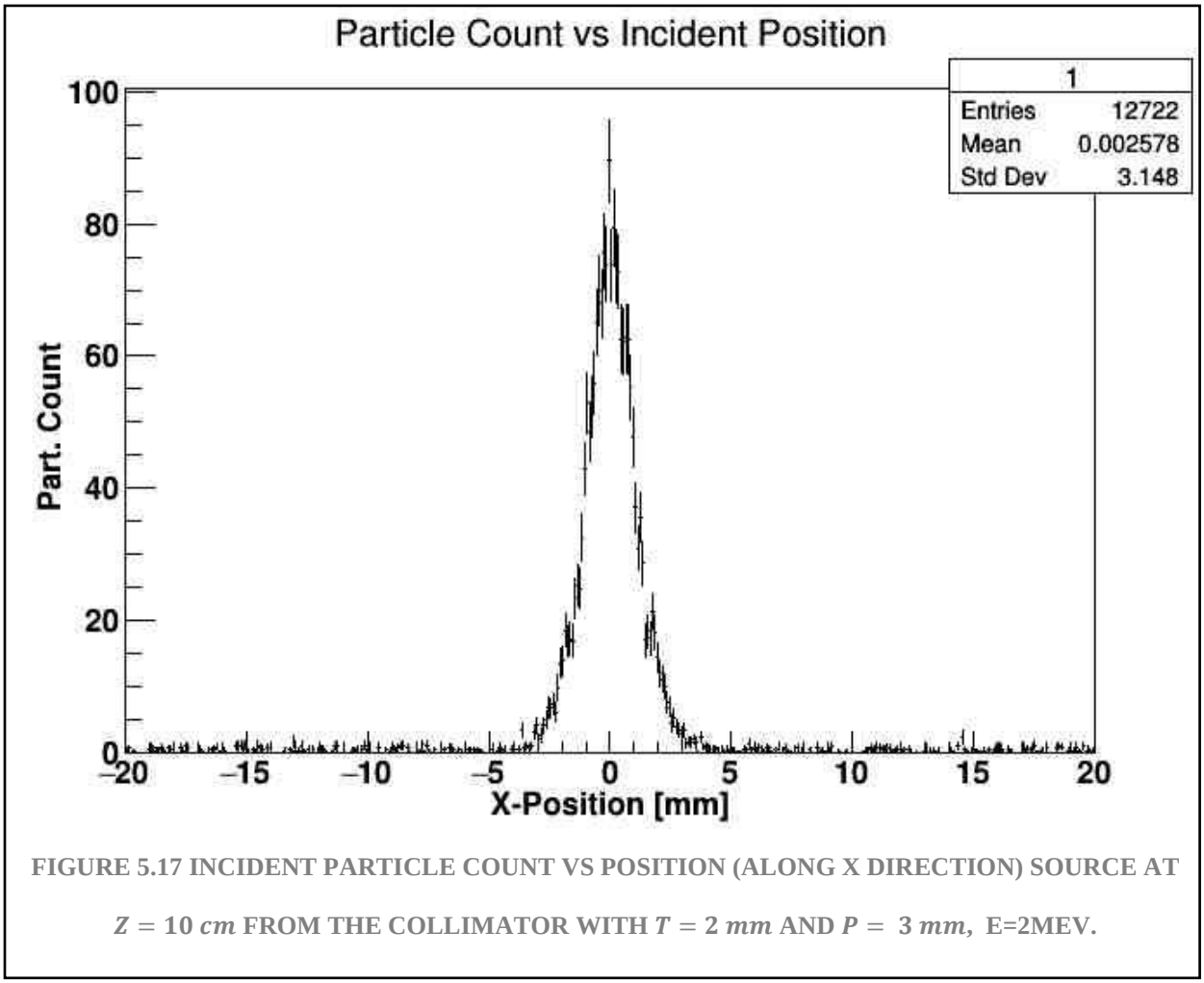

FIGURE 5.17 INCIDENT PARTICLE COUNT VS POSITION (ALONG X DIRECTION) SOURCE AT $Z = 10\ cm$ FROM THE COLLIMATOR WITH $T = 2\ mm$ AND $P = 3\ mm$, E=2MEV.

total integral of histo 1: 2456.39

partial integral of histo 1 (first pitch): 1619.41

partial integral of histo 1 (until second pitch): 1958.43

partial integral of histo 1 (until third pitch): 1989.54

contrast ratio of histo 1 (first pitch):32.6744

contrast ratio of histo 1 (until second pitch):39.5148

contrast ratio of histo 1 (until third pitch):40.1425

In Figure 5.17, there is no clue of the second areas yet.

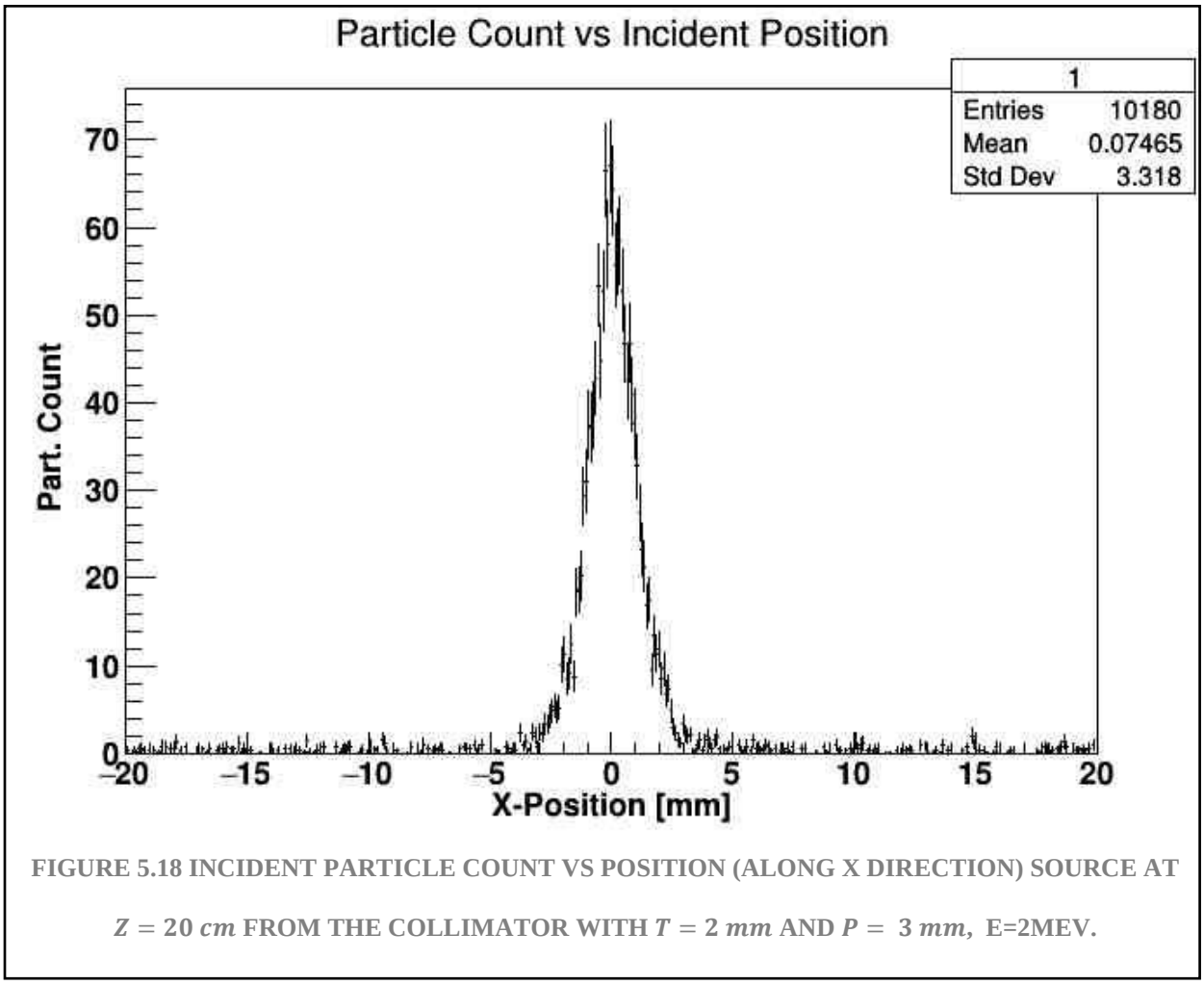

FIGURE 5.18 INCIDENT PARTICLE COUNT VS POSITION (ALONG X DIRECTION) SOURCE AT $Z = 20\ cm$ FROM THE COLLIMATOR WITH $T = 2\ mm$ AND $P = 3\ mm$, E=2MEV.

total integral of histo 1: 1970.04

partial integral of histo 1 (first pitch): 1249.84

partial integral of histo 1 (until second pitch): 1498.99

partial integral of histo 1 (until third pitch): 1528.67

contrast ratio of histo 1 (first pitch):28.1589

contrast ratio of histo 1 (until second pitch):33.7723

contrast ratio of histo 1 (until third pitch):34.441

In Figure 5.18, again the graph doesn't show any hint of the signal in the second areas, although still looks narrow and smaller the gamma signal at the center.

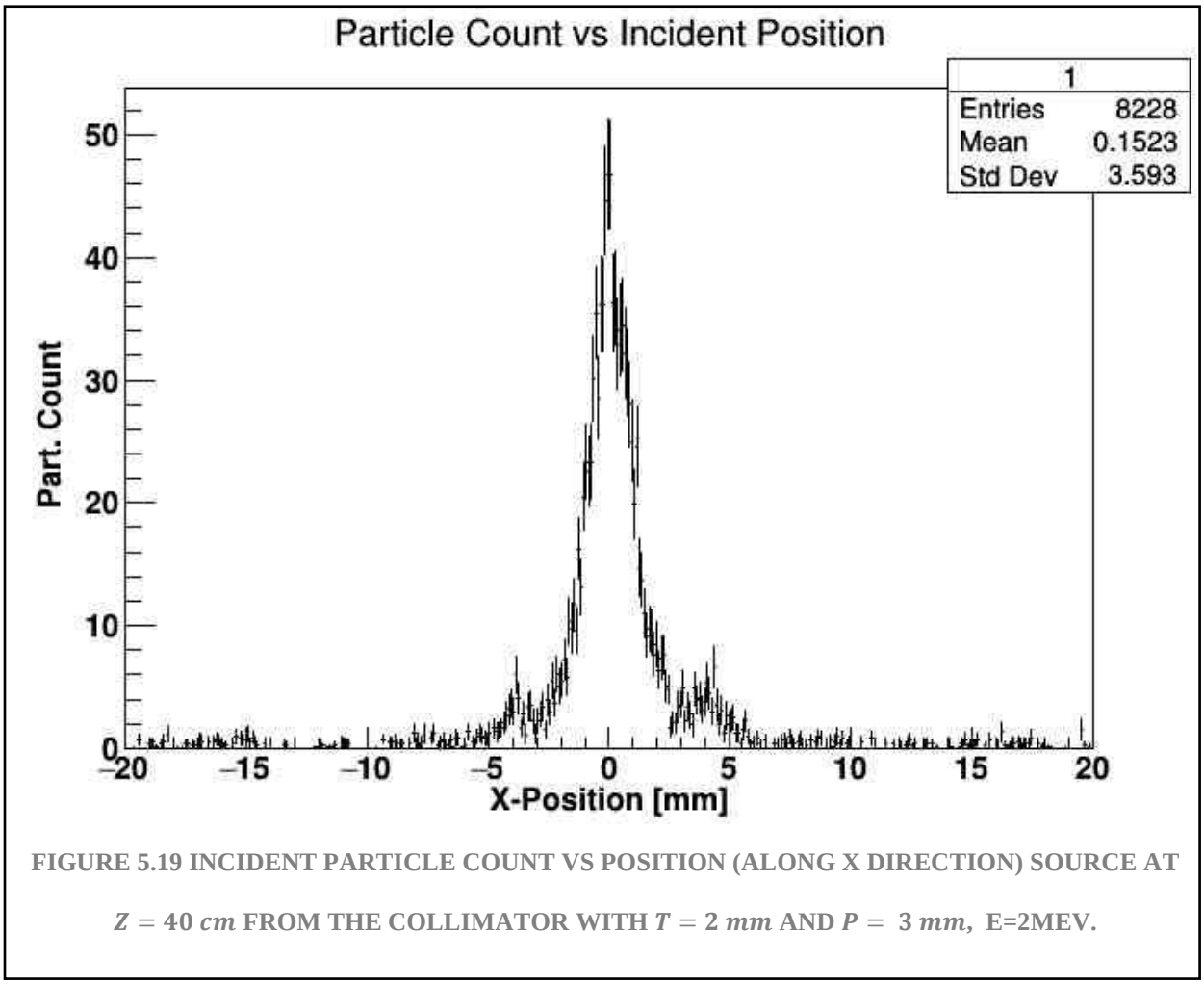

FIGURE 5.19 INCIDENT PARTICLE COUNT VS POSITION (ALONG X DIRECTION) SOURCE AT $Z = 40\ cm$ FROM THE COLLIMATOR WITH $T = 2\ mm$ AND $P = 3\ mm$, E=2MEV.

total integral of histo 1: 1545.66

partial integral of histo 1 (first pitch): 829.172

partial integral of histo 1 (until second pitch): 1126.73

partial integral of histo 1 (until third pitch): 1155.88

contrast ratio of histo 1 (first pitch):21.0905

contrast ratio of histo 1 (until second pitch):28.6591

contrast ratio of histo 1 (until third pitch):29.4006

In Figure 5.19, now it is increasing the signal in the second areas, and as expected, in a shorter range.

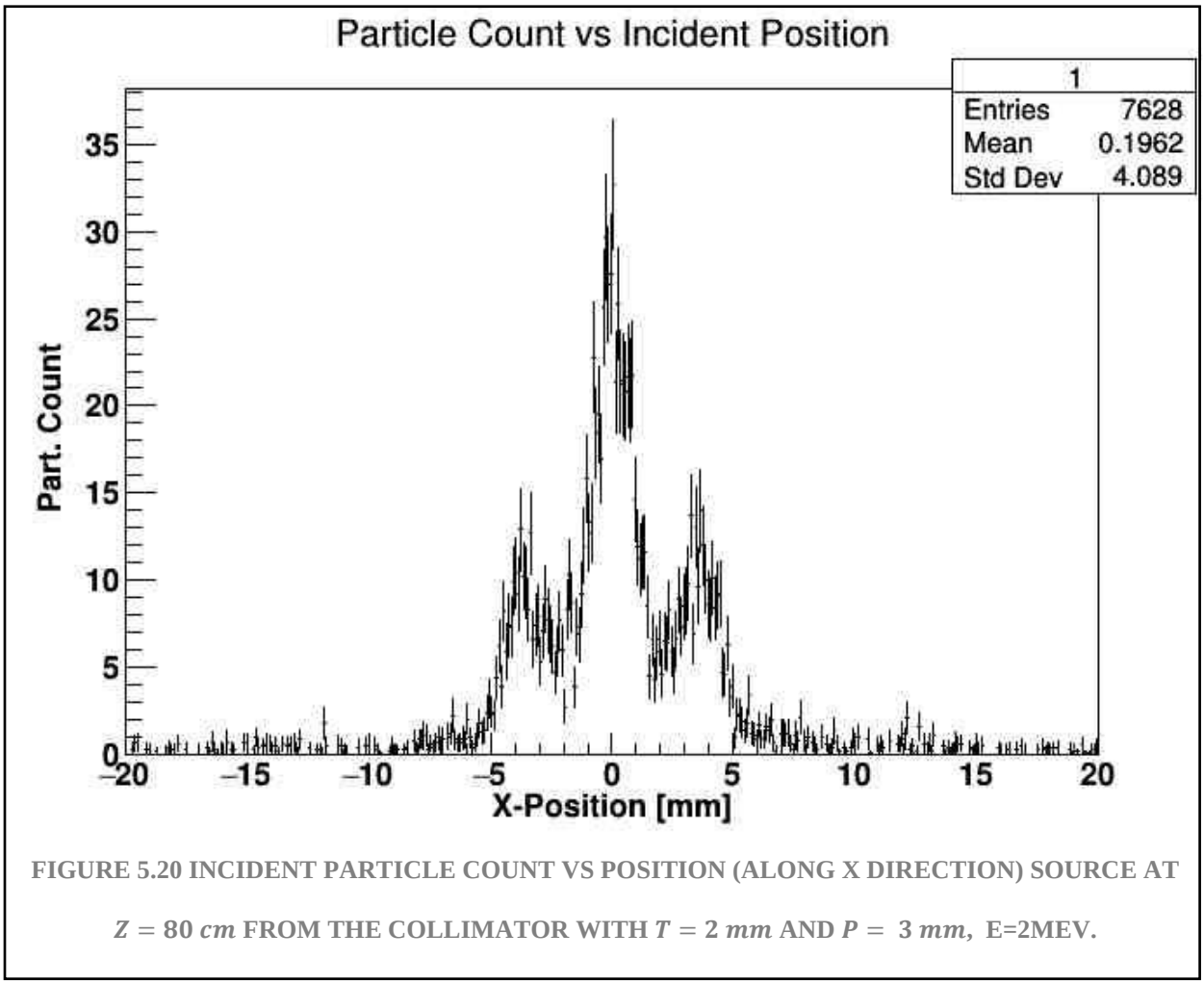

FIGURE 5.20 INCIDENT PARTICLE COUNT VS POSITION (ALONG X DIRECTION) SOURCE AT $Z = 80\ cm$ FROM THE COLLIMATOR WITH $T = 2\ mm$ AND $P = 3\ mm$, E=2MEV.

total integral of histo 1: 1479.37

partial integral of histo 1 (first pitch): 545.79

partial integral of histo 1 (until second pitch): 1111.1

partial integral of histo 1 (until third pitch): 1154.73

contrast ratio of histo 1 (first pitch):14.1902

contrast ratio of histo 1 (until second pitch):28.8879

contrast ratio of histo 1 (until third pitch):30.0222

In Figure 5.20 is a notorious signal captured at the second areas and some noise beside those areas.

5.2 RESULTS CHANGING THICKNESS 2 MEV ENERGY

5.2.1 SIMULATION FOR 4 MM PITCH AND 1 MM THICKNESS

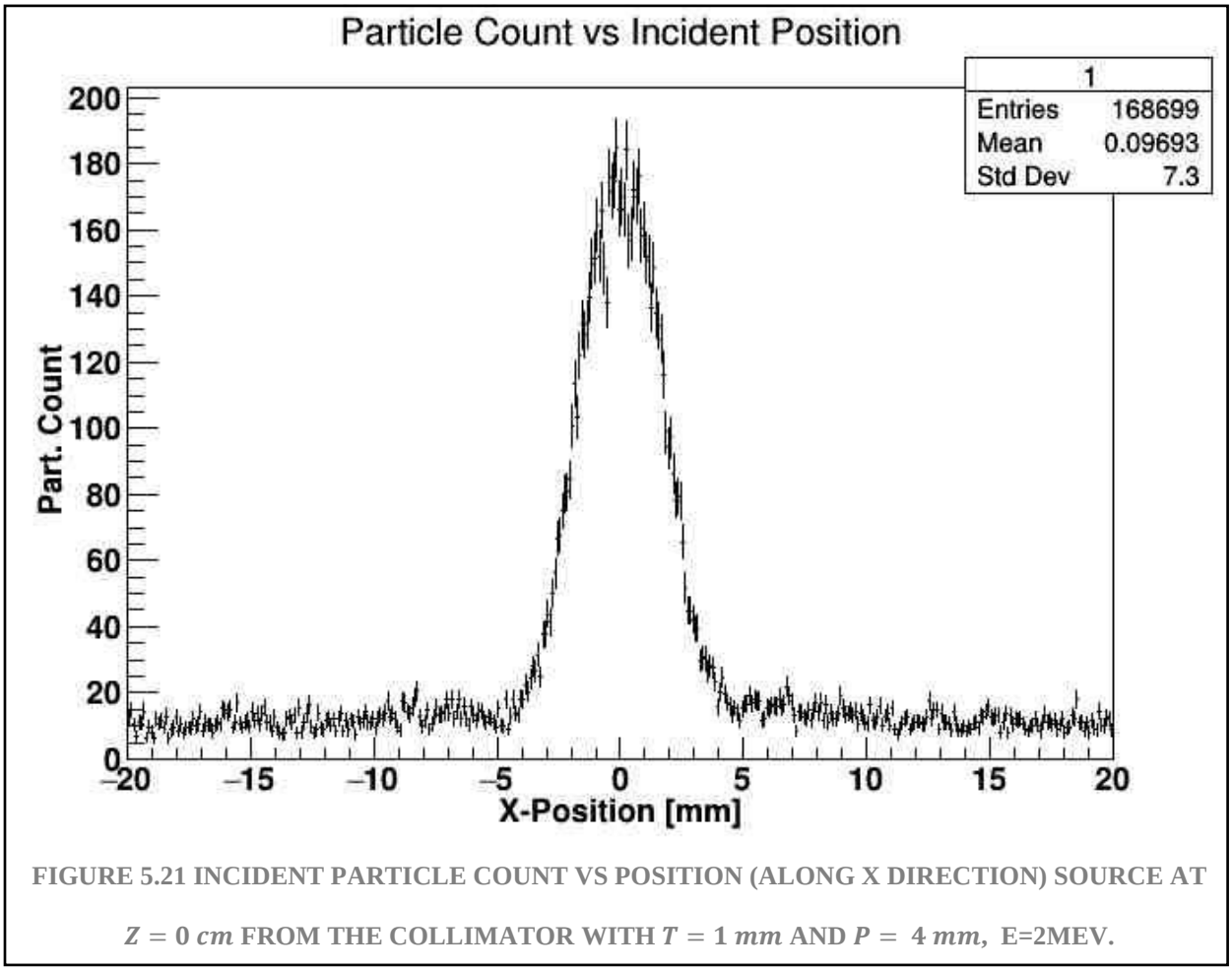

FIGURE 5.21 INCIDENT PARTICLE COUNT VS POSITION (ALONG X DIRECTION) SOURCE AT $Z = 0\ cm$ FROM THE COLLIMATOR WITH $T = 1\ mm$ AND $P = 4\ mm$, E=2MEV.

total integral of histo 1: 30108.4

partial integral of histo 1 (first pitch): 5956.85

partial integral of histo 1 (until second pitch): 8675

partial integral of histo 1 (until third pitch): 9941.11

contrast ratio of histo 1 (first pitch):34.3299

contrast ratio of histo 1 (until second pitch):49.9949

contrast ratio of histo 1 (until third pitch):57.2916

In Figure 5.21, it has a thickness of 1 mm in the collimator, which implies that more signal will be captured (as it appears in the graph, given the base height it has in the gamma count).

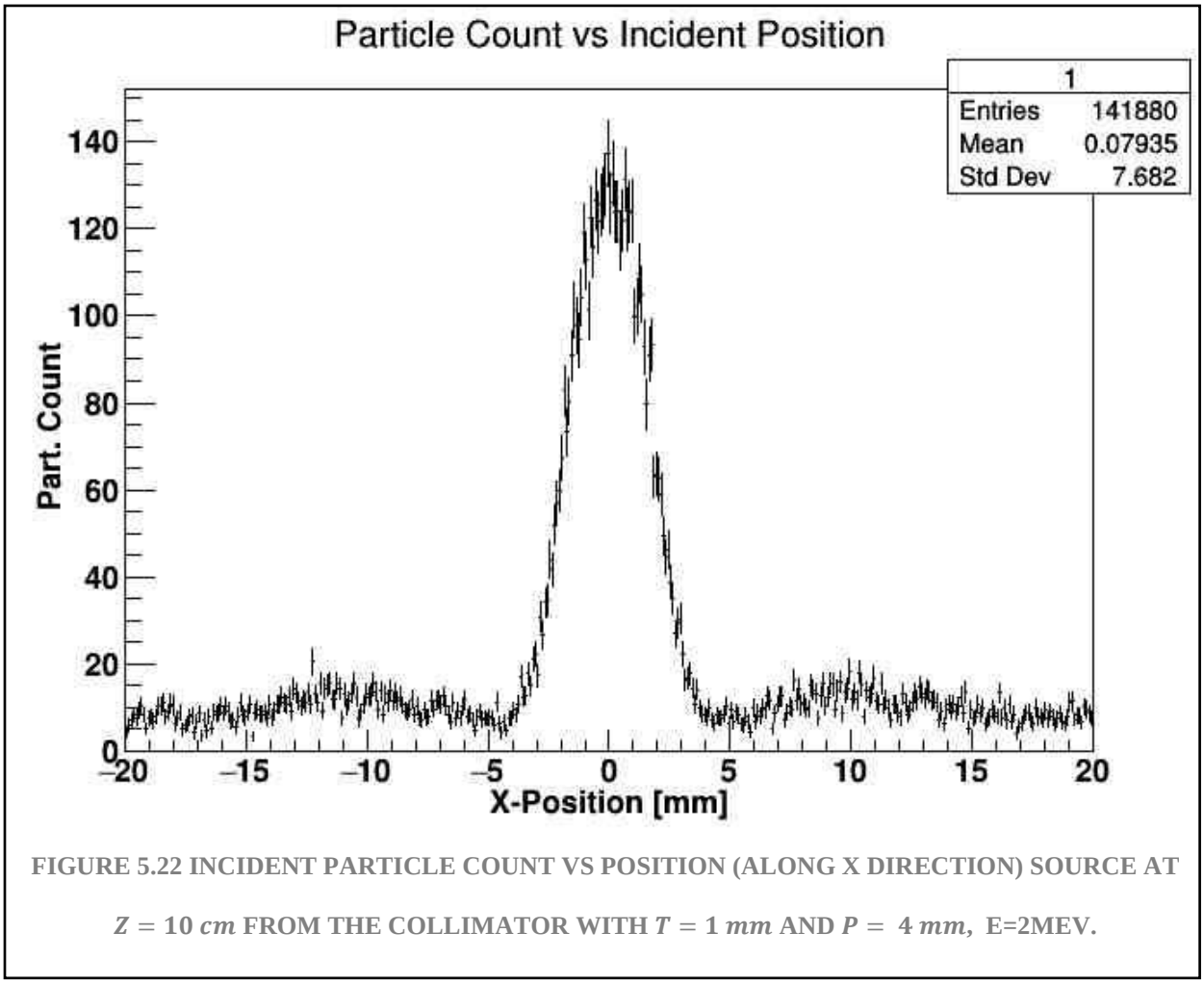

FIGURE 5.22 INCIDENT PARTICLE COUNT VS POSITION (ALONG X DIRECTION) SOURCE AT $Z = 10\ cm$ FROM THE COLLIMATOR WITH $T = 1\ mm$ AND $P = 4\ mm$, E=2MEV.

total integral of histo 1: 25308.4

partial integral of histo 1 (first pitch): 4340.54

partial integral of histo 1 (until second pitch): 5889.89

partial integral of histo 1 (until third pitch): 7076.98

contrast ratio of histo 1 (first pitch):27.2843

contrast ratio of histo 1 (until second pitch):37.0233

contrast ratio of histo 1 (until third pitch):44.4853

In Figure 5.22 there is not much information to mention, because apparently, it is increasing the second areas, but with another different pattern to those already seen.

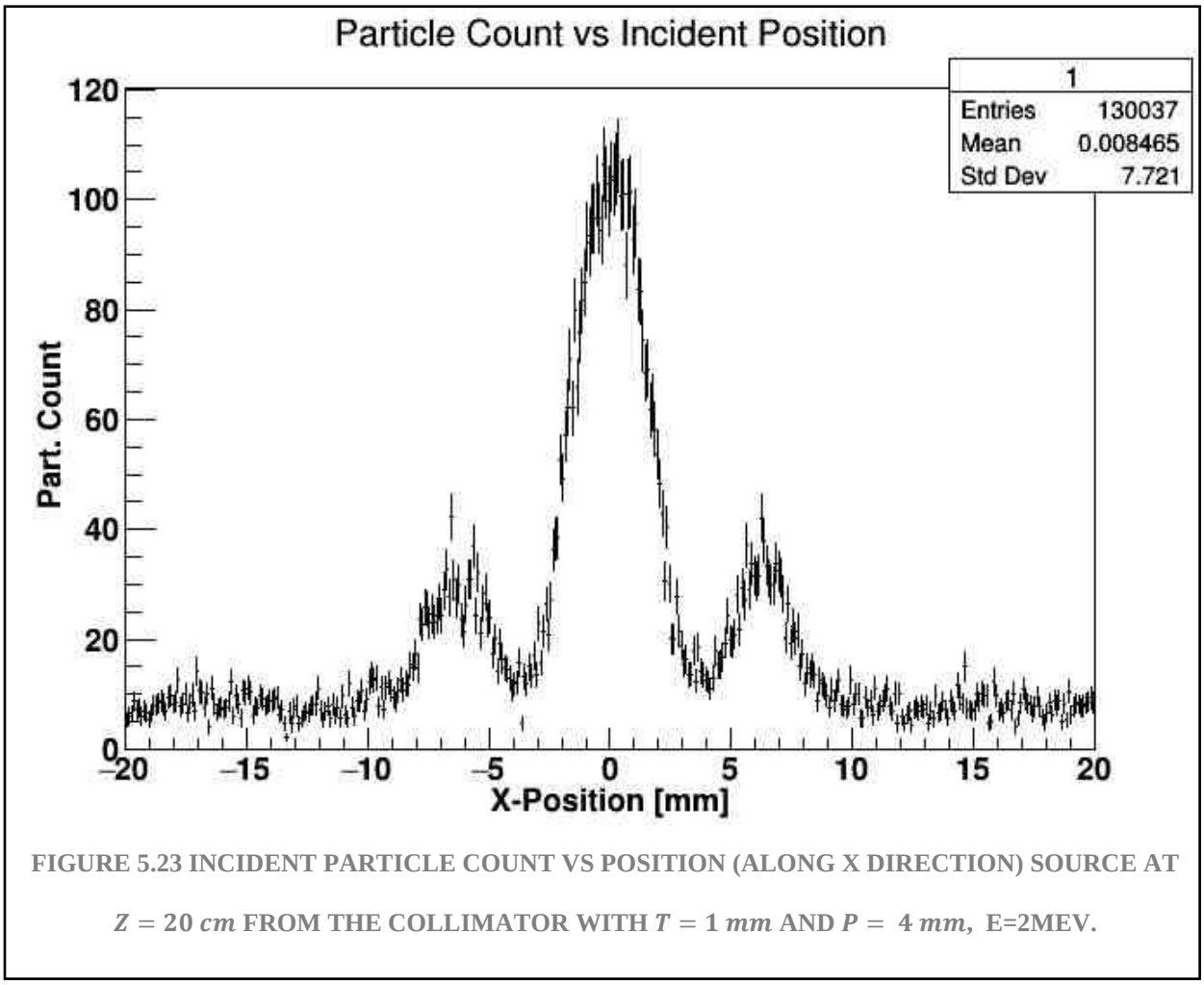

FIGURE 5.23 INCIDENT PARTICLE COUNT VS POSITION (ALONG X DIRECTION) SOURCE AT $Z = 20\ cm$ FROM THE COLLIMATOR WITH $T = 1\ mm$ AND $P = 4\ mm$, E=2MEV.

total integral of histo 1: 23230

partial integral of histo 1 (first pitch): 3439.87

partial integral of histo 1 (until second pitch): 5802.6

partial integral of histo 1 (until third pitch): 7013.54

contrast ratio of histo 1 (first pitch):22.5693

contrast ratio of histo 1 (until second pitch):38.0713

contrast ratio of histo 1 (until third pitch):46.0163

In Figure 5.23 can be seen the signal of the second areas and some increase next to those signals.

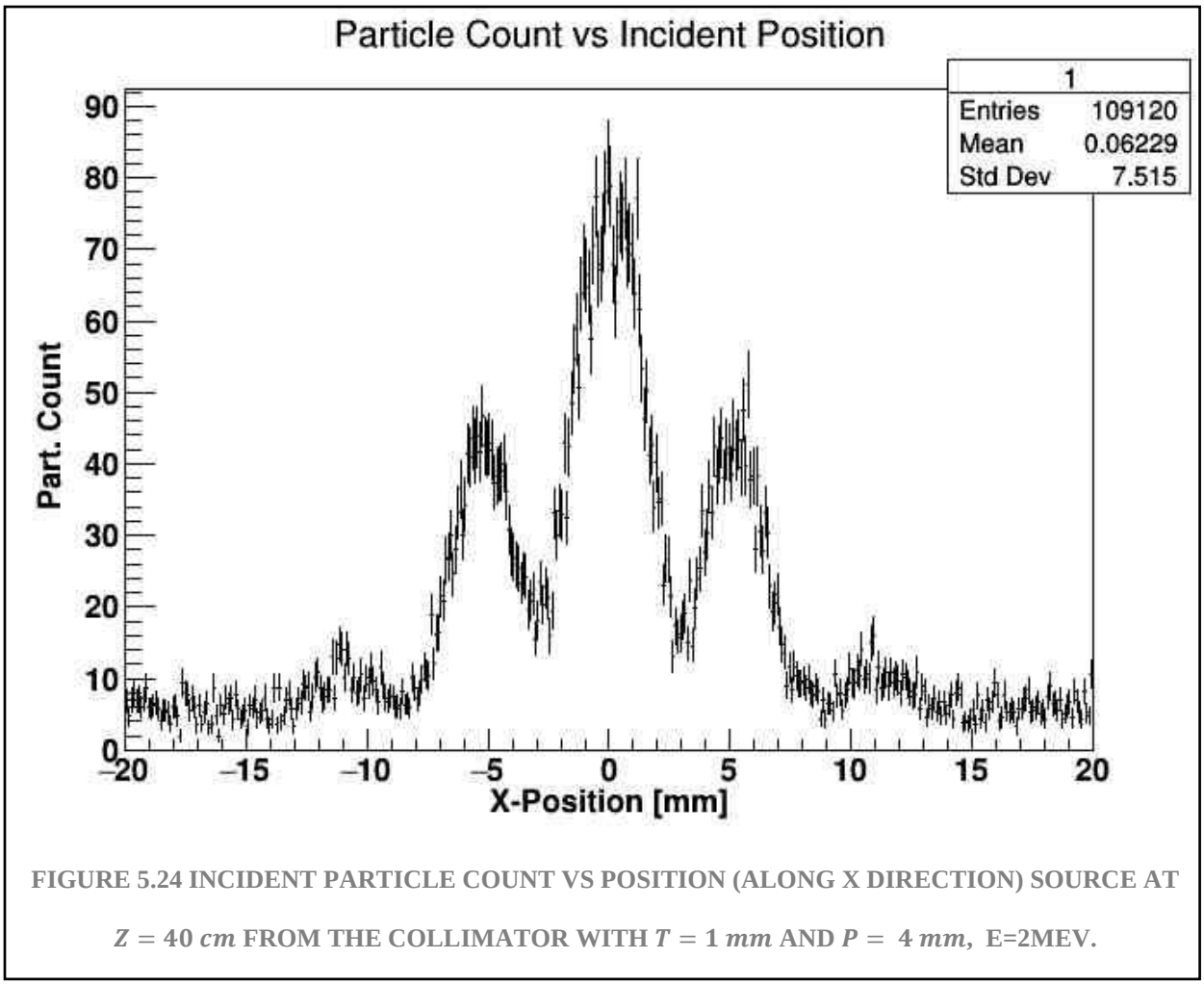

FIGURE 5.24 INCIDENT PARTICLE COUNT VS POSITION (ALONG X DIRECTION) SOURCE AT $Z = 40\ cm$ FROM THE COLLIMATOR WITH $T = 1\ mm$ AND $P = 4\ mm$, E=2MEV.

total integral of histo 1: 19842.1

partial integral of histo 1 (first pitch): 2460.34

partial integral of histo 1 (until second pitch): 5515.01

partial integral of histo 1 (until third pitch): 6476.91

contrast ratio of histo 1 (first pitch):17.4663

contrast ratio of histo 1 (until second pitch):39.1518

contrast ratio of histo 1 (until third pitch):45.9805

In Figure 5.24 are defined the three signals of interest previously seen at different ranges.

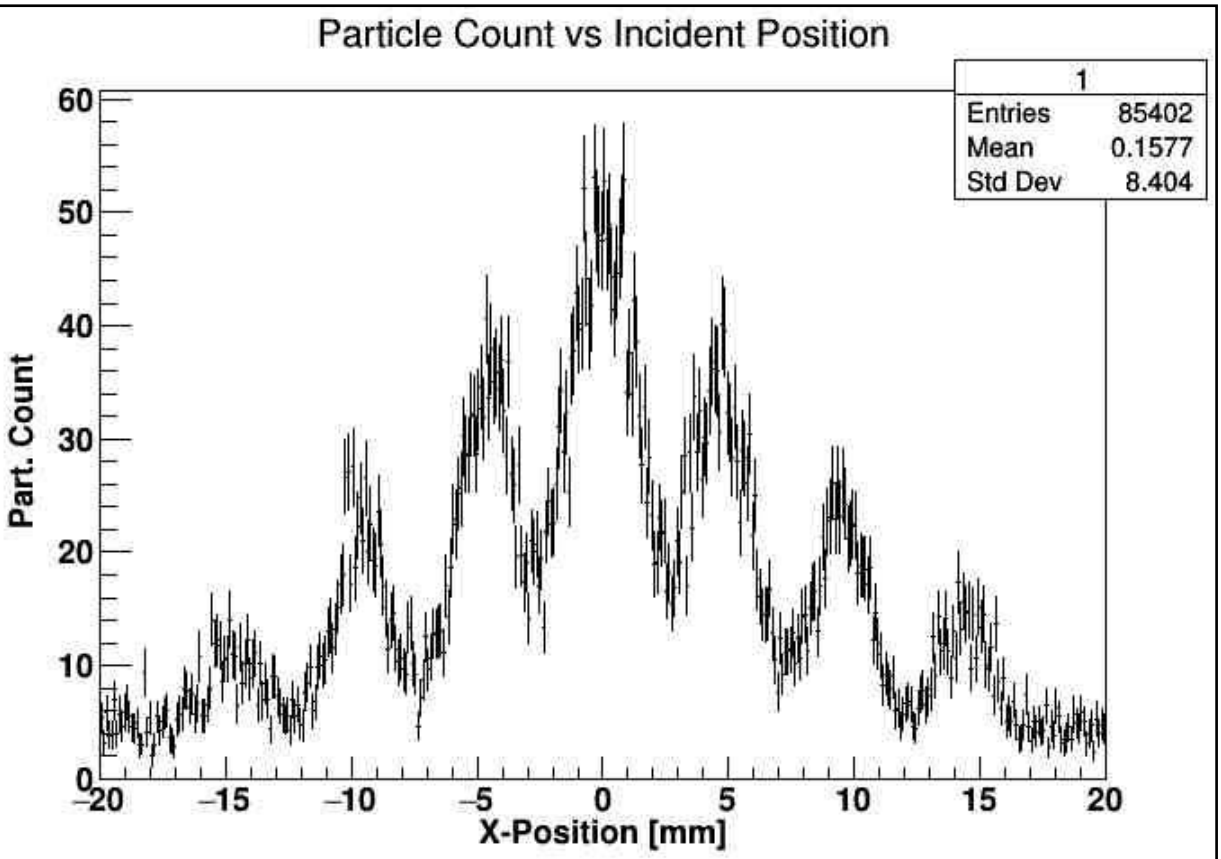

FIGURE 5.25 INCIDENT PARTICLE COUNT VS POSITION (ALONG X DIRECTION) SOURCE AT $Z = 80\ cm$ FROM THE COLLIMATOR WITH $T = 1\ mm$ AND $P = 4\ mm$, E=2MEV.

total integral of histo 1: 15722.2

partial integral of histo 1 (first pitch): 1580.13

partial integral of histo 1 (until second pitch): 4012.54

partial integral of histo 1 (until third pitch): 5498.48

contrast ratio of histo 1 (first pitch):12.6019

contrast ratio of histo 1 (until second pitch):32.0009

contrast ratio of histo 1 (until third pitch):43.8516

In Figure 5.25 is one of the most interesting graphs, which also happens at 80 cm, it can be seen that there are four areas capturing signal.

5.2.2 SIMULATION FOR 4 MM PITCH AND 3 MM THICKNESS

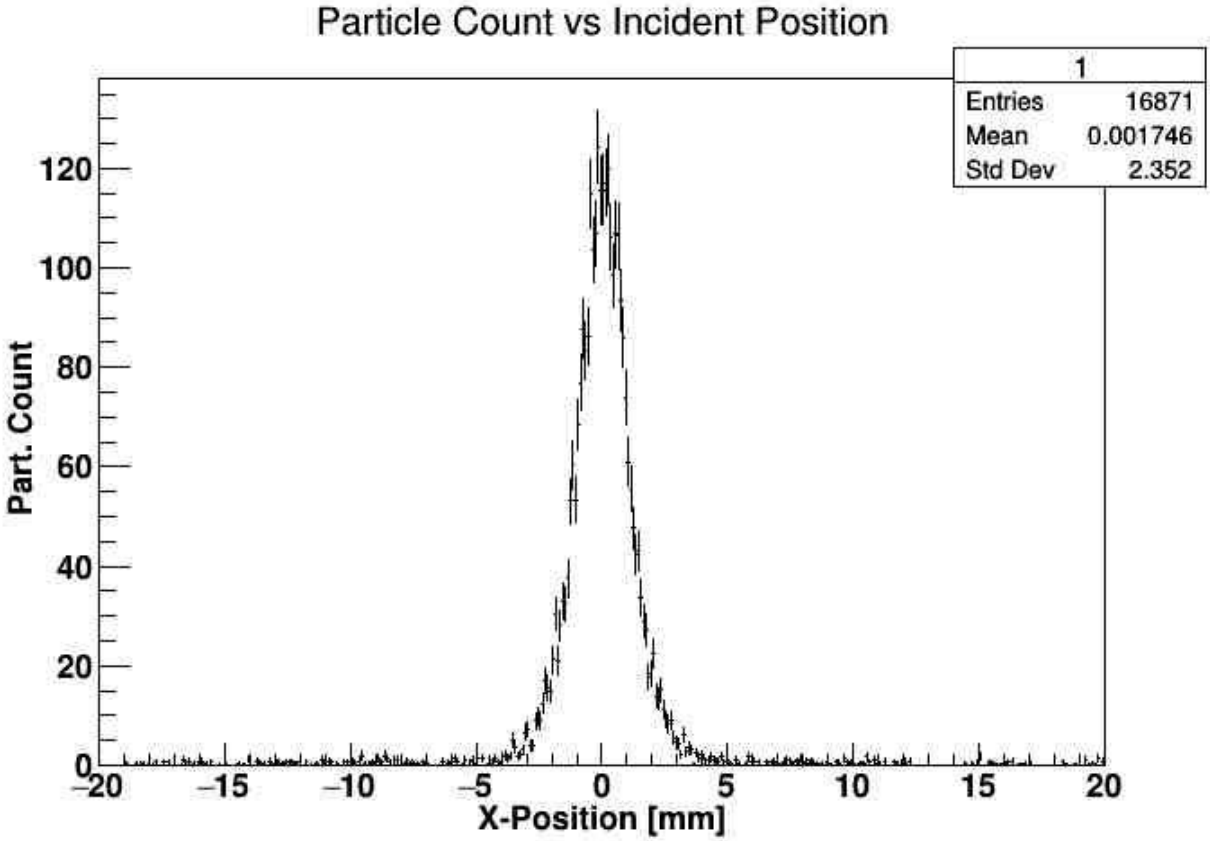

FIGURE 5.26 INCIDENT PARTICLE COUNT VS POSITION (ALONG X DIRECTION) SOURCE AT $Z = 0\ cm$ FROM THE COLLIMATOR WITH $T = 3\ mm$ AND $P = 4\ mm$, E=2MEV.

total integral of histo 1: 3390.24

partial integral of histo 1 (first pitch): 2753.03

partial integral of histo 1 (until second pitch): 3068.91

partial integral of histo 1 (until third pitch): 3110.02

contrast ratio of histo 1 (first pitch):47.2819

contrast ratio of histo 1 (until second pitch):52.707

contrast ratio of histo 1 (until third pitch):53.4131

In Figure 5.26 is the typical well-defined peak but very thin, because of the interspacing of 1mm.

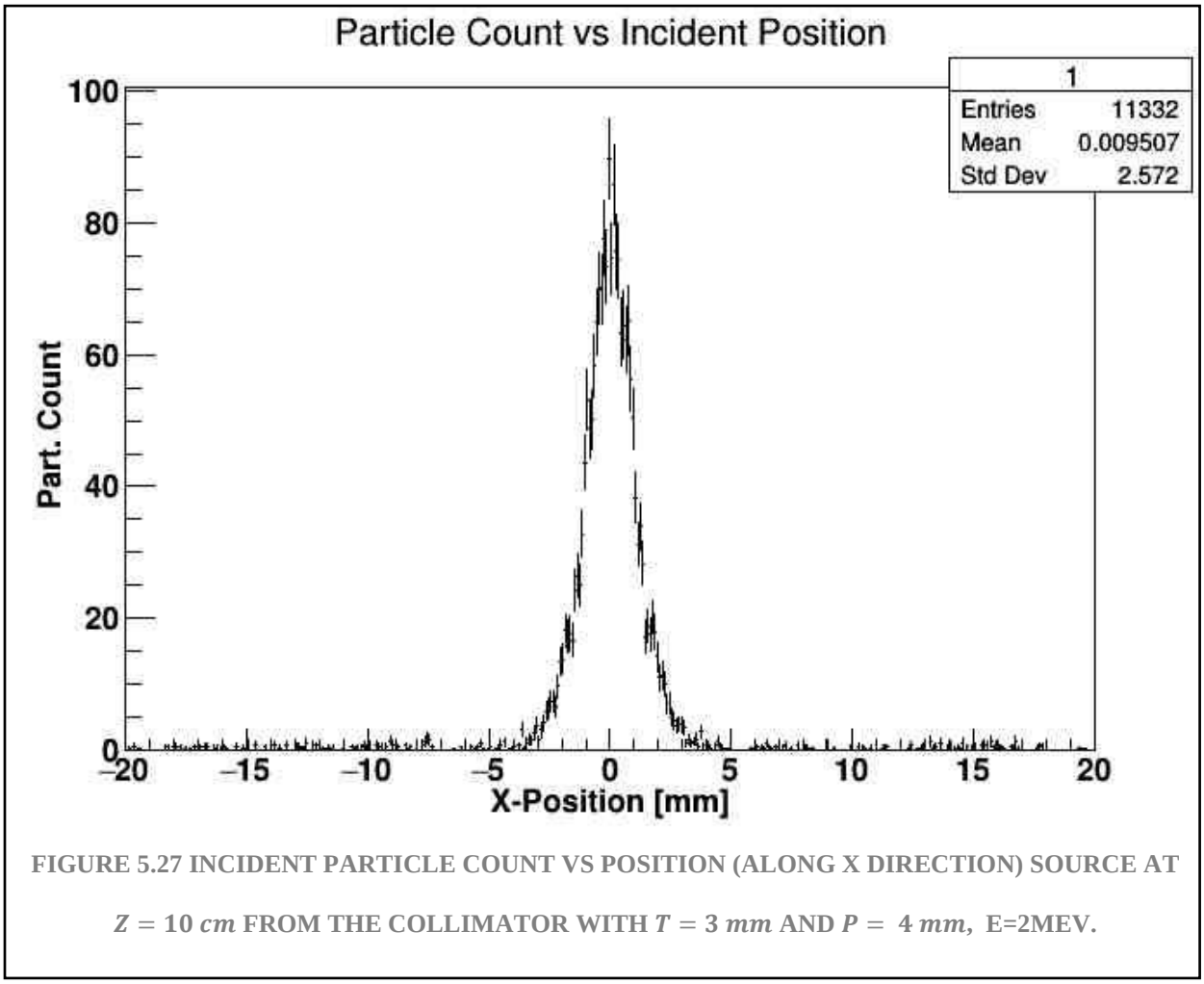

FIGURE 5.27 INCIDENT PARTICLE COUNT VS POSITION (ALONG X DIRECTION) SOURCE AT $Z = 10\ cm$ FROM THE COLLIMATOR WITH $T = 3\ mm$ AND $P = 4\ mm$, E=2MEV.

total integral of histo 1: 2269.15

partial integral of histo 1 (first pitch): 1816.03

partial integral of histo 1 (until second pitch): 1992.94

partial integral of histo 1 (until third pitch): 2028.17

contrast ratio of histo 1 (first pitch):38.1235

contrast ratio of histo 1 (until second pitch):41.8373

contrast ratio of histo 1 (until third pitch):42.5769

In Figure 5.27 is the typical well-defined peak but very thin, because of the interspacing of 1mm.

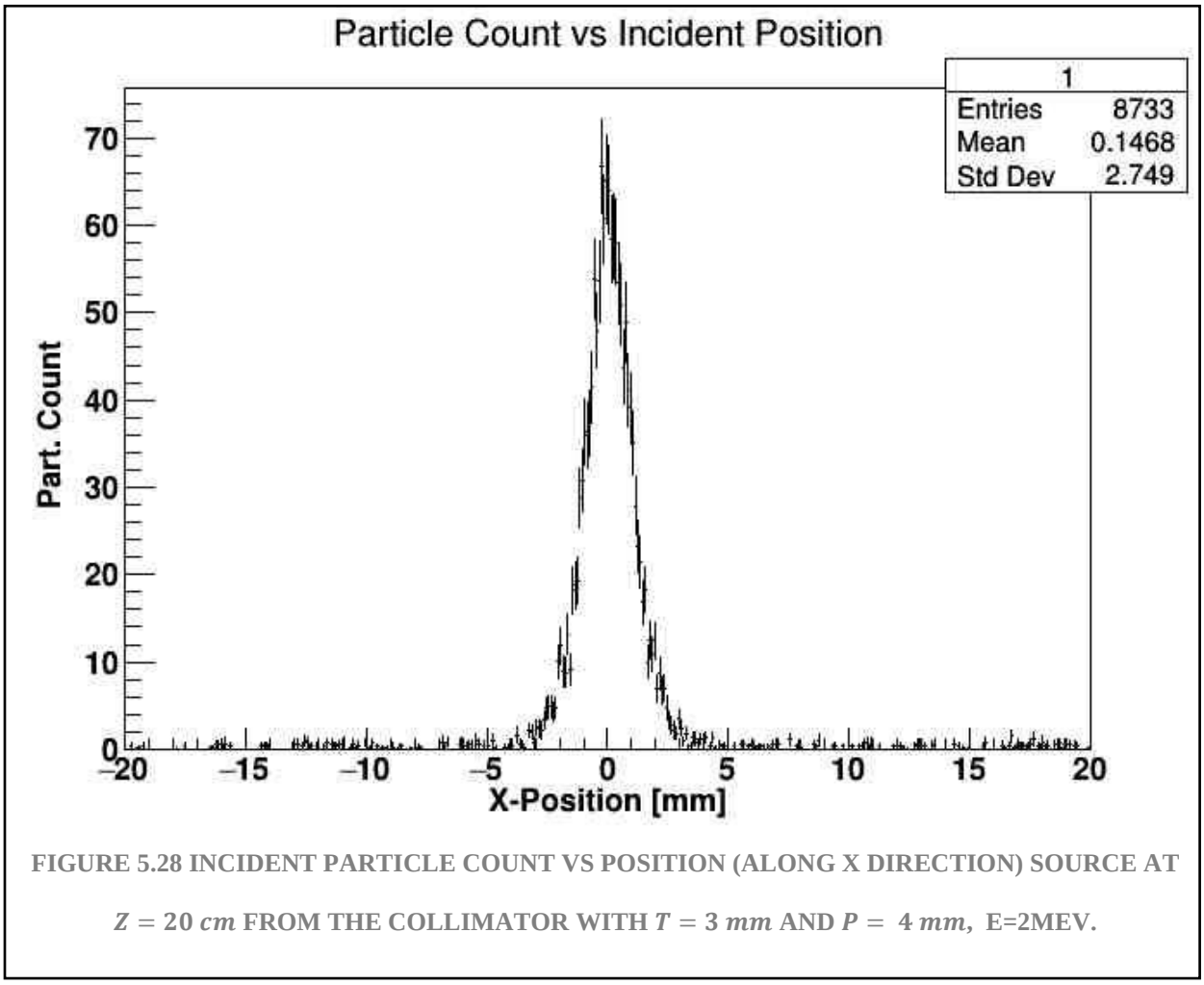

FIGURE 5.28 INCIDENT PARTICLE COUNT VS POSITION (ALONG X DIRECTION) SOURCE AT $Z = 20\ cm$ FROM THE COLLIMATOR WITH $T = 3\ mm$ AND $P = 4\ mm$, E=2MEV.

total integral of histo 1: 1746.5

partial integral of histo 1 (first pitch): 1382.2

partial integral of histo 1 (until second pitch): 1508.71

partial integral of histo 1 (until third pitch): 1534.61

contrast ratio of histo 1 (first pitch):33.074

contrast ratio of histo 1 (until second pitch):36.1012

contrast ratio of histo 1 (until third pitch):36.721

Figure 5.28 remains the same compared to the 10 cm and 0 cm graphs.

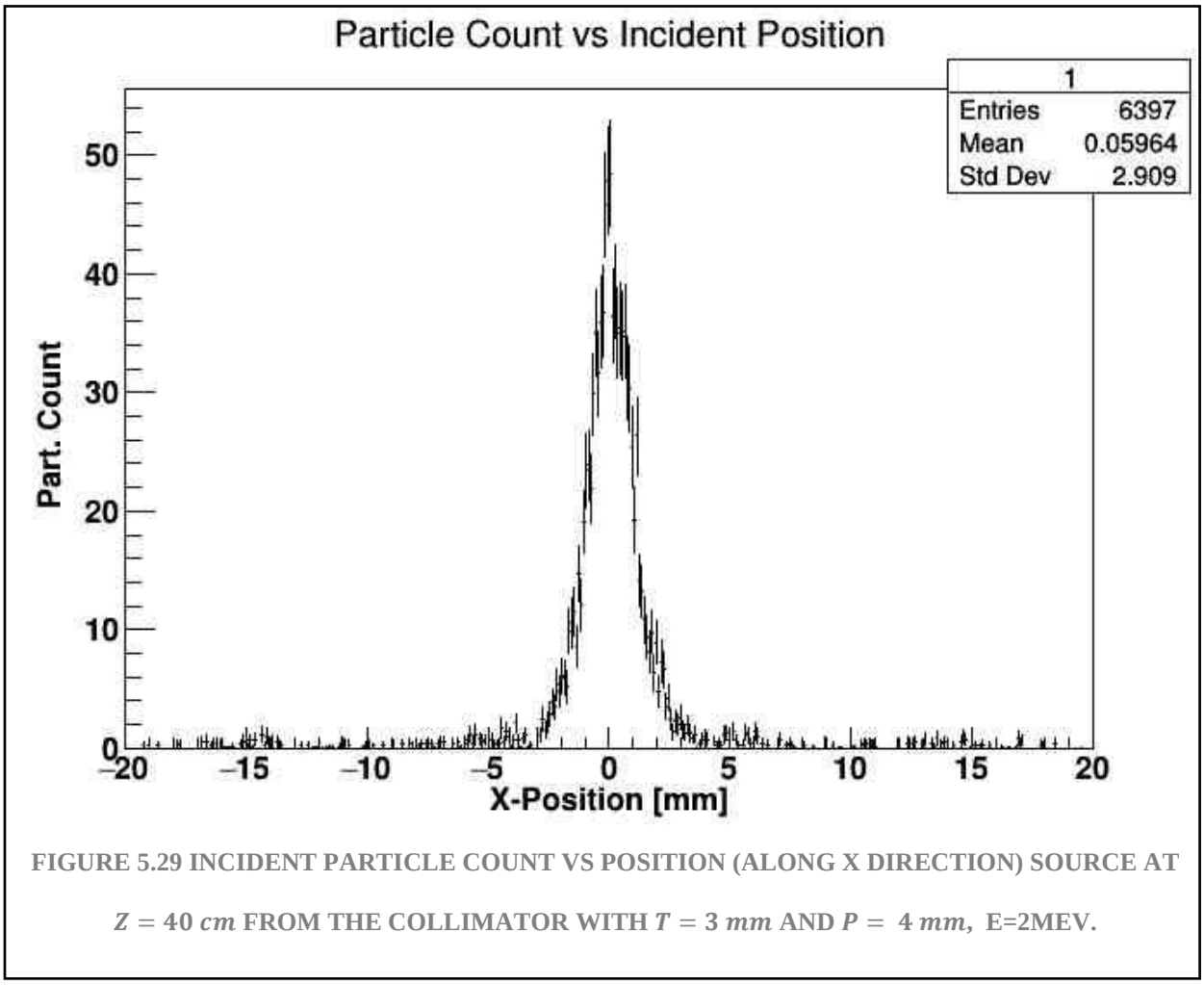

FIGURE 5.29 INCIDENT PARTICLE COUNT VS POSITION (ALONG X DIRECTION) SOURCE AT $Z = 40\ cm$ FROM THE COLLIMATOR WITH $T = 3\ mm$ AND $P = 4\ mm$, E=2MEV.

total integral of histo 1: 1261.8

partial integral of histo 1 (first pitch): 918.211

partial integral of histo 1 (until second pitch): 1033.4

partial integral of histo 1 (until third pitch): 1058.39

contrast ratio of histo 1 (first pitch):25.8492

contrast ratio of histo 1 (until second pitch):29.092

contrast ratio of histo 1 (until third pitch):29.7955

Figure 5.29 has a smaller gamma count and a little signal on the sides of the central peak.

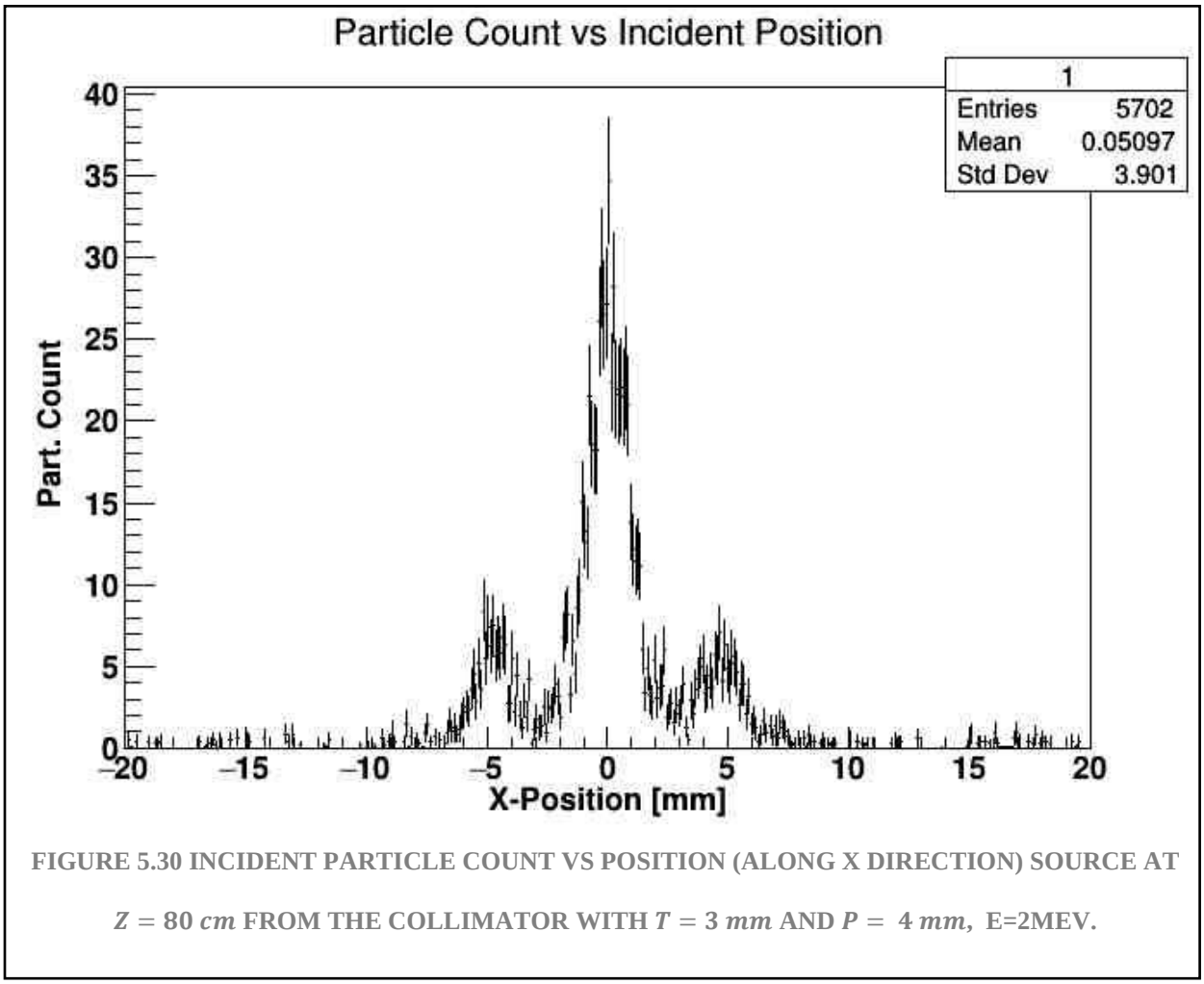

FIGURE 5.30 INCIDENT PARTICLE COUNT VS POSITION (ALONG X DIRECTION) SOURCE AT $Z = 80\ cm$ FROM THE COLLIMATOR WITH $T = 3\ mm$ AND $P = 4\ mm$, E=2MEV.

total integral of histo 1: 1113.96

partial integral of histo 1 (first pitch): 589.614

partial integral of histo 1 (until second pitch): 920.173

partial integral of histo 1 (until third pitch): 936.266

contrast ratio of histo 1 (first pitch):17.6658

contrast ratio of histo 1 (until second pitch):27.5698

contrast ratio of histo 1 (until third pitch):28.052

Figure 5.30 shows again a capture of the signal in the second areas, but one difference is the amount of radiation captured.

5.3 RESULTS CHANGING PITCH WITH 5 MEV ENERGY

5.3.1 SIMULATION FOR 2 MM THICKNESS AND 4 MM PITCH

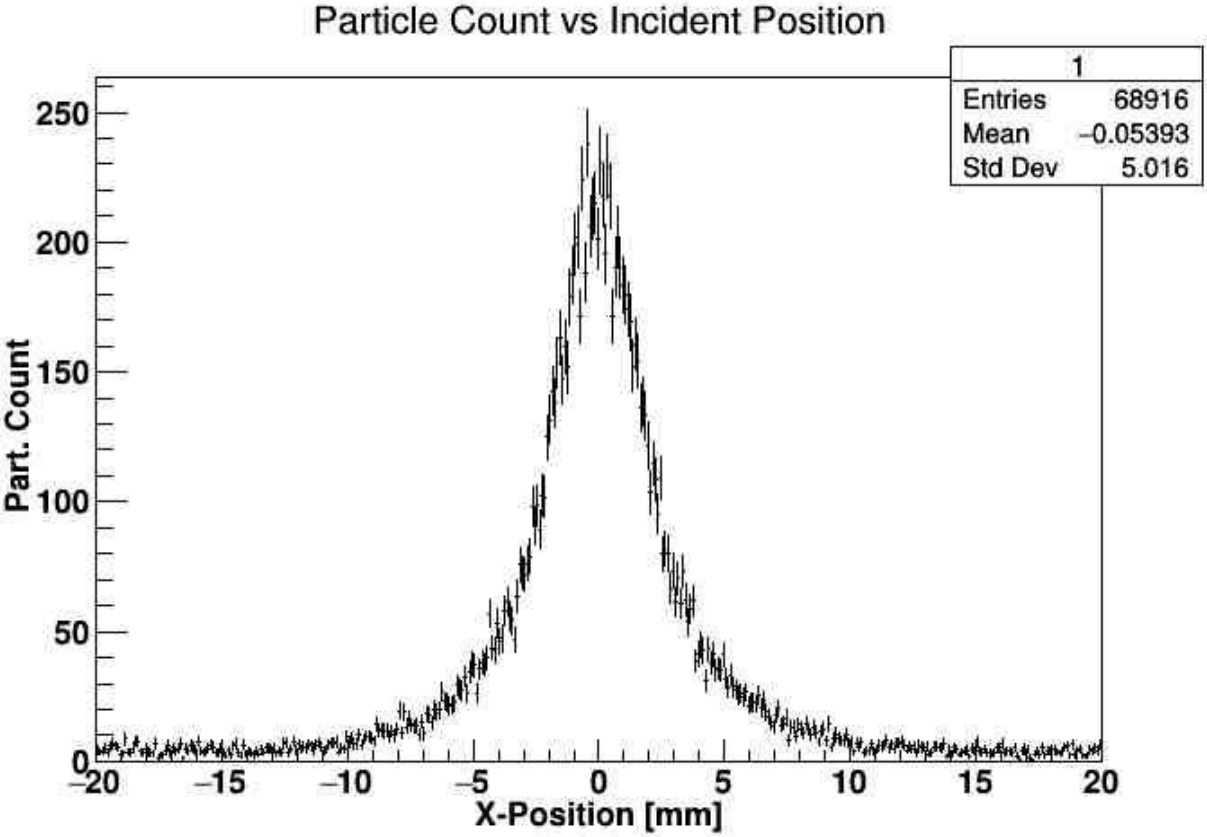

FIGURE 5.31 INCIDENT PARTICLE COUNT VS POSITION (ALONG X DIRECTION) SOURCE AT $Z = 0\ cm$ FROM THE COLLIMATOR WITH $E = 5\ MeV,\ T = 2\ mm$ AND $P = 4\ mm$.

total integral of histo 1: 18735.4

partial integral of histo 1 (first pitch): 7288.24

partial integral of histo 1 (until second pitch): 12231.2

partial integral of histo 1 (until third pitch): 13053.2

contrast ratio of histo 1 (first pitch):53.2466

contrast ratio of histo 1 (until second pitch):89.3586

contrast ratio of histo 1 (until third pitch):95.3645

Figure 5.31 has an energy of 5 MeV, compared to the same parameters graph, it can be seen that the ranges of the signal is wider.

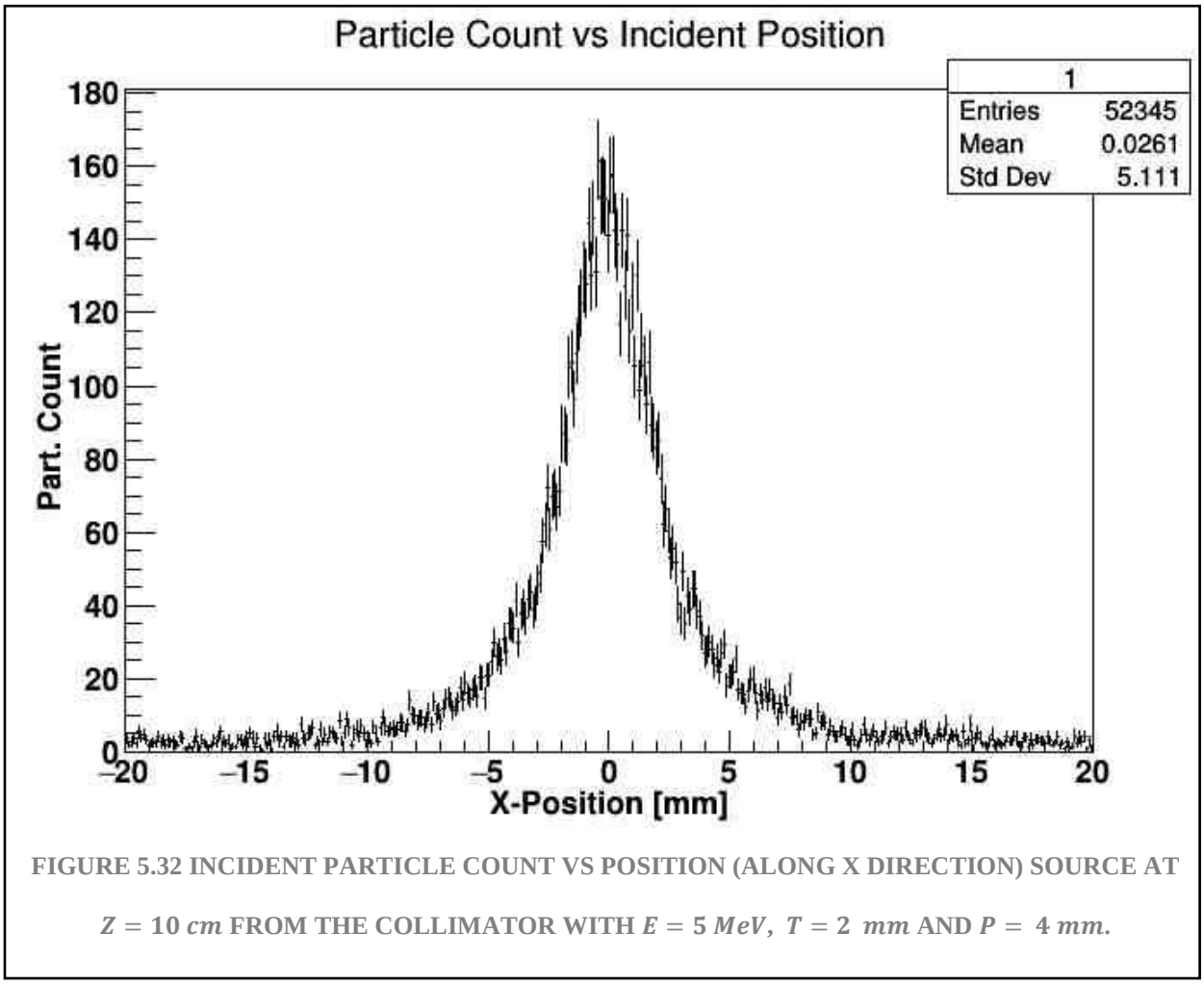

FIGURE 5.32 INCIDENT PARTICLE COUNT VS POSITION (ALONG X DIRECTION) SOURCE AT $Z = 10\ cm$ FROM THE COLLIMATOR WITH $E = 5\ MeV,\ T = 2\ mm$ AND $P = 4\ mm$.

total integral of histo 1: 14177.4

partial integral of histo 1 (first pitch): 4931.83

partial integral of histo 1 (until second pitch): 8237.96

partial integral of histo 1 (until third pitch): 8859.26

contrast ratio of histo 1 (first pitch):41.42

contrast ratio of histo 1 (until second pitch):69.1865

contrast ratio of histo 1 (until third pitch):74.4045

Figure 5.32 has the same pattern compared to the same parameters, but it displays a notorious noise besides the main peak.

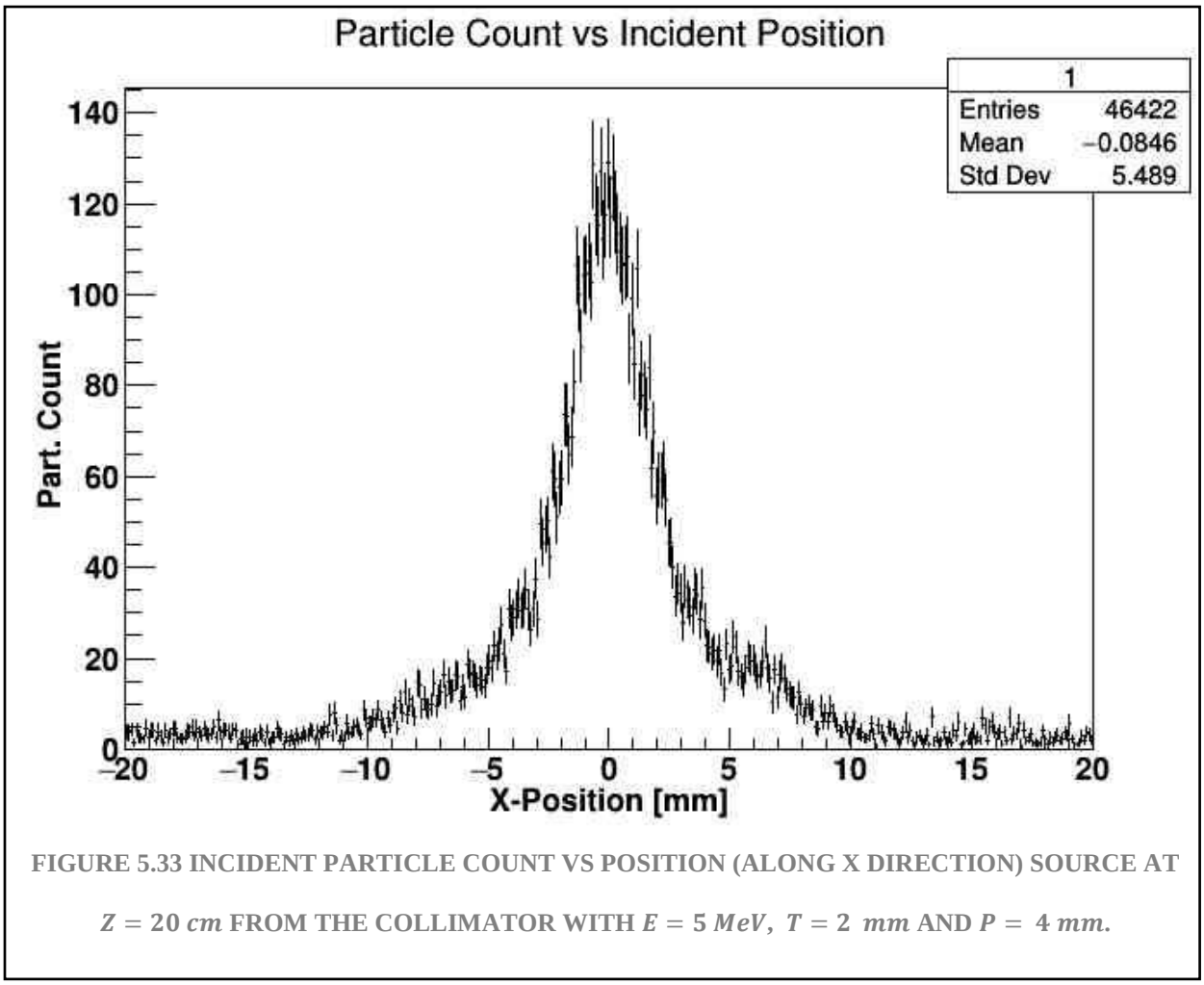

FIGURE 5.33 INCIDENT PARTICLE COUNT VS POSITION (ALONG X DIRECTION) SOURCE AT $Z = 20\ cm$ FROM THE COLLIMATOR WITH $E = 5\ MeV,\ T = 2\ mm$ AND $P = 4\ mm$.

total integral of histo 1: 12366.6

partial integral of histo 1 (first pitch): 3905.83

partial integral of histo 1 (until second pitch): 6771.55

partial integral of histo 1 (until third pitch): 7327.34

contrast ratio of histo 1 (first pitch):35.1228

contrast ratio of histo 1 (until second pitch):60.8924

contrast ratio of histo 1 (until third pitch):65.8902

Figure 5.33 has a smaller (half) signal compared to Figure 5.31, and it apparently begins to show the pattern of the second areas, although not very marked.

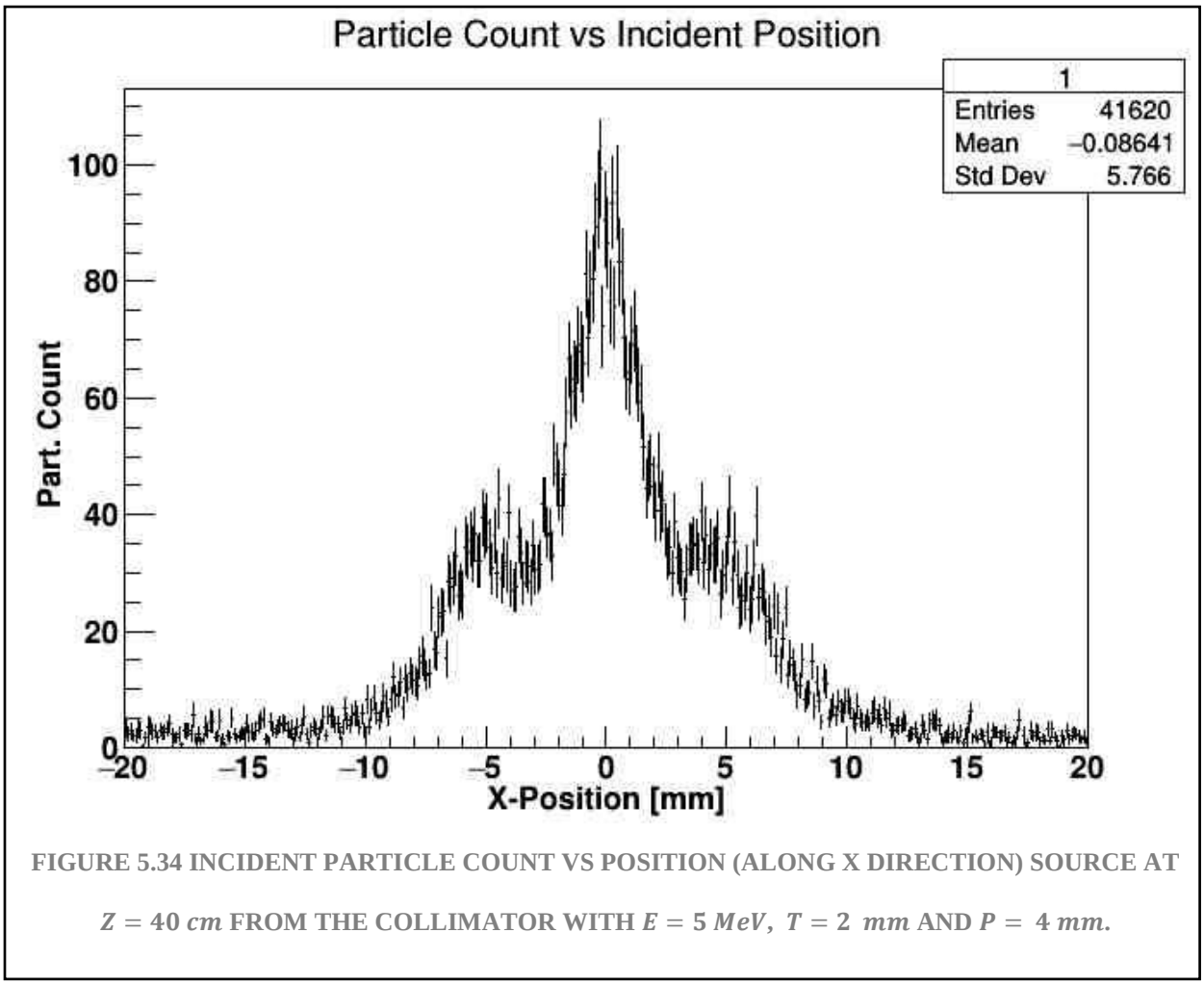

FIGURE 5.34 INCIDENT PARTICLE COUNT VS POSITION (ALONG X DIRECTION) SOURCE AT $Z = 40\ cm$ FROM THE COLLIMATOR WITH $E = 5\ MeV,\ T = 2\ mm$ AND $P = 4\ mm$.

total integral of histo 1: 11238

partial integral of histo 1 (first pitch): 2805.46

partial integral of histo 1 (until second pitch): 6299.45

partial integral of histo 1 (until third pitch): 6953.8

contrast ratio of histo 1 (first pitch):26.4643

contrast ratio of histo 1 (until second pitch):59.4234

contrast ratio of histo 1 (until third pitch):65.596

Figure 5.34 shows the signal of the second areas, but there is not defined the end of the first zone (first area) as it does for 2 MeV (Figure 5.4).

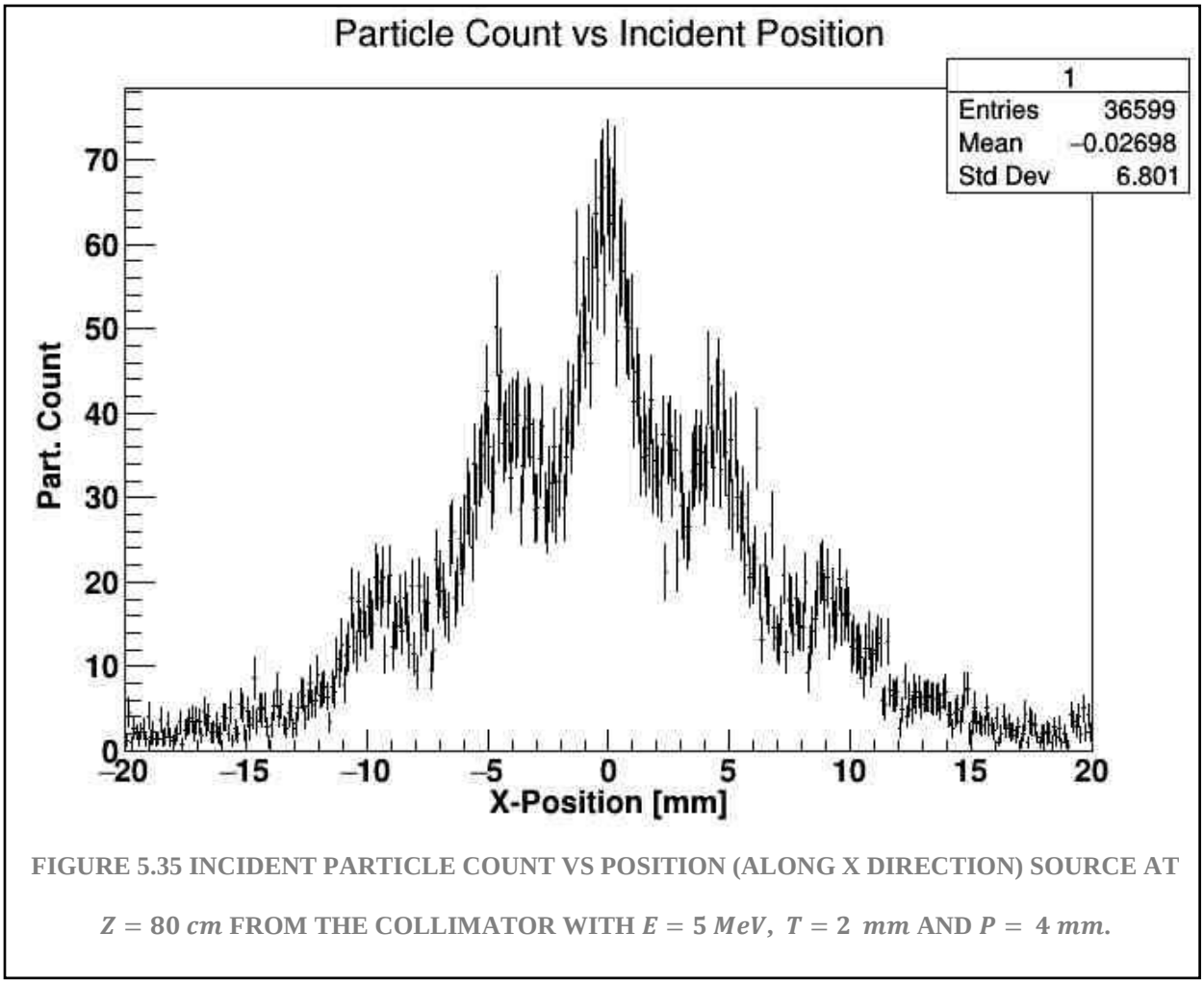

FIGURE 5.35 INCIDENT PARTICLE COUNT VS POSITION (ALONG X DIRECTION) SOURCE AT $Z = 80\ cm$ FROM THE COLLIMATOR WITH $E = 5\ MeV,\ T = 2\ mm$ AND $P = 4\ mm$.

total integral of histo 1: 10046.2

partial integral of histo 1 (first pitch): 1985.81

partial integral of histo 1 (until second pitch): 5348.61

partial integral of histo 1 (until third pitch): 6648.47

contrast ratio of histo 1 (first pitch):19.8124

contrast ratio of histo 1 (until second pitch):53.3631

contrast ratio of histo 1 (until third pitch):66.3317

Figure 5.35 shows the signal of the second areas, but there is not defined the end of the first zone (first area) as it does for 2 MeV (Figure 5.4).

5.3.2 SIMULATION FOR 2 MM THICKNESS AND 5 MM PITCH

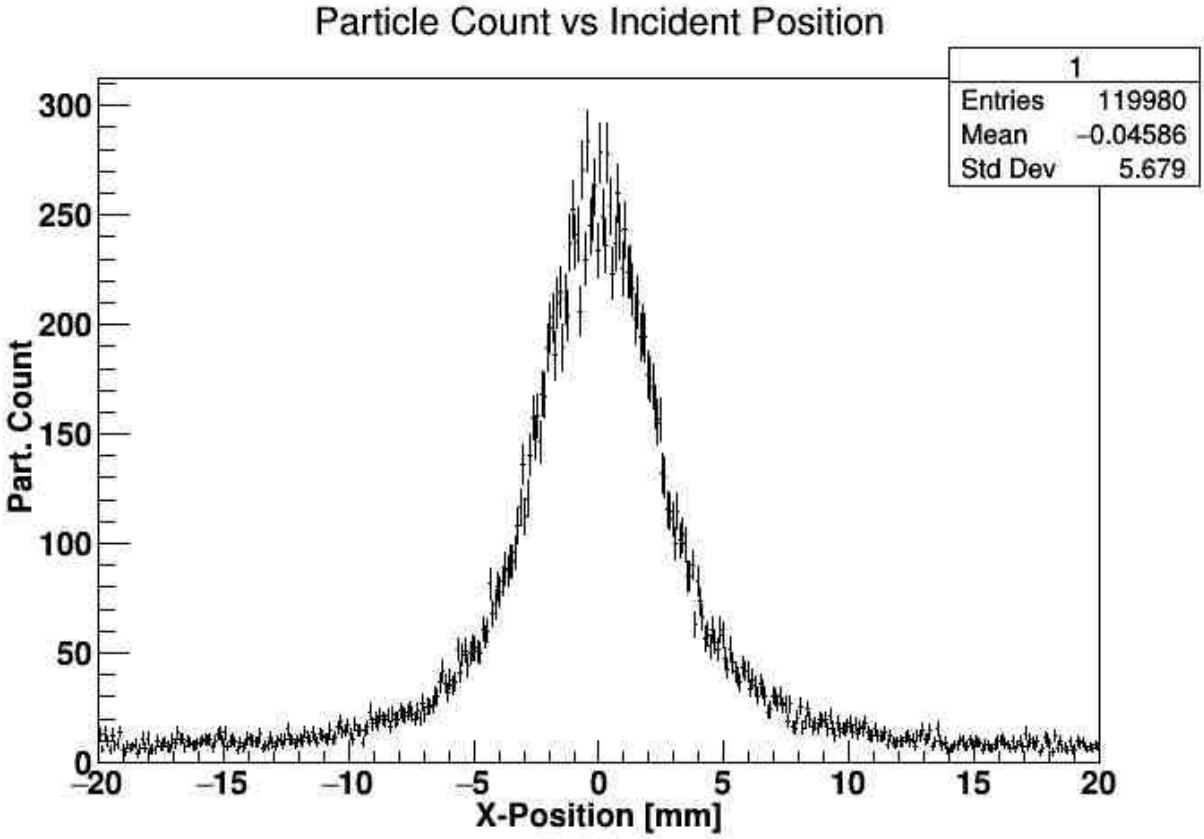

FIGURE 5.36 INCIDENT PARTICLE COUNT VS POSITION (ALONG X DIRECTION) SOURCE AT $Z = 0\ cm$ FROM THE COLLIMATOR WITH $E = 5\ MeV,\ T = 2\ mm$ AND $P = 5\ mm$.

total integral of histo 1: 31811.8

partial integral of histo 1 (first pitch): 10939.5

partial integral of histo 1 (until second pitch): 17742.9

partial integral of histo 1 (until third pitch): 19251.5

contrast ratio of histo 1 (first pitch):61.3341

contrast ratio of histo 1 (until second pitch):99.4786

contrast ratio of histo 1 (until third pitch):107.937

Figure 5.36 shows again a wider range for the given parameters.

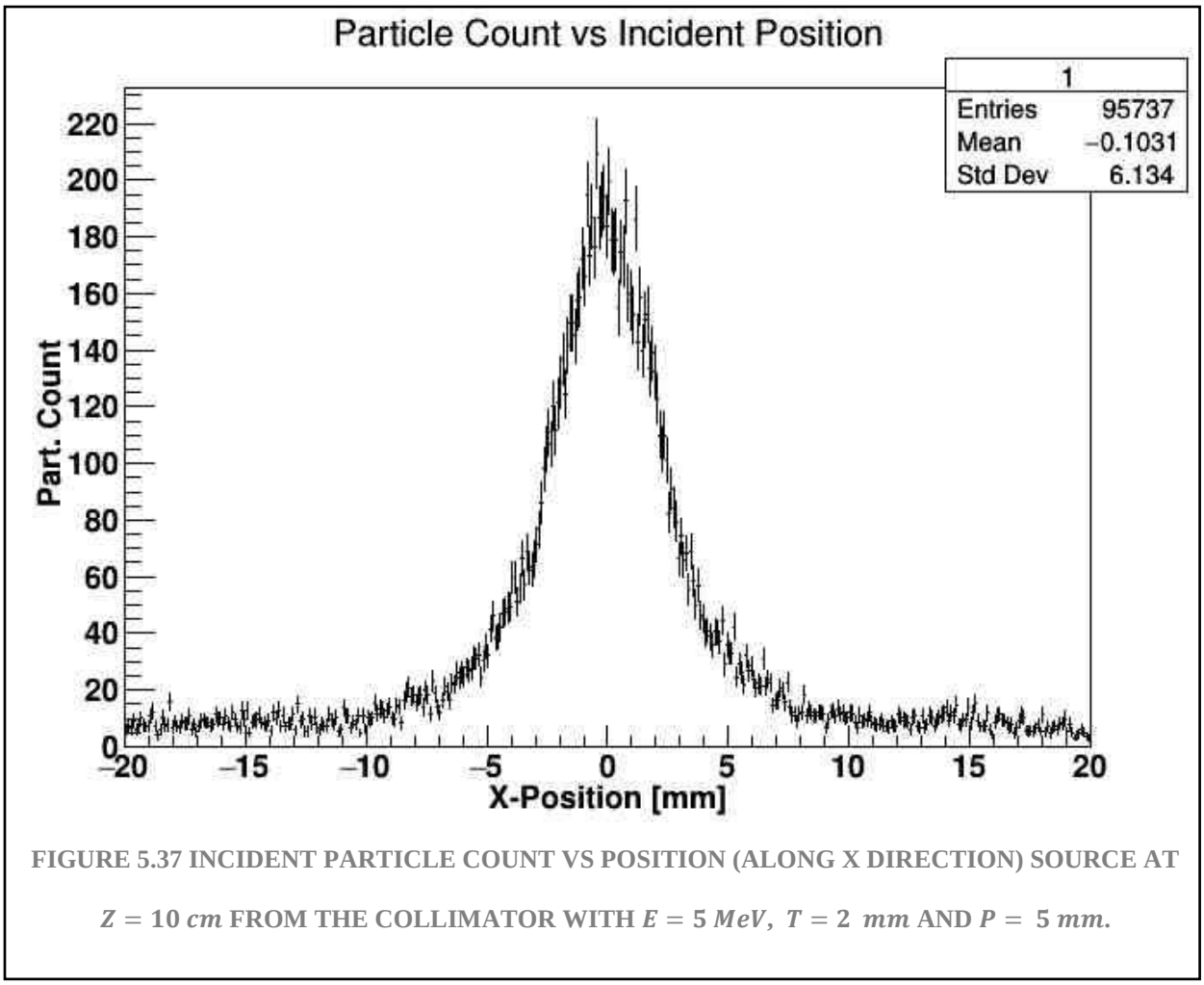

FIGURE 5.37 INCIDENT PARTICLE COUNT VS POSITION (ALONG X DIRECTION) SOURCE AT $Z = 10\ cm$ FROM THE COLLIMATOR WITH $E = 5\ MeV,\ T = 2\ mm$ AND $P = 5\ mm$.

total integral of histo 1: 25200

partial integral of histo 1 (first pitch): 7788.73

partial integral of histo 1 (until second pitch): 12279.7

partial integral of histo 1 (until third pitch): 13582.9

contrast ratio of histo 1 (first pitch):49.0643

contrast ratio of histo 1 (until second pitch):77.3548

contrast ratio of histo 1 (until third pitch):85.5639

Figure 5.37 shows again the noise on the sides of the main peak.

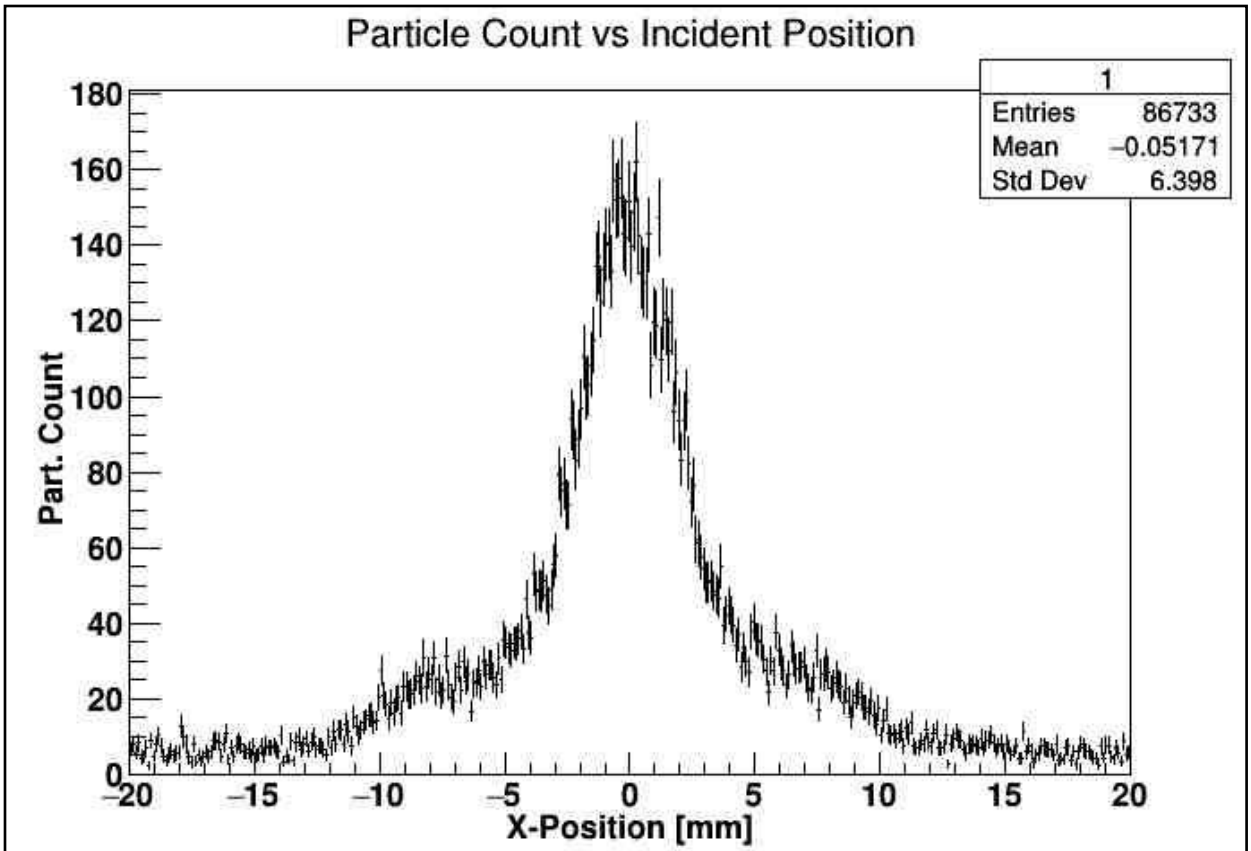

FIGURE 5.38 INCIDENT PARTICLE COUNT VS POSITION (ALONG X DIRECTION) SOURCE AT $Z = 20\ cm$ FROM THE COLLIMATOR WITH $E = 5\ MeV,\ T = 2\ mm$ AND $P = 5\ mm$.

total integral of histo 1: 22577.5

partial integral of histo 1 (first pitch): 6069.54

partial integral of histo 1 (until second pitch): 10639.2

partial integral of histo 1 (until third pitch): 11924.7

contrast ratio of histo 1 (first pitch):40.3941

contrast ratio of histo 1 (until second pitch):70.806

contrast ratio of histo 1 (until third pitch):79.3618

Figure 5.38 now shows a diffuse signal on the sides of the main peak, but with a signal input from the second areas.

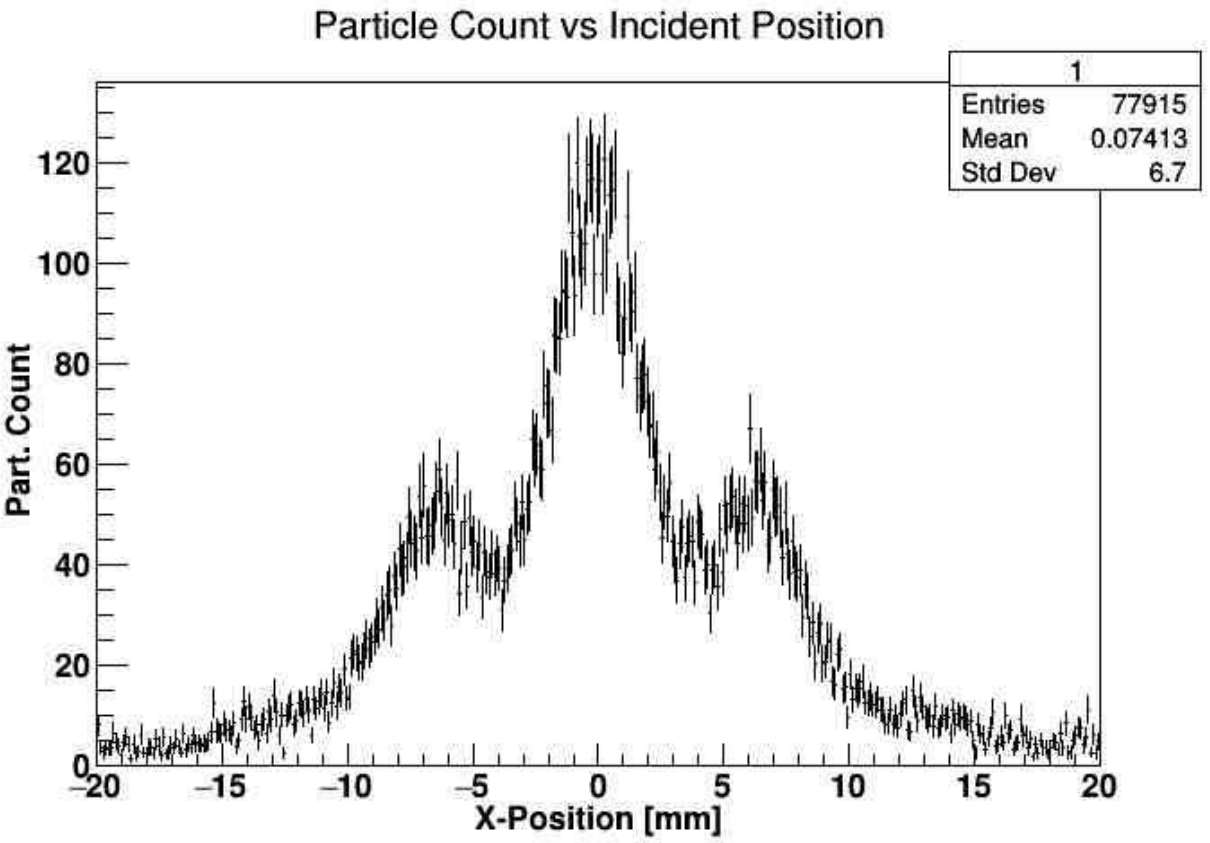

FIGURE 5.39 INCIDENT PARTICLE COUNT VS POSITION (ALONG X DIRECTION) SOURCE AT $Z = 40\ cm$ FROM THE COLLIMATOR WITH $E = 5\ MeV,\ T = 2\ mm$ AND $P = 5\ mm$.

total integral of histo 1: 20891.6

partial integral of histo 1 (first pitch): 4596.83

partial integral of histo 1 (until second pitch): 10457.6

partial integral of histo 1 (until third pitch): 11849.4

contrast ratio of histo 1 (first pitch):31.8033

contrast ratio of histo 1 (until second pitch):72.3514

contrast ratio of histo 1 (until third pitch):81.9805

Figure 5.39 has activity at the first two capture areas and as it should be known, it has a high count compared to the corresponding graph for 2 MeV.

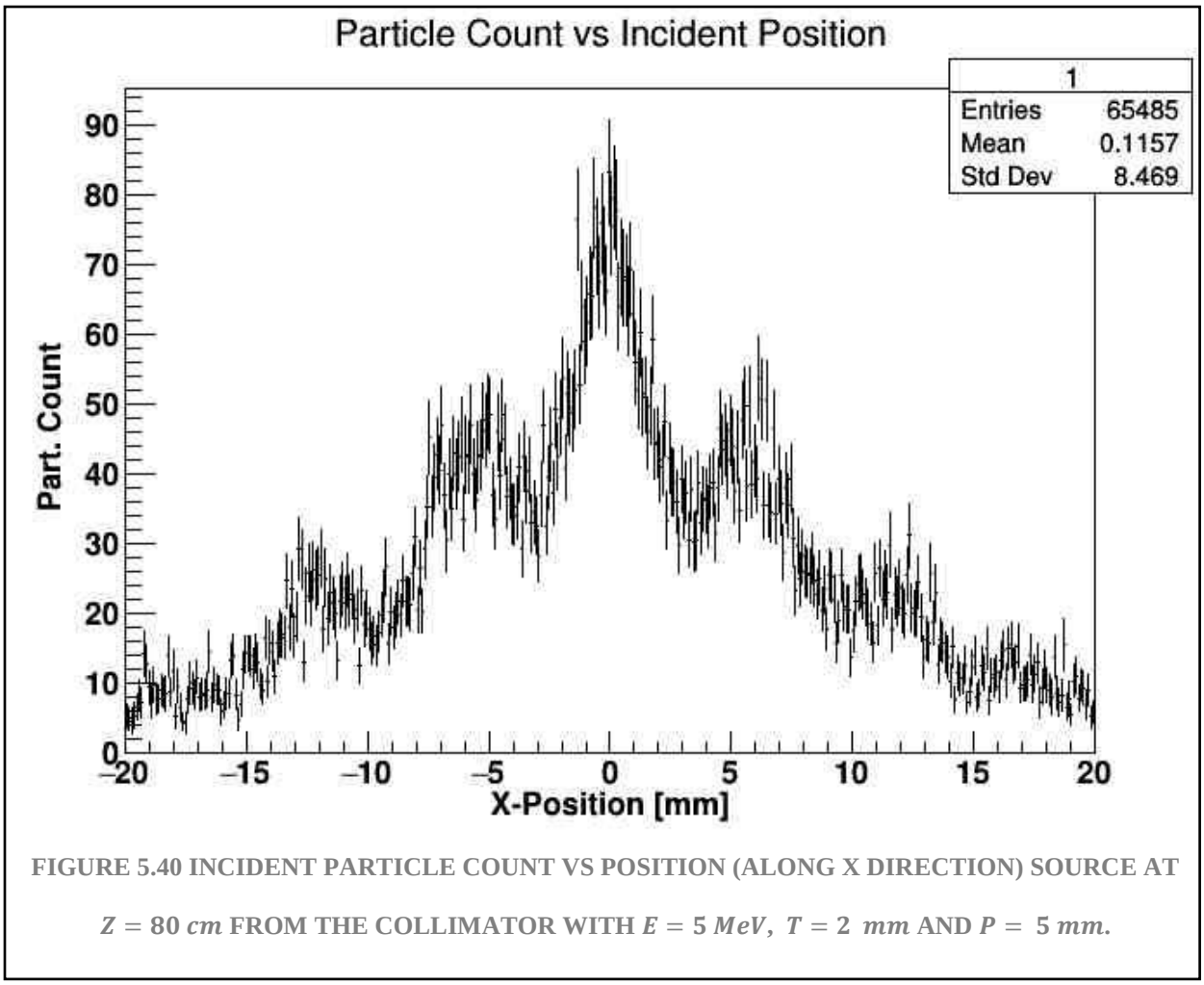

FIGURE 5.40 INCIDENT PARTICLE COUNT VS POSITION (ALONG X DIRECTION) SOURCE AT $Z = 80\ cm$ FROM THE COLLIMATOR WITH $E = 5\ MeV,\ T = 2\ mm$ AND $P = 5\ mm$.

total integral of histo 1: 17711.8

partial integral of histo 1 (first pitch): 2934.95

partial integral of histo 1 (until second pitch): 7795.45

partial integral of histo 1 (until third pitch): 10184.3

contrast ratio of histo 1 (first pitch):22.0531

contrast ratio of histo 1 (until second pitch):58.5747

contrast ratio of histo 1 (until third pitch):76.5244

Figure 5.40 is interesting because those seem characteristic peaks for a radial uniform source at 80 cm away from the detector with 5 MeV of energy.

5.3.3 SIMULATION FOR 2 MM THICKNESS AND 6 MM PITCH

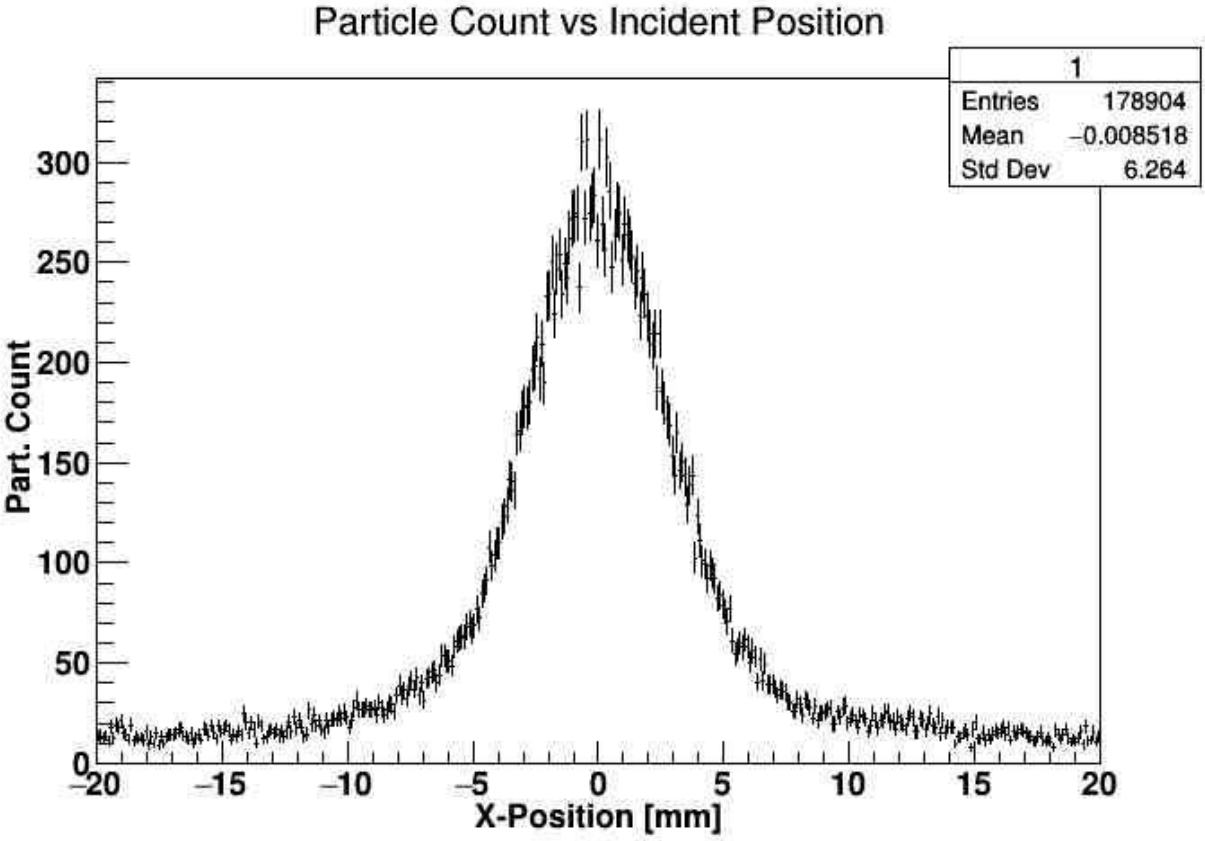

FIGURE 5.41 INCIDENT PARTICLE COUNT VS POSITION (ALONG X DIRECTION) SOURCE AT $Z = 0\ cm$ FROM THE COLLIMATOR WITH $E = 5\ MeV,\ T = 2\ mm$ AND $P = 6\ mm$.

total integral of histo 1: 46839

partial integral of histo 1 (first pitch): 14478.2

partial integral of histo 1 (until second pitch): 23293.4

partial integral of histo 1 (until third pitch): 25851.7

contrast ratio of histo 1 (first pitch):66.8978

contrast ratio of histo 1 (until second pitch):107.629

contrast ratio of histo 1 (until third pitch):119.45

Figure 5.41 shows a lot of gamma count at the center and a wide range.

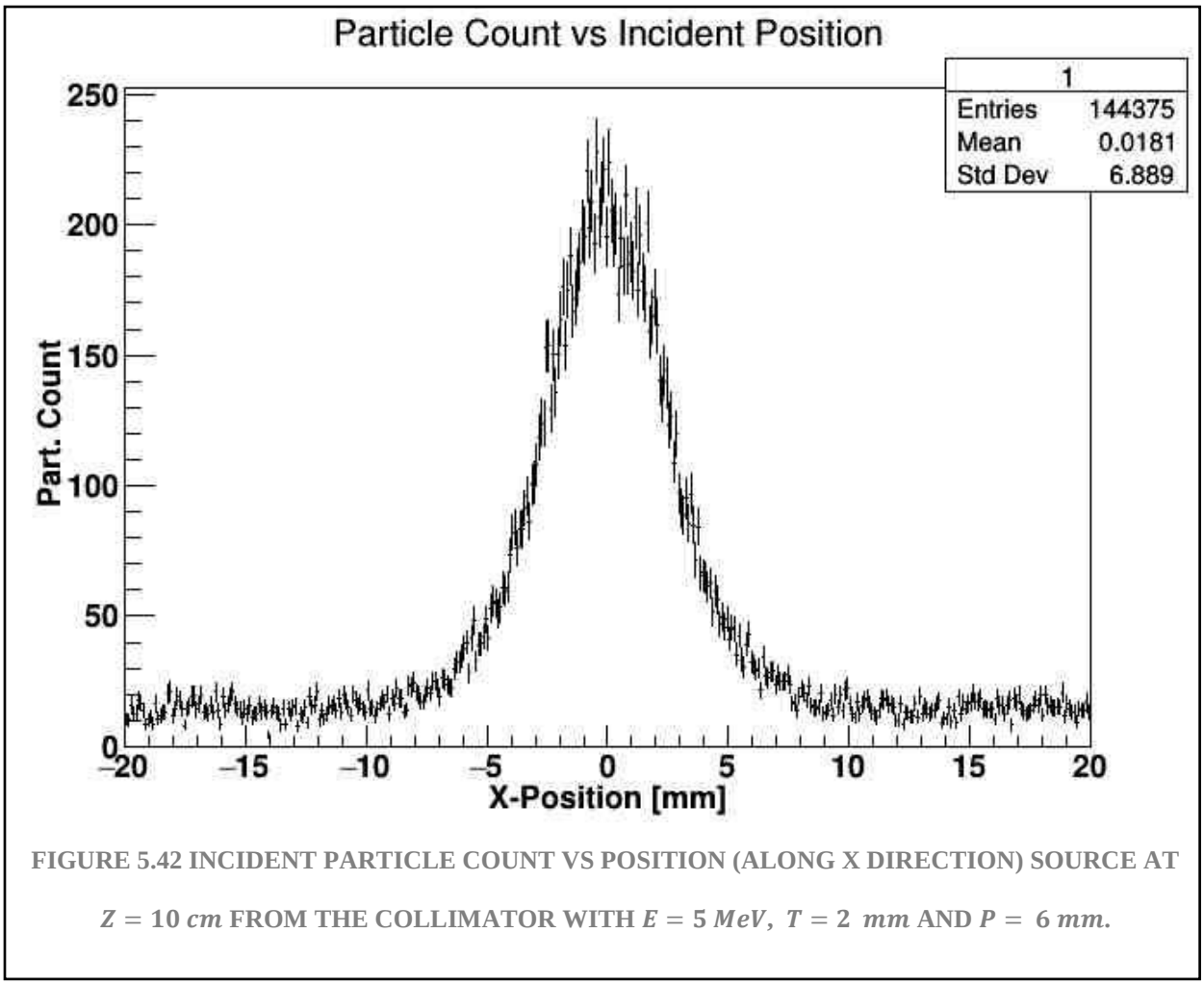

FIGURE 5.42 INCIDENT PARTICLE COUNT VS POSITION (ALONG X DIRECTION) SOURCE AT $Z = 10\ cm$ FROM THE COLLIMATOR WITH $E = 5\ MeV,\ T = 2\ mm$ AND $P = 6\ mm$.

total integral of histo 1: 37590.9

partial integral of histo 1 (first pitch): 9195.87

partial integral of histo 1 (until second pitch): 15390.8

partial integral of histo 1 (until third pitch): 17438.5

contrast ratio of histo 1 (first pitch):47.4299

contrast ratio of histo 1 (until second pitch):79.3815

contrast ratio of histo 1 (until third pitch):89.9433

Figure 5.42 shows the same as before, some initial height in the signal, nothing new.

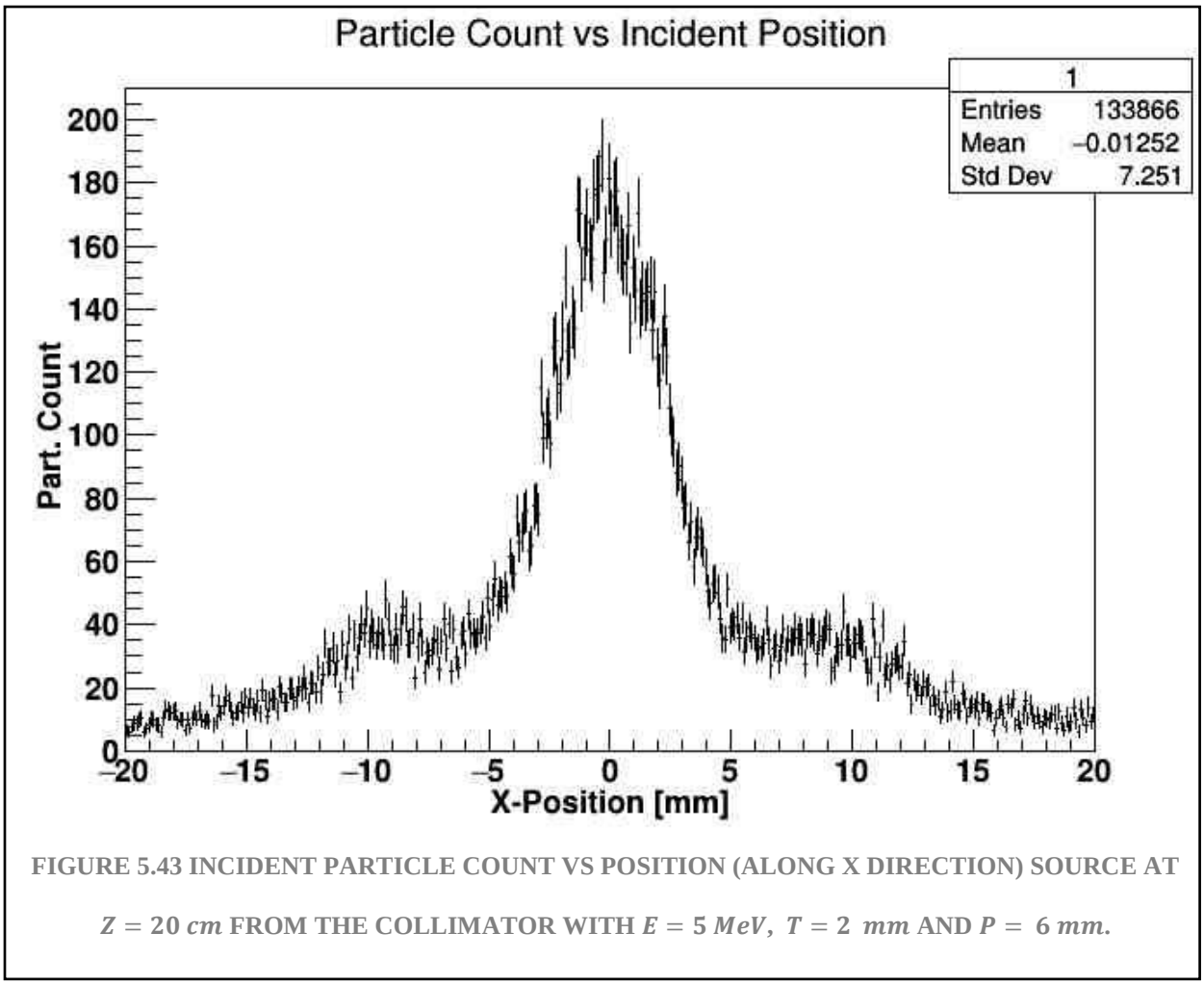

FIGURE 5.43 INCIDENT PARTICLE COUNT VS POSITION (ALONG X DIRECTION) SOURCE AT $Z = 20\ cm$ FROM THE COLLIMATOR WITH $E = 5\ MeV,\ T = 2\ mm$ AND $P = 6\ mm$.

total integral of histo 1: 34896.6

partial integral of histo 1 (first pitch): 8447.64

partial integral of histo 1 (until second pitch): 14967.5

partial integral of histo 1 (until third pitch): 17443

contrast ratio of histo 1 (first pitch):45.2214

contrast ratio of histo 1 (until second pitch):80.1229

contrast ratio of histo 1 (until third pitch):93.375

Figure 5.43 has the initial signal capture of the second areas.

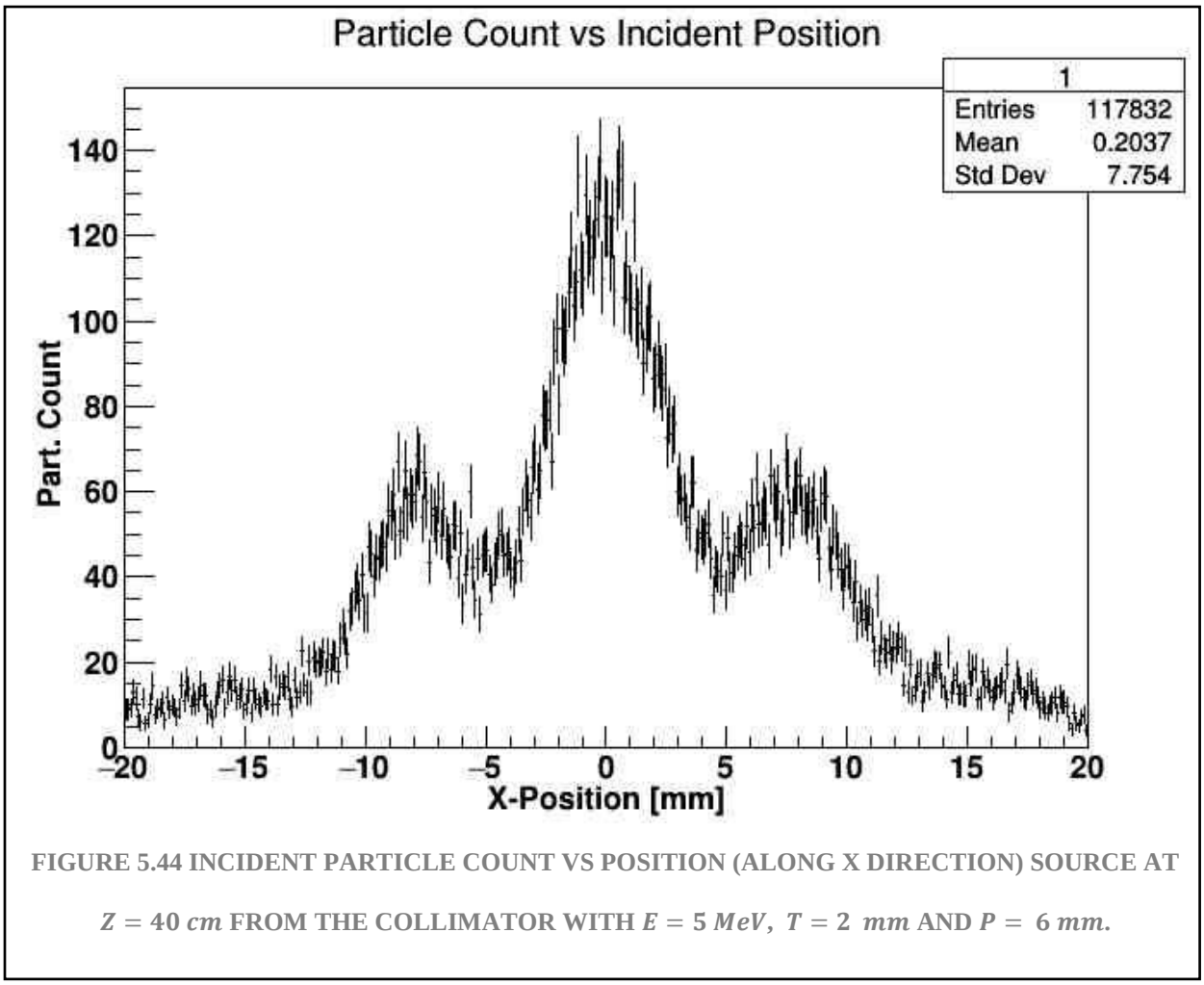

FIGURE 5.44 INCIDENT PARTICLE COUNT VS POSITION (ALONG X DIRECTION) SOURCE AT $Z = 40\ cm$ FROM THE COLLIMATOR WITH $E = 5\ MeV,\ T = 2\ mm$ AND $P = 6\ mm$.

total integral of histo 1: 31268.8

partial integral of histo 1 (first pitch): 6099.11

partial integral of histo 1 (until second pitch): 13835.2

partial integral of histo 1 (until third pitch): 16148.3

contrast ratio of histo 1 (first pitch):34.4914

contrast ratio of histo 1 (until second pitch):78.2403

contrast ratio of histo 1 (until third pitch):91.3213

Figure 5.44 shows an interesting signal pattern since the separation is not well defined in the graph.

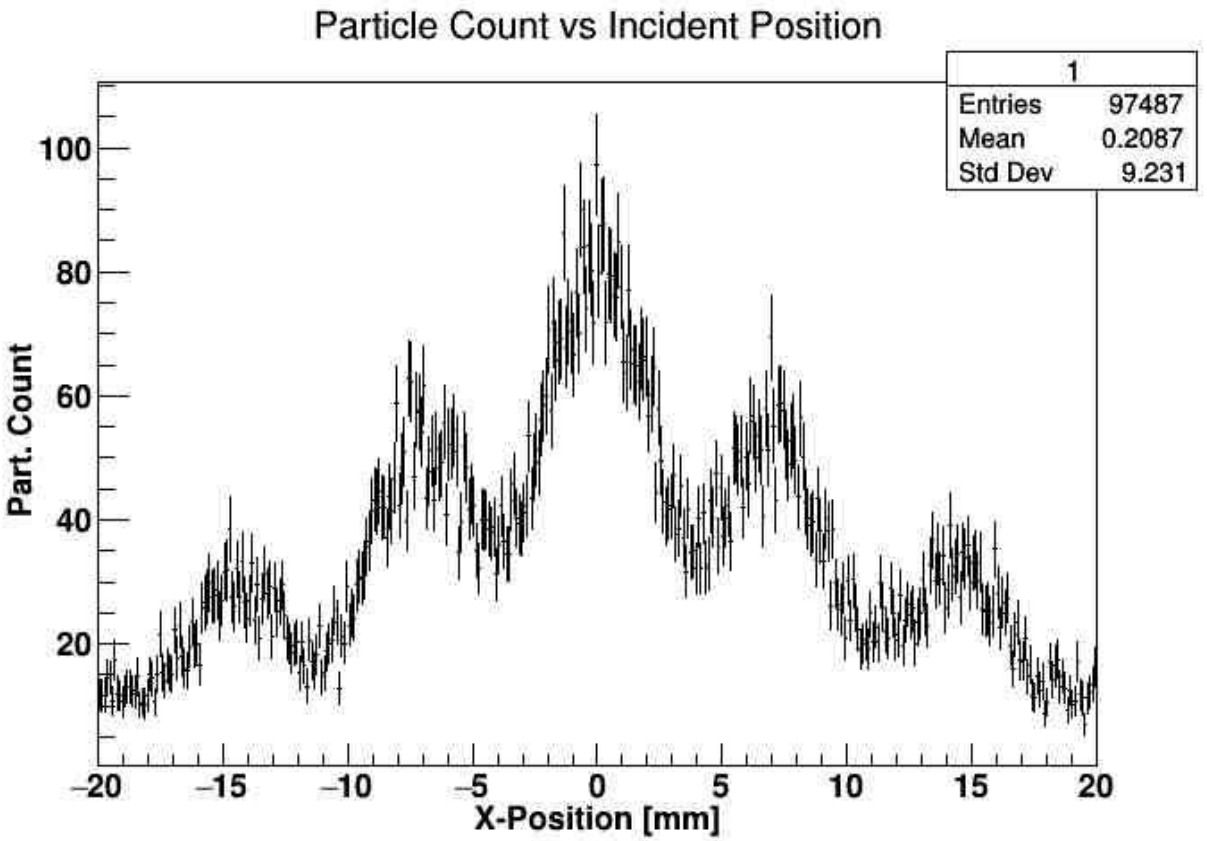

FIGURE 5.45 INCIDENT PARTICLE COUNT VS POSITION (ALONG X DIRECTION) SOURCE AT $Z = 80\ cm$ FROM THE COLLIMATOR WITH $E = 5\ MeV,\ T = 2\ mm$ AND $P = 6\ mm$.

total integral of histo 1: 26400.8

partial integral of histo 1 (first pitch): 4005.13

partial integral of histo 1 (until second pitch): 10453.1

partial integral of histo 1 (until third pitch): 14068.1

contrast ratio of histo 1 (first pitch):24.6495

contrast ratio of histo 1 (until second pitch):64.3337

contrast ratio of histo 1 (until third pitch):86.582

Figure 5.45 has a very good definition of signal in the second and the third areas.

5.3.4 SIMULATION FOR 2 MM THICKNESS AND 3 MM PITCH

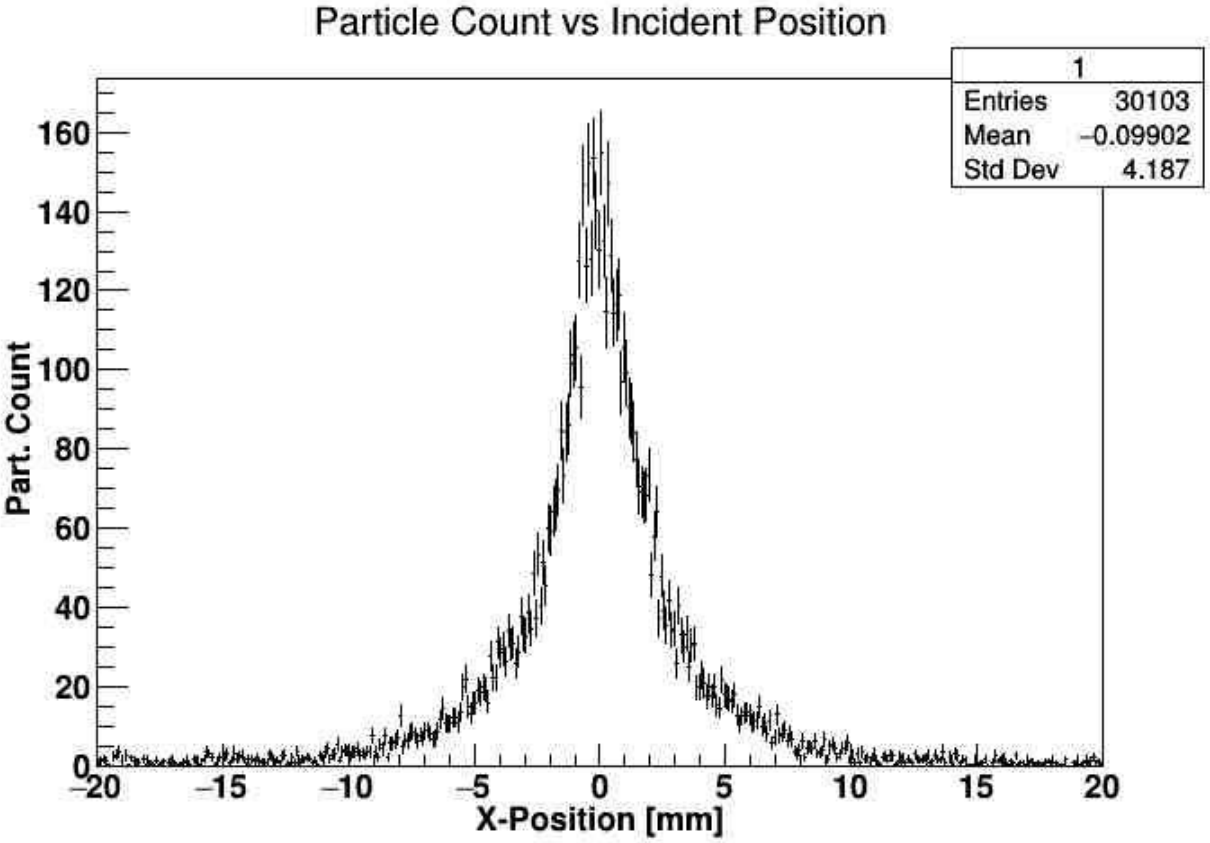

FIGURE 5.46 INCIDENT PARTICLE COUNT VS POSITION (ALONG X DIRECTION) SOURCE AT $Z = 0\ cm$ FROM THE COLLIMATOR WITH $E = 5\ MeV,\ T = 2\ mm$ AND $P = 3\ mm$.

total integral of histo 1: 8483.77

partial integral of histo 1 (first pitch): 3510.98

partial integral of histo 1 (until second pitch): 6414.28

partial integral of histo 1 (until third pitch): 6883.81

contrast ratio of histo 1 (first pitch):38.1184

contrast ratio of histo 1 (until second pitch):69.6392

contrast ratio of histo 1 (until third pitch):74.7368

Figure 5.46 is again the peak centered, although quite different compared to the same parameters for 2 MeV.

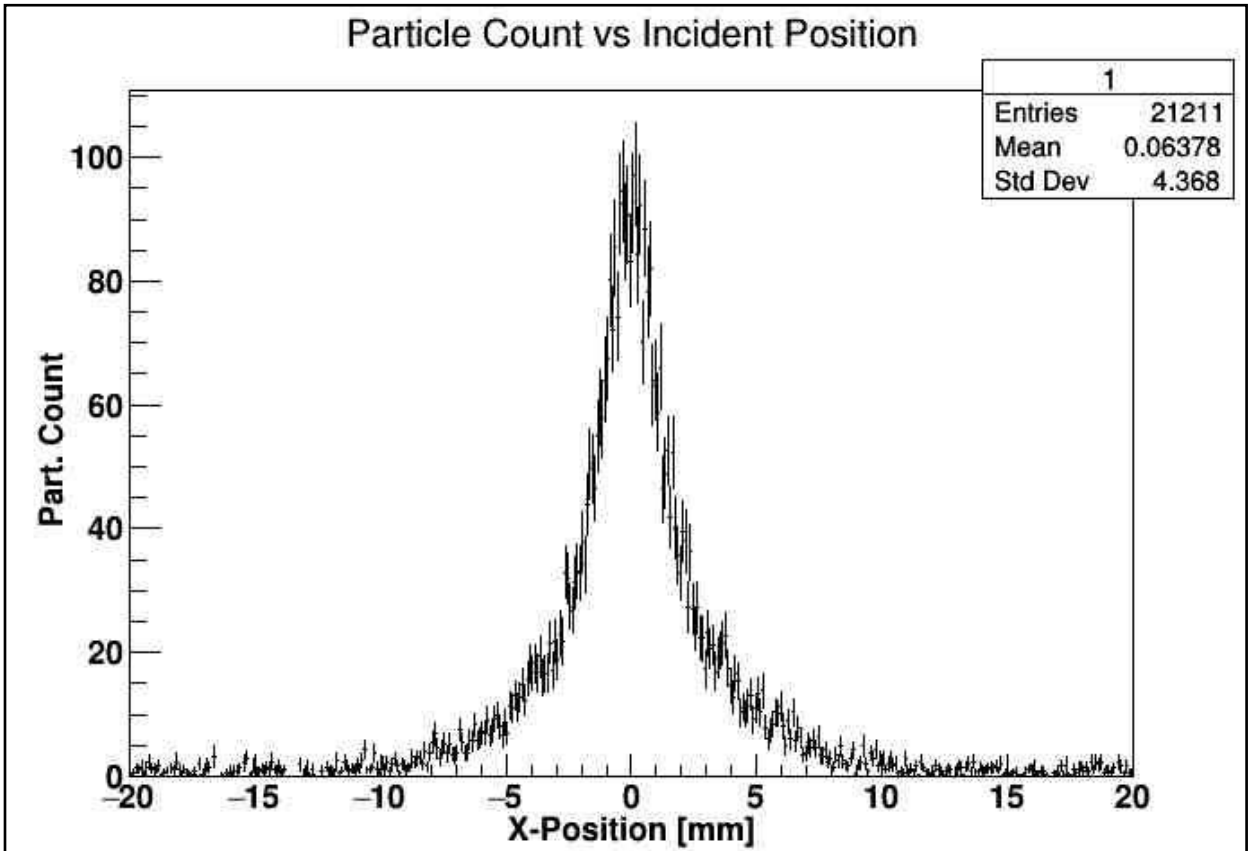

FIGURE 5.47 INCIDENT PARTICLE COUNT VS POSITION (ALONG X DIRECTION) SOURCE AT $Z = 10\ cm$ FROM THE COLLIMATOR WITH $E = 5\ MeV,\ T = 2\ mm$ AND $P = 3\ mm$.

total integral of histo 1: 5814.71

partial integral of histo 1 (first pitch): 2246.77

partial integral of histo 1 (until second pitch): 4057.56

partial integral of histo 1 (until third pitch): 4338.34

contrast ratio of histo 1 (first pitch):29.4642

contrast ratio of histo 1 (until second pitch):53.2109

contrast ratio of histo 1 (until third pitch):56.8932

Figure 5.47 has no changes, except for a small increase in noise around the peak.

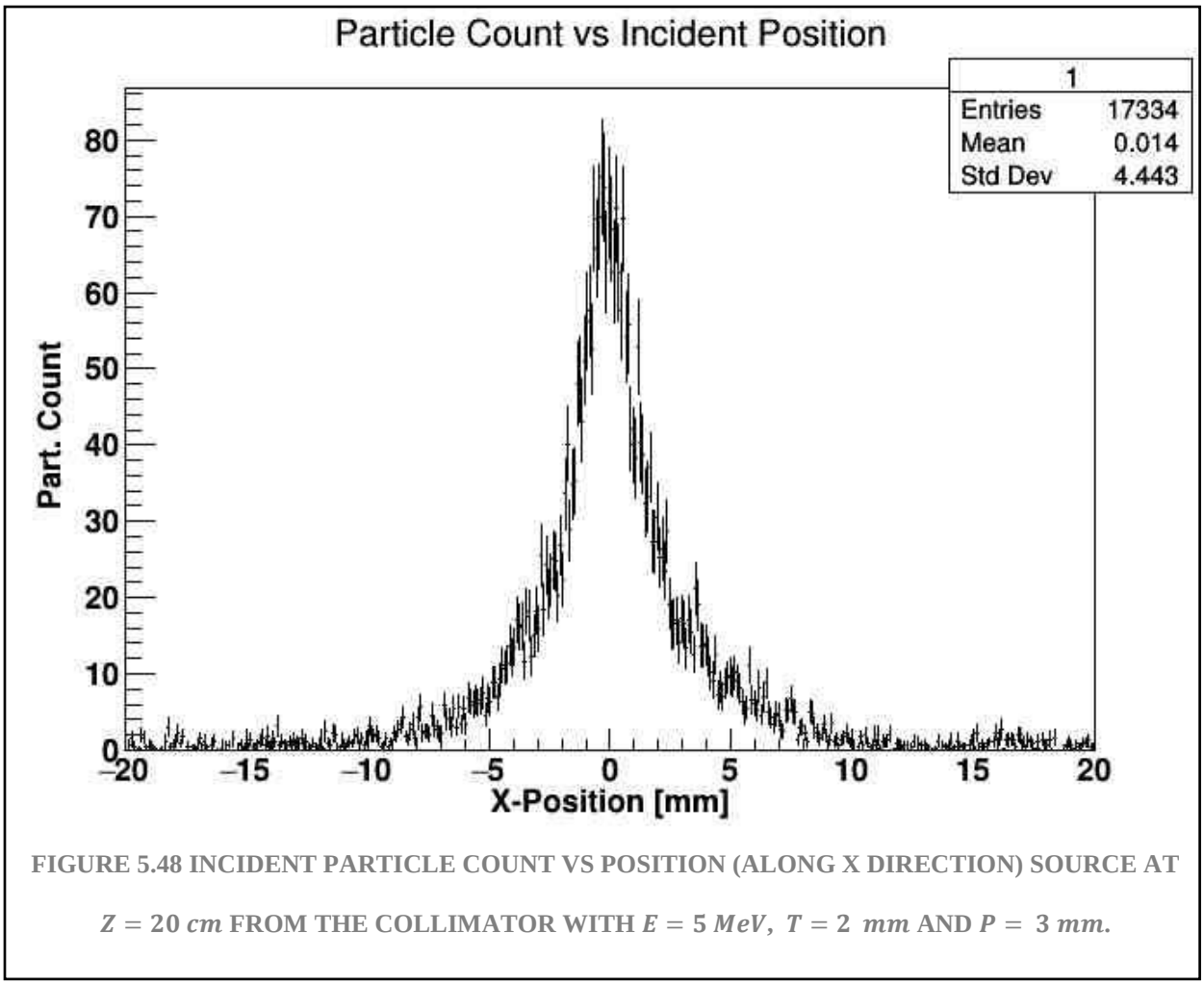

FIGURE 5.48 INCIDENT PARTICLE COUNT VS POSITION (ALONG X DIRECTION) SOURCE AT $Z = 20\ cm$ FROM THE COLLIMATOR WITH $E = 5\ MeV,\ T = 2\ mm$ AND $P = 3\ mm$.

total integral of histo 1: 4696.19

partial integral of histo 1 (first pitch): 1703.94

partial integral of histo 1 (until second pitch): 3117.64

partial integral of histo 1 (until third pitch): 3345.52

contrast ratio of histo 1 (first pitch):24.8646

contrast ratio of histo 1 (until second pitch):45.4939

contrast ratio of histo 1 (until third pitch):48.8192

Figure 5.48 has no change at all, but it doesn't seem so continuous as the last image.

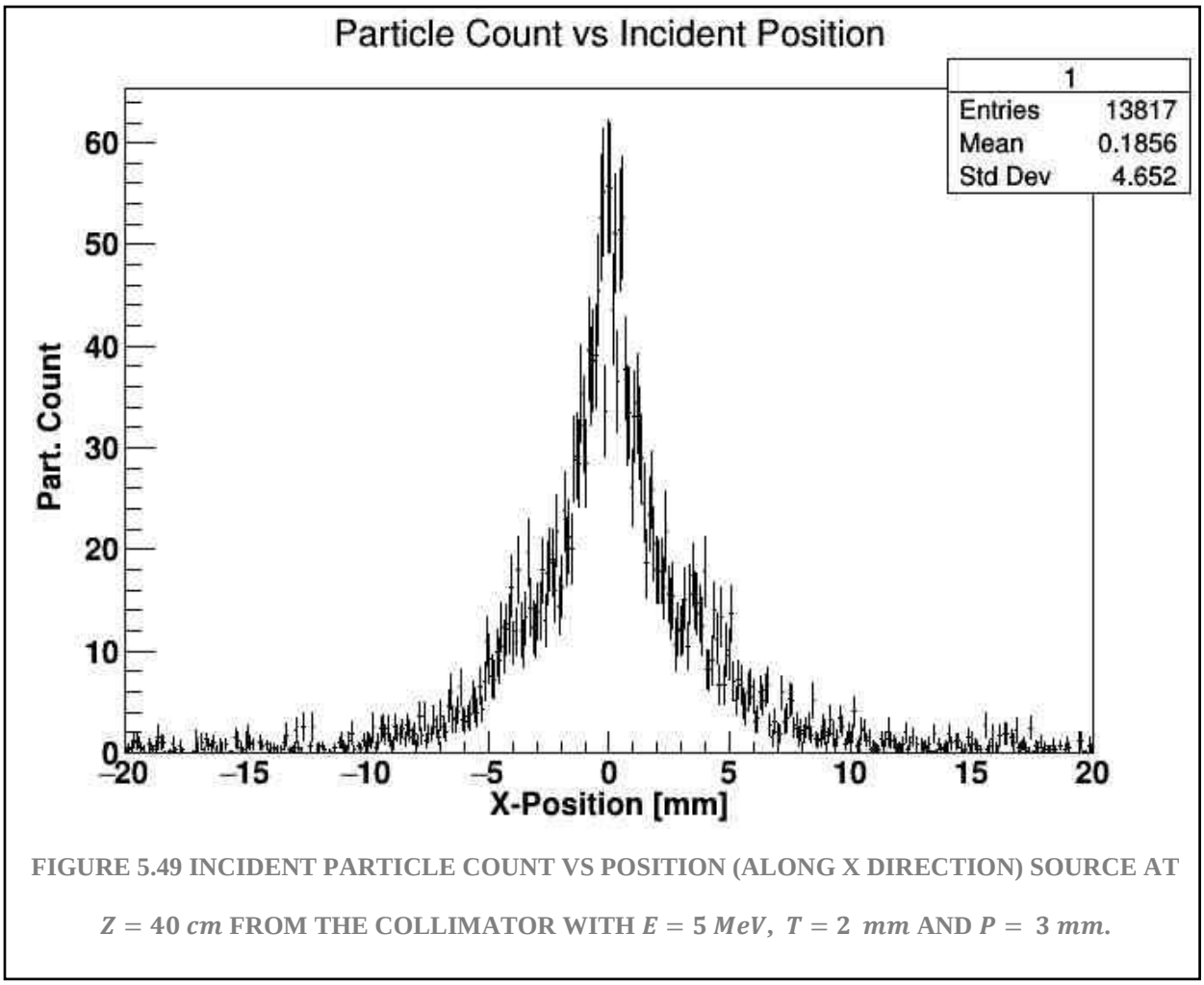

FIGURE 5.49 INCIDENT PARTICLE COUNT VS POSITION (ALONG X DIRECTION) SOURCE AT $Z = 40\ cm$ FROM THE COLLIMATOR WITH $E = 5\ MeV,\ T = 2\ mm$ AND $P = 3\ mm$.

total integral of histo 1: 3668.97

partial integral of histo 1 (first pitch): 1173.55

partial integral of histo 1 (until second pitch): 2335.43

partial integral of histo 1 (until third pitch): 2527.66

contrast ratio of histo 1 (first pitch):19.3744

contrast ratio of histo 1 (until second pitch):38.5562

contrast ratio of histo 1 (until third pitch):41.7298

Figure 5.49, it can be said that is a widening given the signal captured in the second regions.

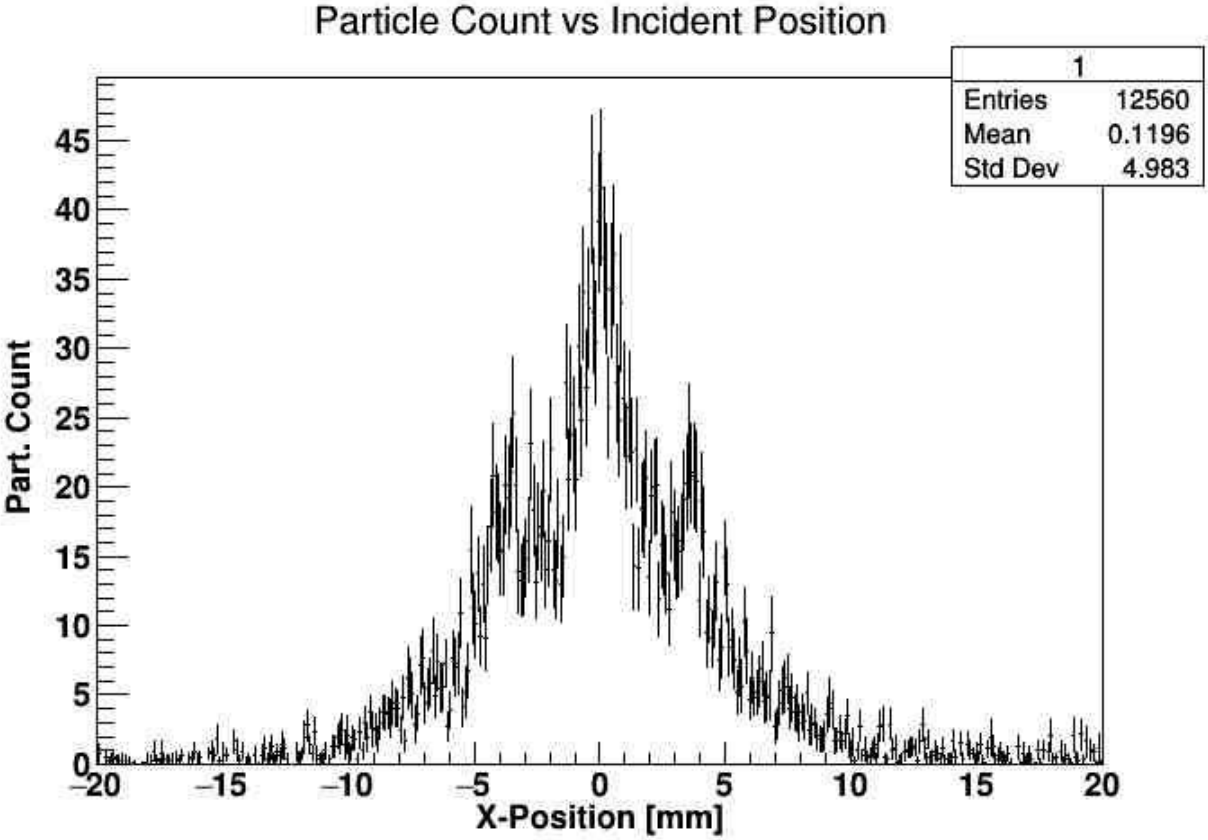

FIGURE 5.50 INCIDENT PARTICLE COUNT VS POSITION (ALONG X DIRECTION) SOURCE AT $Z = 80\ cm$ FROM THE COLLIMATOR WITH $E = 5\ MeV,\ T = 2\ mm$ AND $P = 3\ mm$.

total integral of histo 1: 3482.61

partial integral of histo 1 (first pitch): 868.119

partial integral of histo 1 (until second pitch): 2197.99

partial integral of histo 1 (until third pitch): 2486.23

contrast ratio of histo 1 (first pitch):14.7105

contrast ratio of histo 1 (until second pitch):37.2455

contrast ratio of histo 1 (until third pitch):42.1297

Figure 5.50, now it shows no clue of any other region, compared to the 2 MeV image, it seems the same pattern but intensified.

5.4 RESULTS CHANGING THICKNESS 5 MEV ENERGY

5.4.1 SIMULATION FOR 4 MM PITCH AND 1 MM THICKNESS

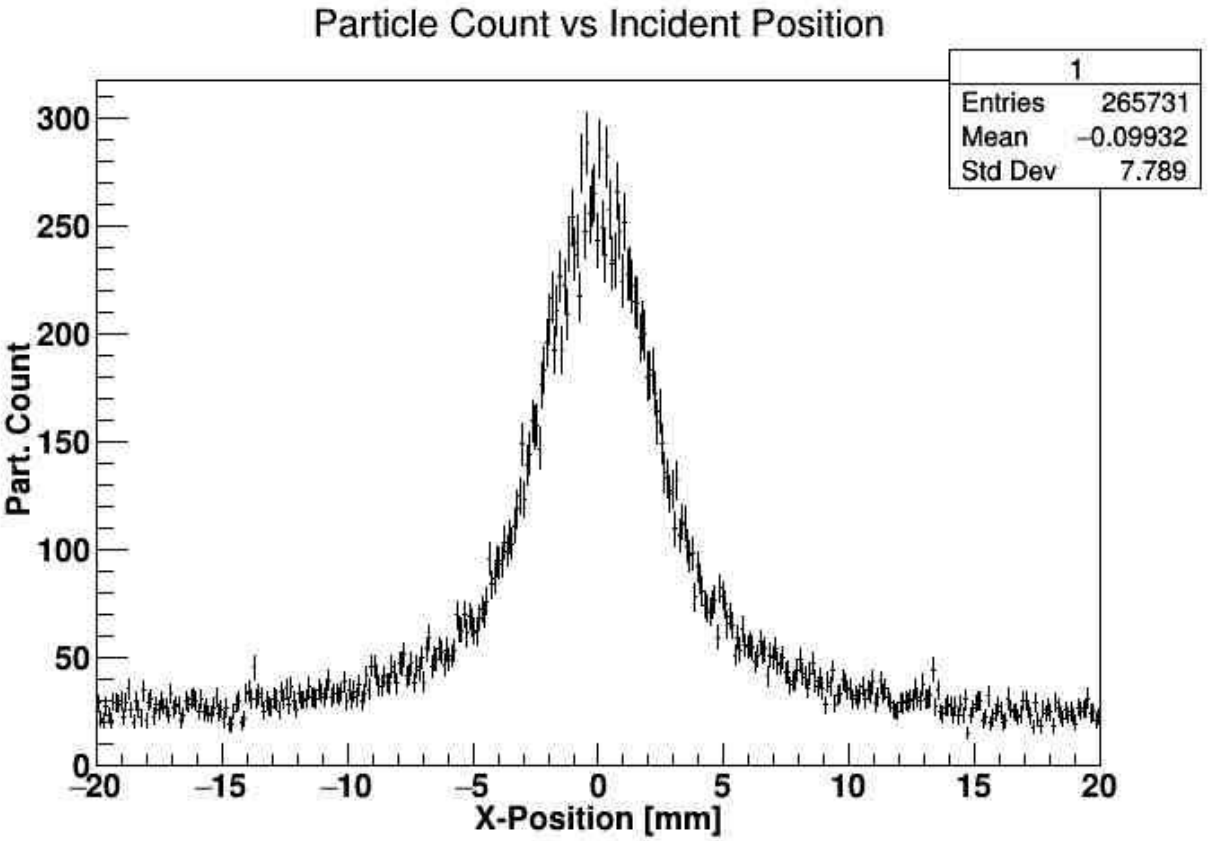

FIGURE 5.51 INCIDENT PARTICLE COUNT VS POSITION (ALONG X DIRECTION) SOURCE AT $Z = 0\ cm$ FROM THE COLLIMATOR WITH $E = 5\ MeV,\ T = 1\ mm$ AND $P = 4\ mm$.

total integral of histo 1: 67962.6

partial integral of histo 1 (first pitch): 9570.54

partial integral of histo 1 (until second pitch): 18463.3

partial integral of histo 1 (until third pitch): 22169.8

contrast ratio of histo 1 (first pitch):36.7114

contrast ratio of histo 1 (until second pitch):70.8228

contrast ratio of histo 1 (until third pitch):85.0406

In Figure 5.51, it can be seen that it allows passing enough gamma particles given the separation of the set.

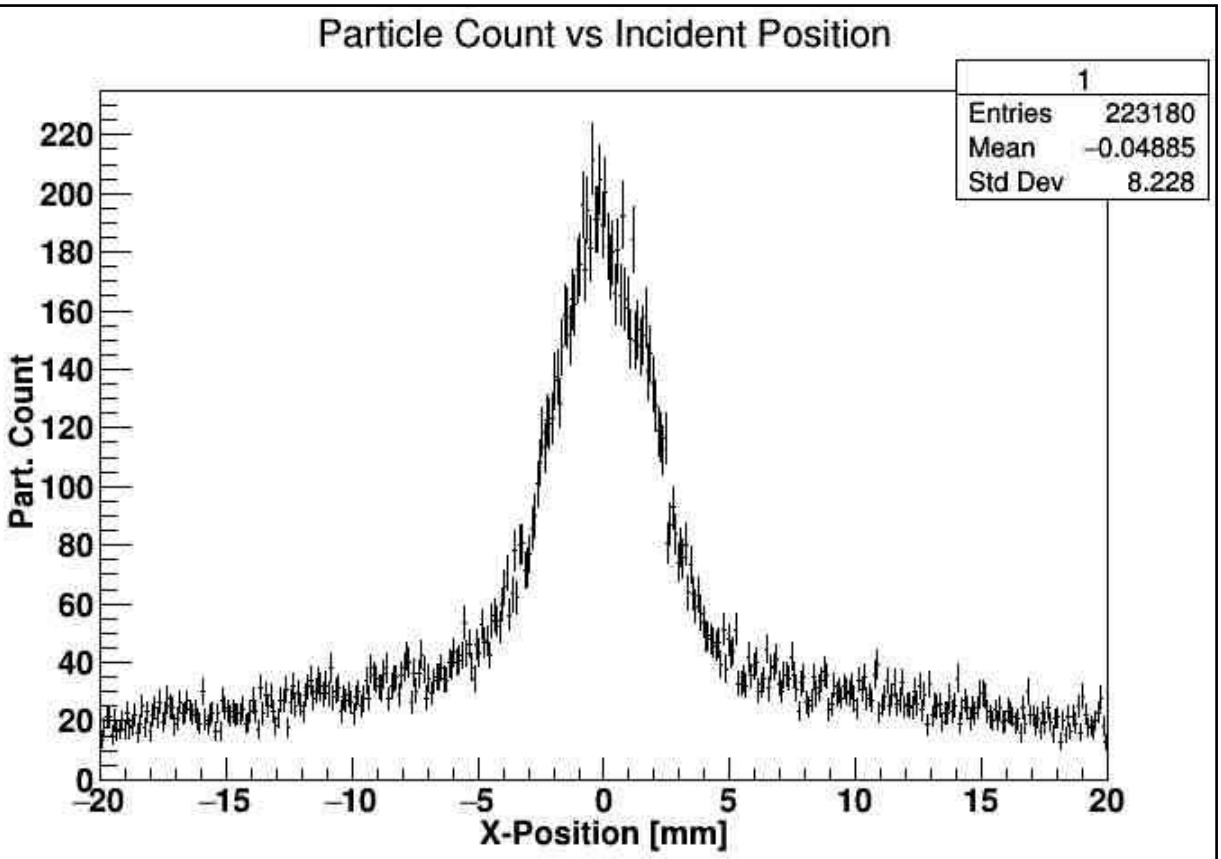

FIGURE 5.52 INCIDENT PARTICLE COUNT VS POSITION (ALONG X DIRECTION) SOURCE AT $Z = 10\ cm$ FROM THE COLLIMATOR WITH $E = 5\ MeV,\ T = 1\ mm$ AND $P = 4\ mm$.

total integral of histo 1: 56839.8

partial integral of histo 1 (first pitch): 6832.21

partial integral of histo 1 (until second pitch): 12685

partial integral of histo 1 (until third pitch): 15801.6

contrast ratio of histo 1 (first pitch):28.6573

contrast ratio of histo 1 (until second pitch):53.2065

contrast ratio of histo 1 (until third pitch):66.2788

Figure 5.52 now shows more signal around it.

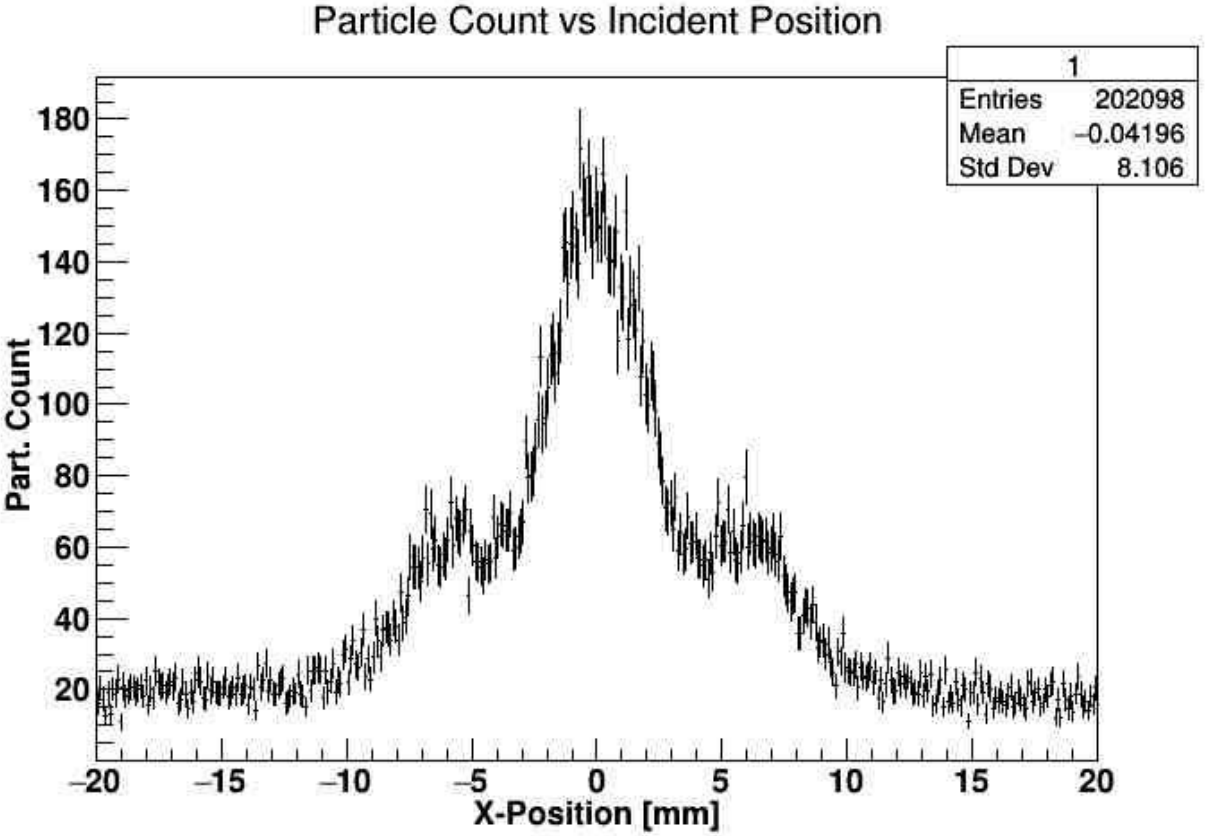

FIGURE 5.53 INCIDENT PARTICLE COUNT VS POSITION (ALONG X DIRECTION) SOURCE AT $Z = 20\ cm$ FROM THE COLLIMATOR WITH $E = 5\ MeV,\ T = 1\ mm$ AND $P = 4\ mm$.

total integral of histo 1: 52065.5

partial integral of histo 1 (first pitch): 5562.27

partial integral of histo 1 (until second pitch): 12192.3

partial integral of histo 1 (until third pitch): 15404.1

contrast ratio of histo 1 (first pitch):24.3768

contrast ratio of histo 1 (until second pitch):53.433

contrast ratio of histo 1 (until third pitch):67.5088

In Figure 5.53 it is sufficient to say that the two signal regions are active and have an extra height, compared with the graph of the same parameters but with the energy of 2 MeV.

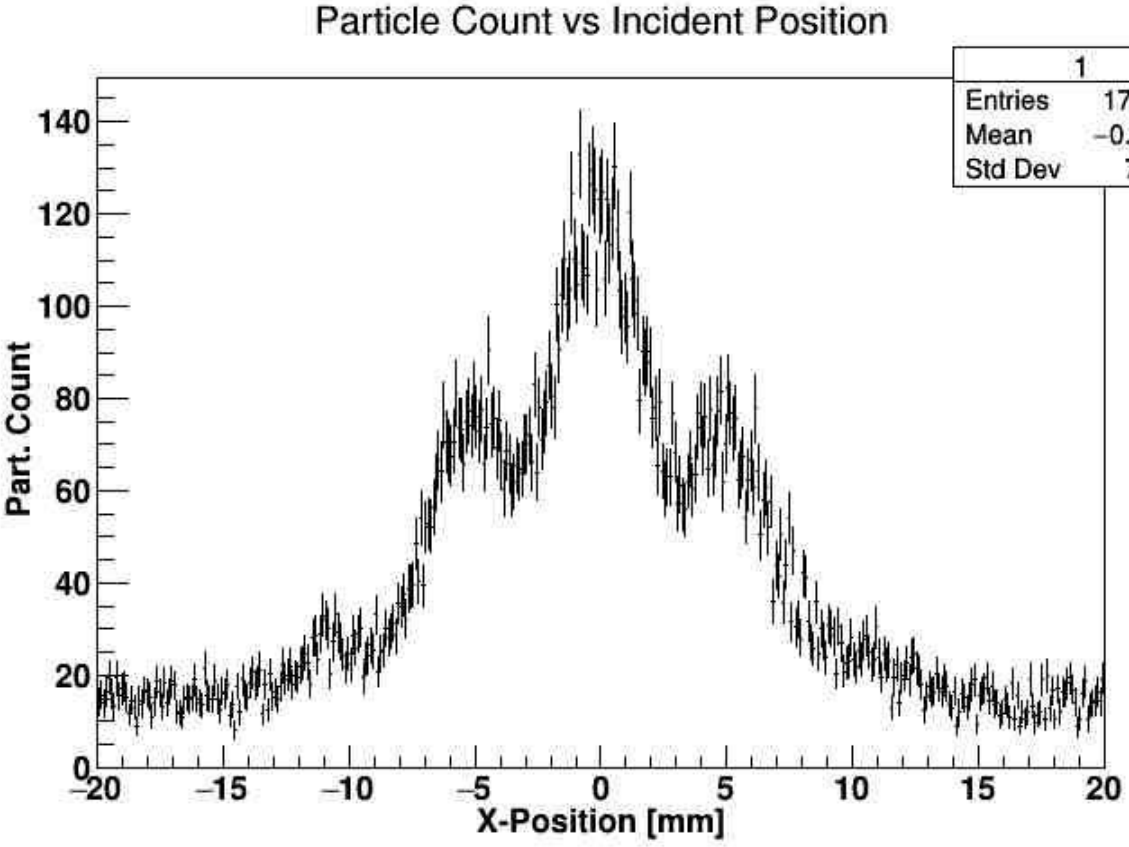

FIGURE 5.54 INCIDENT PARTICLE COUNT VS POSITION (ALONG X DIRECTION) SOURCE AT $Z = 40\ cm$ FROM THE COLLIMATOR WITH $E = 5\ MeV,\ T = 1\ mm$ AND $P = 4\ mm$.

total integral of histo 1: 44661.2

partial integral of histo 1 (first pitch): 4348.9

partial integral of histo 1 (until second pitch): 11099.9

partial integral of histo 1 (until third pitch): 13973.6

contrast ratio of histo 1 (first pitch):20.5785

contrast ratio of histo 1 (until second pitch):52.5236

contrast ratio of histo 1 (until third pitch):66.1214

Figure 5.54 has again the first two zones capturing signal and some noise at the sides.

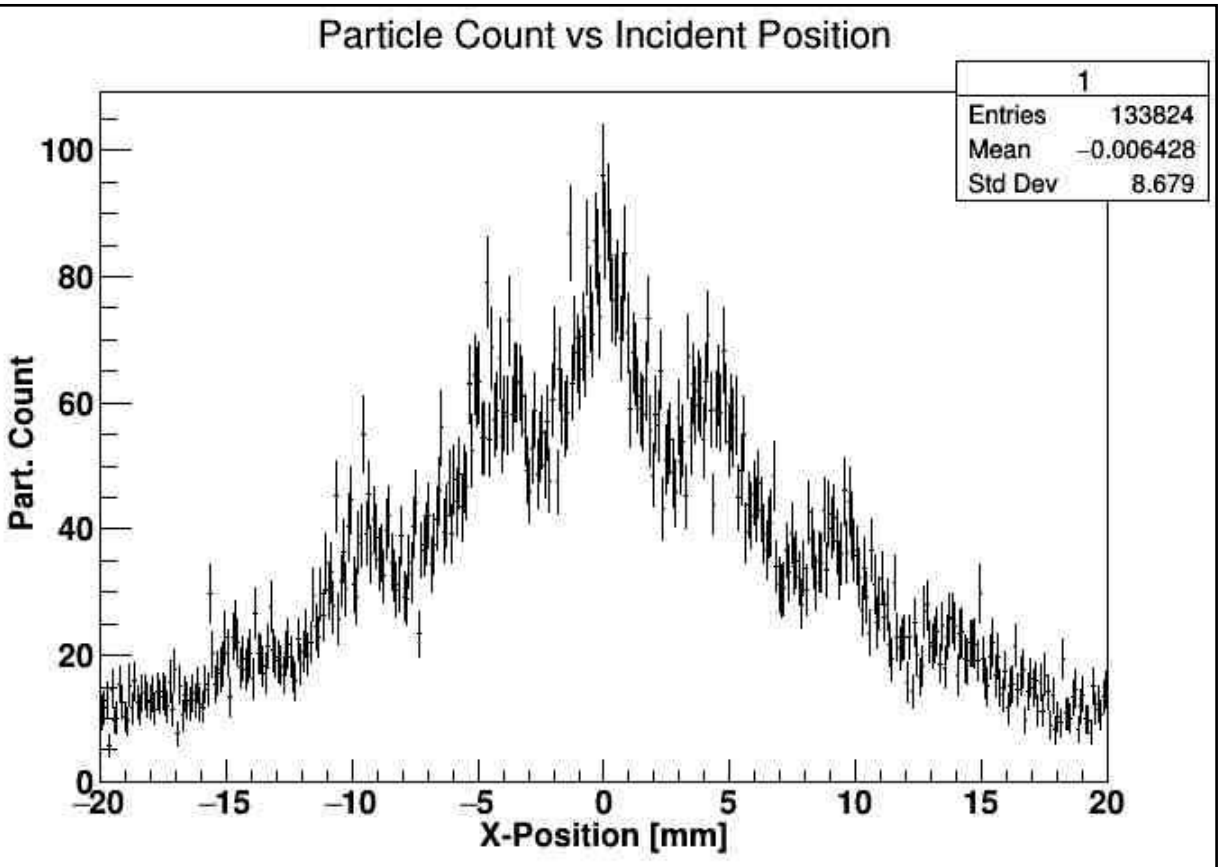

FIGURE 5.55 INCIDENT PARTICLE COUNT VS POSITION (ALONG X DIRECTION) SOURCE AT $Z = 80\ cm$ FROM THE COLLIMATOR WITH $E = 5\ MeV,\ T = 1\ mm$ AND $P = 4\ mm$.

total integral of histo 1: 35444.6

partial integral of histo 1 (first pitch): 2885.14

partial integral of histo 1 (until second pitch): 8160.45

partial integral of histo 1 (until third pitch): 11480.1

contrast ratio of histo 1 (first pitch):15.3247

contrast ratio of histo 1 (until second pitch):43.345

contrast ratio of histo 1 (until third pitch):60.9777

Figure 5.55 is very interesting because it looks like a mountain not very pronounced.

5.4.2 SIMULATION FOR 4 MM PITCH AND 3 MM THICKNESS

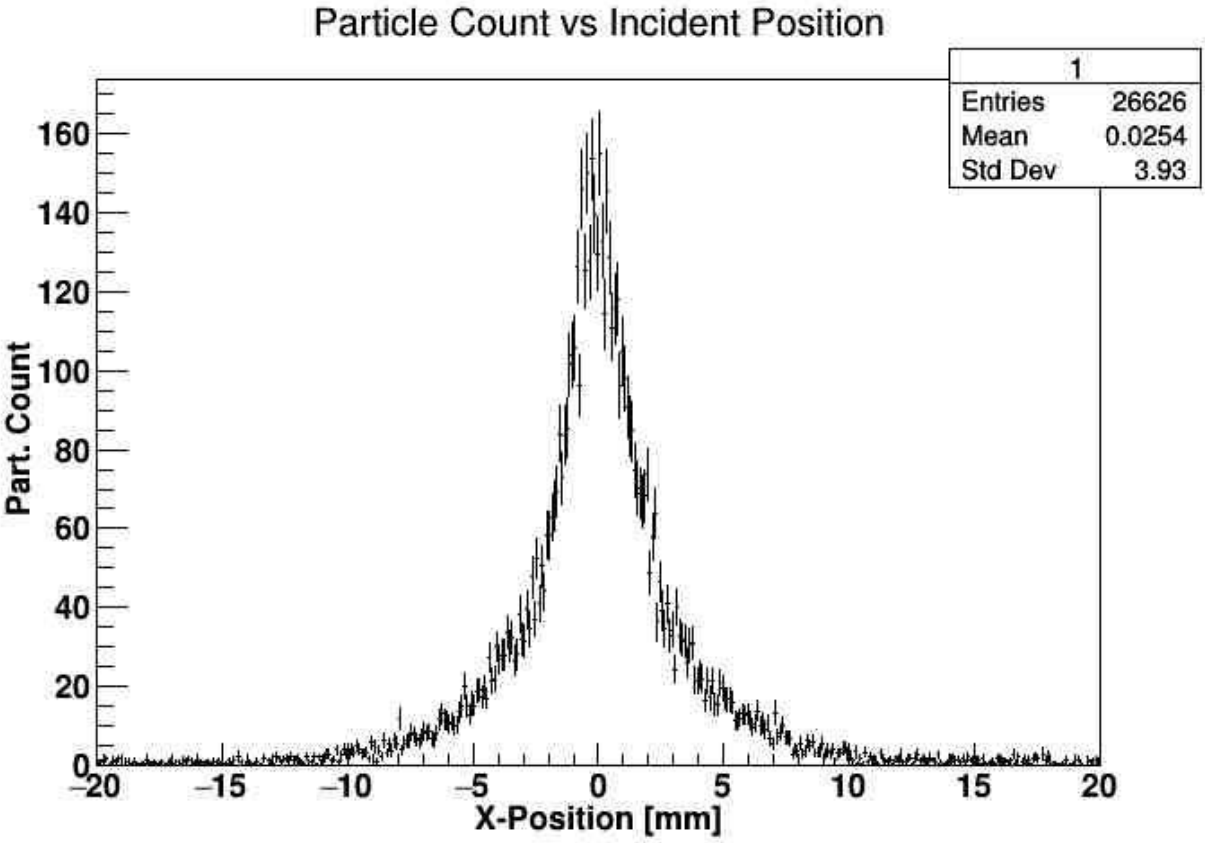

FIGURE 5.56 INCIDENT PARTICLE COUNT VS POSITION (ALONG X DIRECTION) SOURCE AT $Z = 0\ cm$ FROM THE COLLIMATOR WITH $E = 5\ MeV,\ T = 3\ mm$ AND $P = 4\ mm$.

total integral of histo 1: 7754.27

partial integral of histo 1 (first pitch): 4151

partial integral of histo 1 (until second pitch): 6658.25

partial integral of histo 1 (until third pitch): 6875.44

contrast ratio of histo 1 (first pitch):47.1392

contrast ratio of histo 1 (until second pitch):75.6118

contrast ratio of histo 1 (until third pitch):78.0782

Figure 5.56 is again the peak centered.

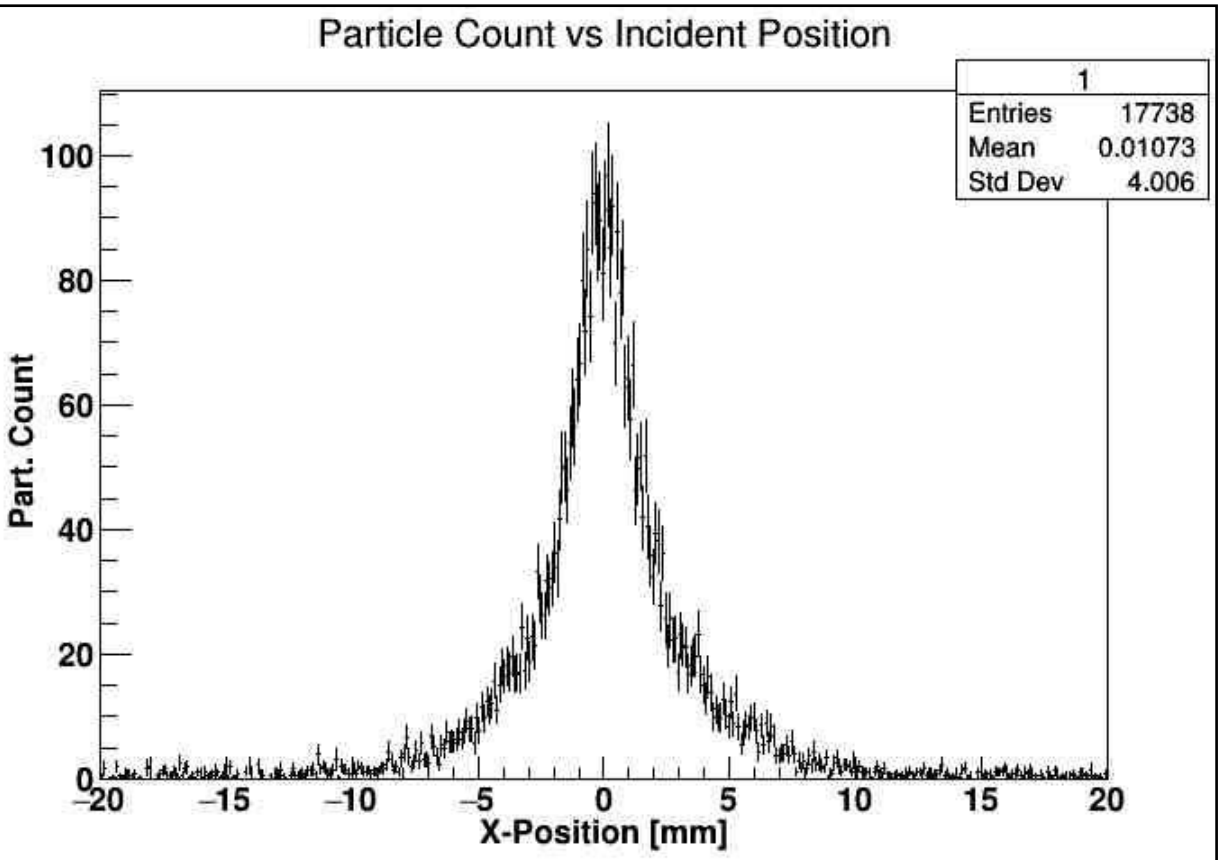

FIGURE 5.57 INCIDENT PARTICLE COUNT VS POSITION (ALONG X DIRECTION) SOURCE AT $Z = 10\ cm$ FROM THE COLLIMATOR WITH $E = 5\ MeV,\ T = 3\ mm$ AND $P = 4\ mm.$

total integral of histo 1: 7754.27

partial integral of histo 1 (first pitch): 4151

partial integral of histo 1 (until second pitch): 6658.25

partial integral of histo 1 (until third pitch): 6875.44

contrast ratio of histo 1 (first pitch):47.1392

contrast ratio of histo 1 (until second pitch):75.6118

contrast ratio of histo 1 (until third pitch):78.0782

Figure 5.57 seems to be the same as the previous one, but with a slower signal in the central peak.

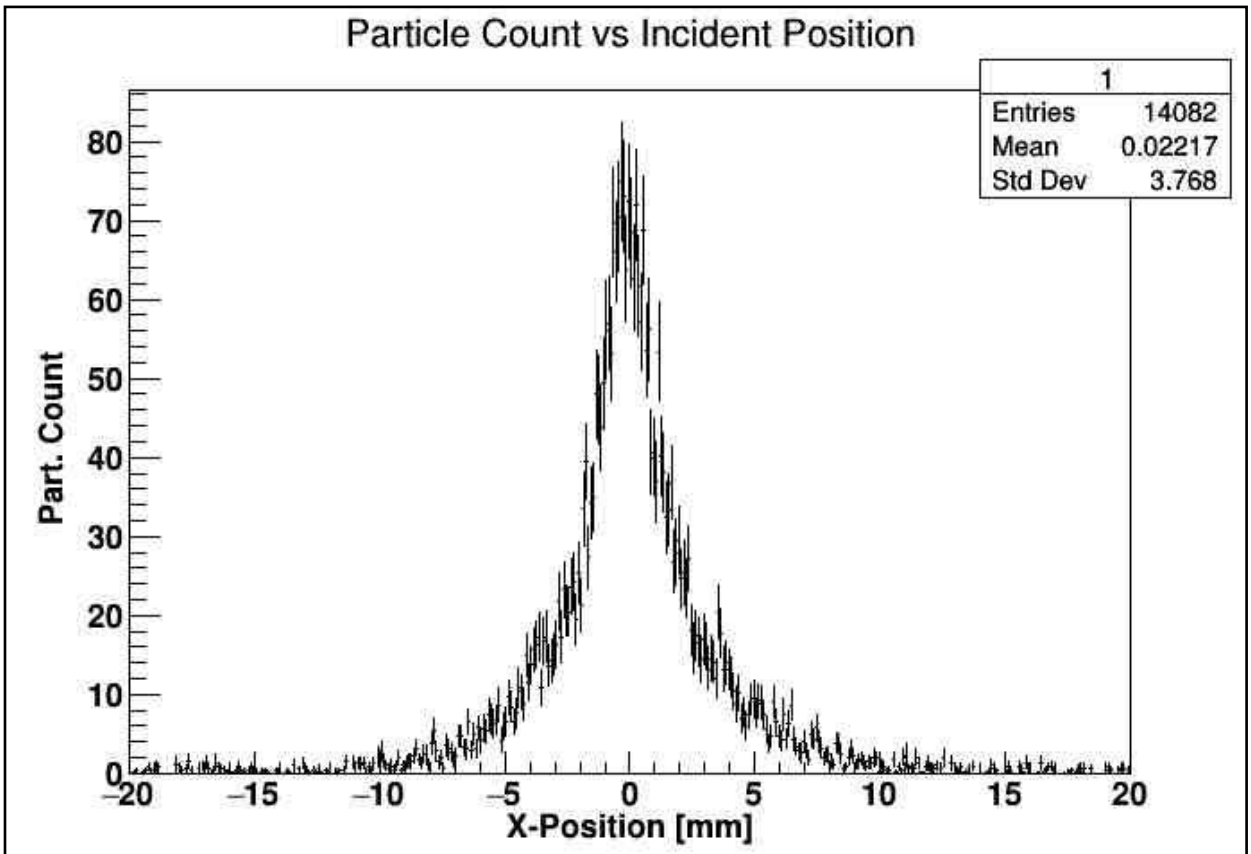

FIGURE 5.58 INCIDENT PARTICLE COUNT VS POSITION (ALONG X DIRECTION) SOURCE AT $Z = 20\ cm$ FROM THE COLLIMATOR WITH $E = 5\ MeV,\ T = 3\ mm$ AND $P = 4\ mm$.

total integral of histo 1: 3995.98

partial integral of histo 1 (first pitch): 1997.99

partial integral of histo 1 (until second pitch): 3192.8

partial integral of histo 1 (until third pitch): 3280.6

contrast ratio of histo 1 (first pitch):31.6069

contrast ratio of histo 1 (until second pitch):50.508

contrast ratio of histo 1 (until third pitch):51.8969

Figure 5.58 shows again no changes, it is because of its separation of 1 mm.

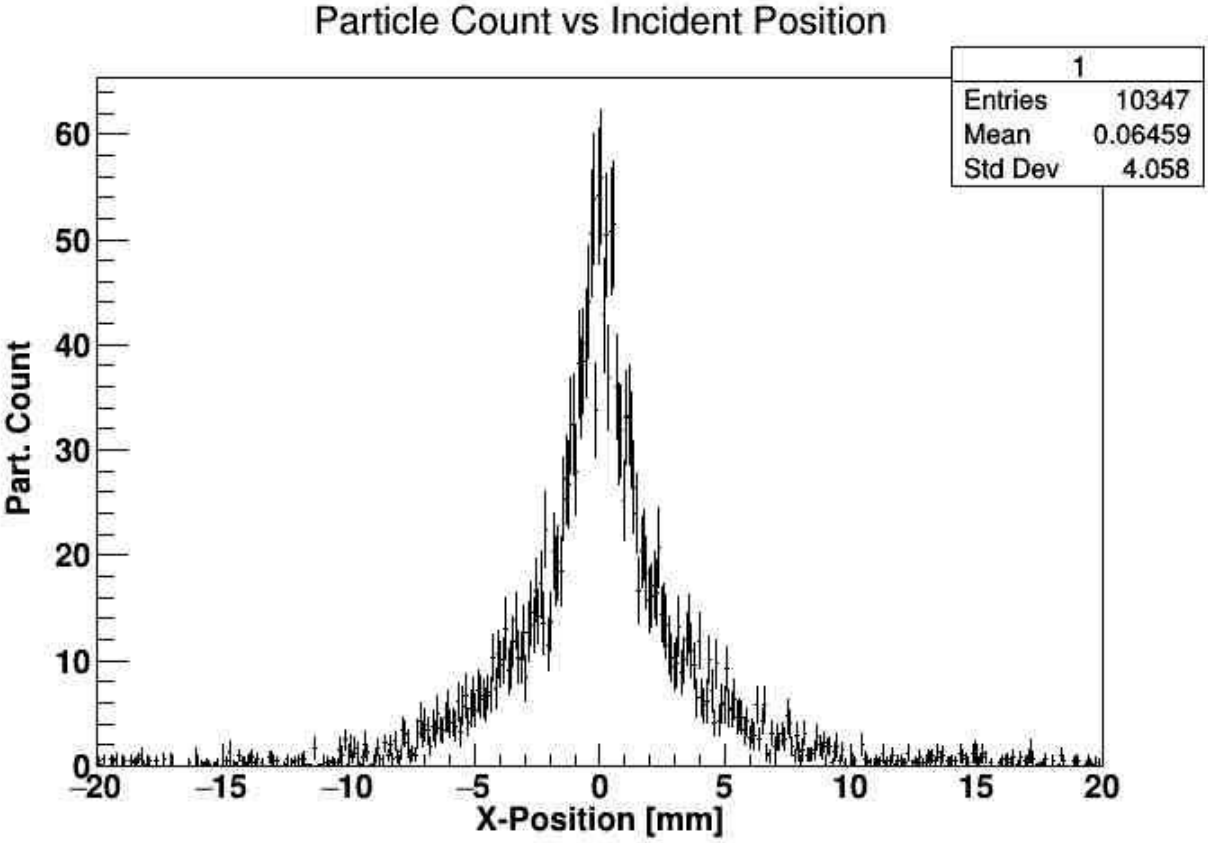

FIGURE 5.59 INCIDENT PARTICLE COUNT VS POSITION (ALONG X DIRECTION) SOURCE AT $Z = 40\ cm$ FROM THE COLLIMATOR WITH $E = 5\ MeV,\ T = 3\ mm$ AND $P = 4\ mm$.

total integral of histo 1: 2864.15

partial integral of histo 1 (first pitch): 1315.86

partial integral of histo 1 (until second pitch): 2199.51

partial integral of histo 1 (until third pitch): 2274.03

contrast ratio of histo 1 (first pitch):24.5874

contrast ratio of histo 1 (until second pitch):41.0987

contrast ratio of histo 1 (until third pitch):42.491

Figure 5.59 doesn't have changes at all, except for the reduction of gamma count in the central peak.

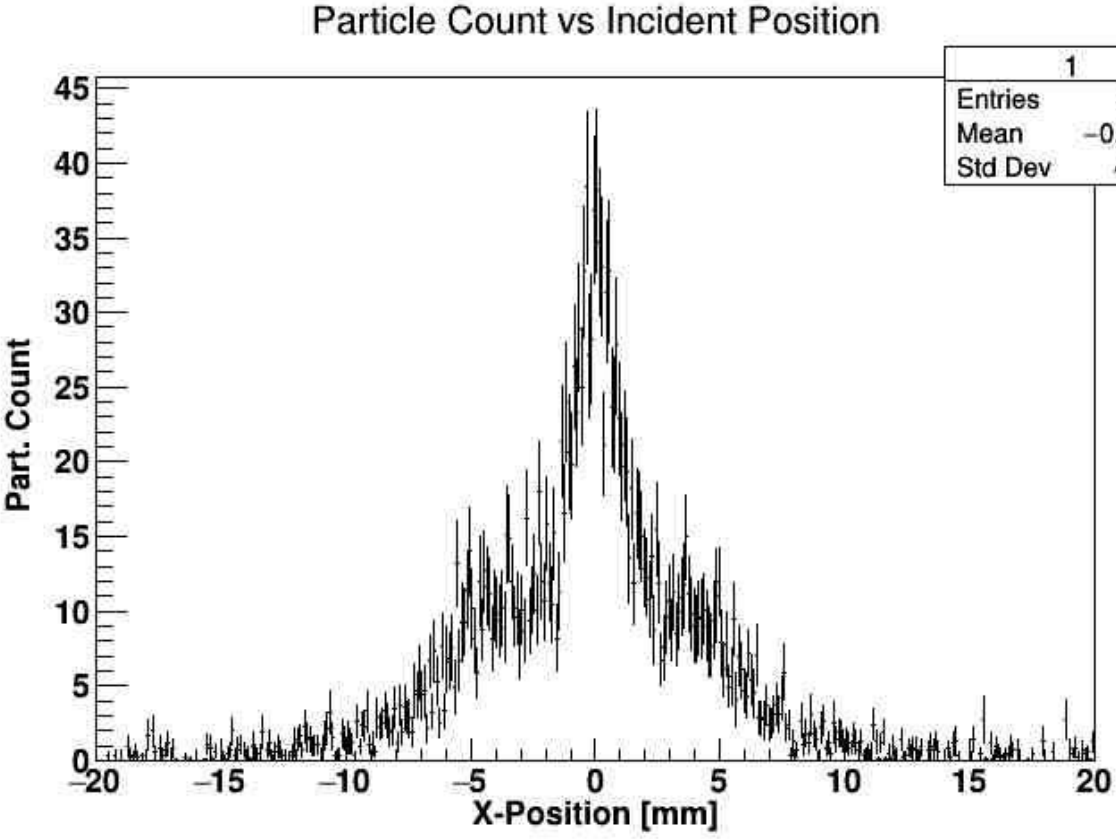

FIGURE 5.60 INCIDENT PARTICLE COUNT VS POSITION (ALONG X DIRECTION) SOURCE AT $Z = 80\ cm$ FROM THE COLLIMATOR WITH $E = 5\ MeV,\ T = 3\ mm$ AND $P = 4\ mm$.

total integral of histo 1: 2485.84

partial integral of histo 1 (first pitch): 905.966

partial integral of histo 1 (until second pitch): 1872.52

partial integral of histo 1 (until third pitch): 1992.82

contrast ratio of histo 1 (first pitch):18.1709

contrast ratio of histo 1 (until second pitch):37.5569

contrast ratio of histo 1 (until third pitch):39.9697

Figure 5.60 has the signal in the second region, it is to be observed that there is no noise around the measurements, even though it has an energy of 5 MeV.

5.5 ANALYSIS OF THE PREVIOUS DATA

5.5.1 ANALYSIS FOR ENERGY WITH 2 MEV

The analysis was made with the distances between the source and the collimator as the x-axis (Z= 0 cm, 10 cm, 20 cm, 40 cm and 80 cm), and the y-axis is the contrast to ratio (CNR) that is defined in section 4.3, at the top of each graph will be the parameters of the simulation such as, pitch (p), thickness (t) and energy (E); the data collection will be placed in the respective areas of the detector, where area 1 will be the first zone of the detector (central zone) and so forth.

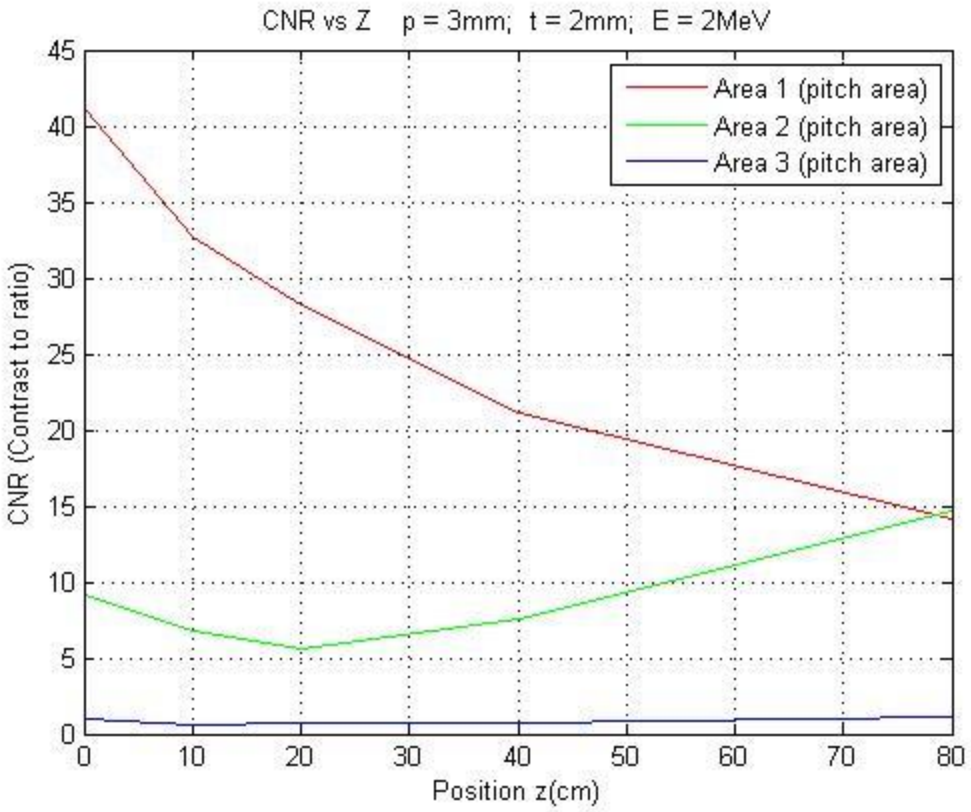

FIGURE 5.61 CNR VS POSITION (ALONG Z DIRECTION) FOR P=3 MM, T=2 MM E=2 MEV

Figure 5.61 shows a natural drop of the signal in the central (first) area, like any radial source, but the interesting thing happens when the second area or second zone capture more signal than its previous measurements, on the other hand, the third area for this case is almost null, meaning that it filters all signals except the first two zones.

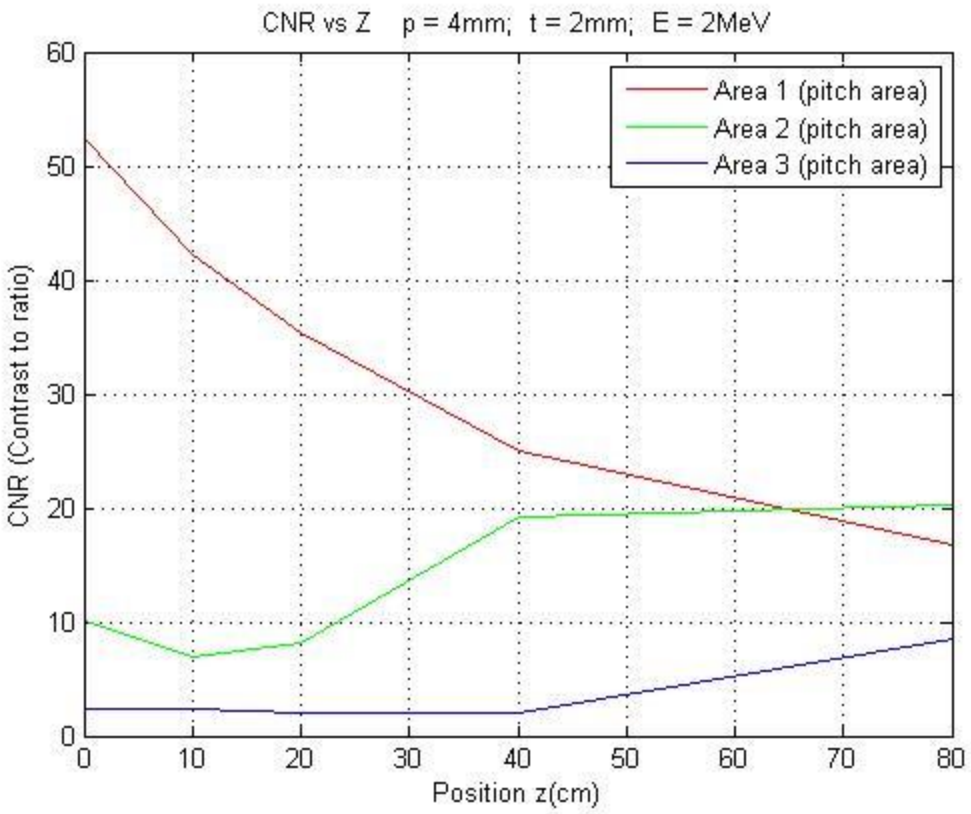

FIGURE 5.62 CNR VS POSITION (ALONG Z DIRECTION) FOR P=4 MM, T=2 MM E=2 MEV

Figure 5.62 will be our starting point to compare the graphs unless some other is mentioned. This is selected given the symmetry that it has in pitch and thickness. The above graph shows again a natural drop in the first area as is expected, but the signal of the second area shows a more pronounced growth between 20 and 40 cm, it is also observed that increases the signal capture between 40 cm and 80 cm. it is also interesting to see the crossing of the signals captured in the first and second zones.

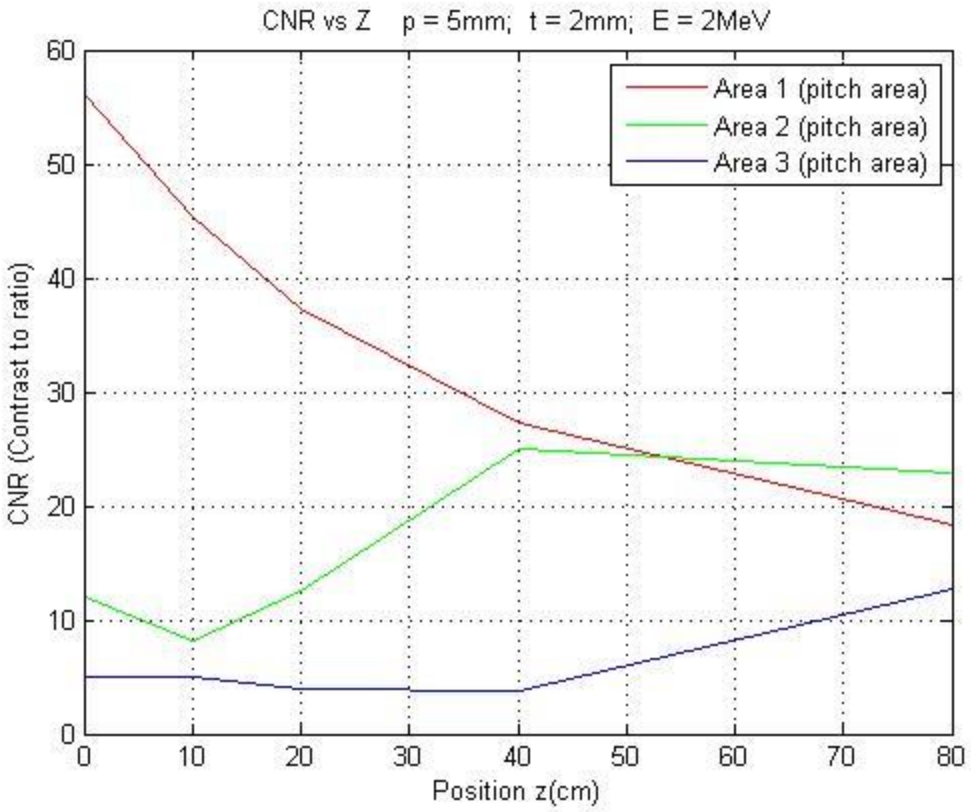

FIGURE 5.63 CNR VS POSITION (ALONG Z DIRECTION) FOR P=5 MM, T=2 MM E=2 MEV

Figure 5.63 shows again the drop behavior for the first zone, but the interesting thing happens when the first and second area intersects at a shorter distance (between 50 and 60 cm), and the third zone illustrates a notorious increase of signal in 80 cm.

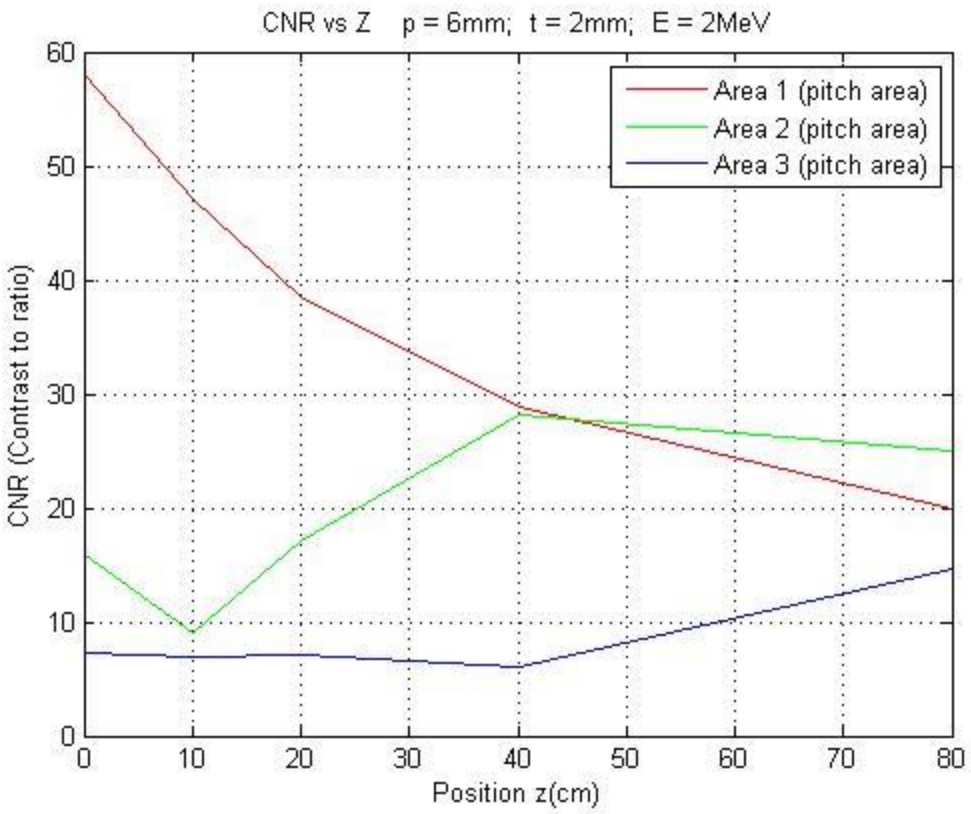

FIGURE 5.64 CNR VS POSITION (ALONG Z DIRECTION) FOR P=6 MM, T=2 MM E=2 MEV

From now on, I will not say the trivial, Figure 5.64 now shows an intersection at a smaller distance than the Figure 5.63, and again an increase in the signal in the third zone, highlighting more the point at 80 cm. The third zone has a higher signal due to the interspacing of the collimator (4 mm).

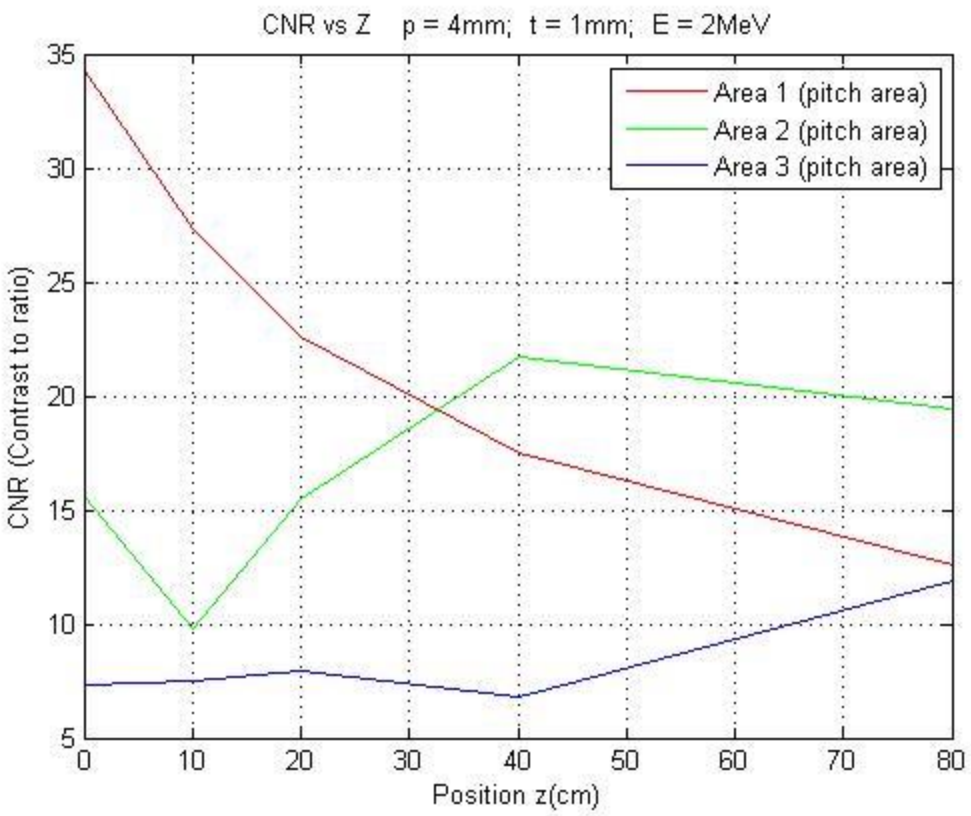

FIGURE 5.65 CNR VS POSITION (ALONG Z DIRECTION) FOR P=4 MM, T=1 MM E=2 MEV

Figure 5.65 has a different nature in the second zone, it can be clearly seen that it has an increased signal at 40 cm not seen before, although is known that it has a spacing of 3 mm as Figure 5.63, so it displays some similarity and does it for 5.64. An important matter here is that the third region in 80 cm shows that the first zone and the third zone have almost the same CNR or signal.

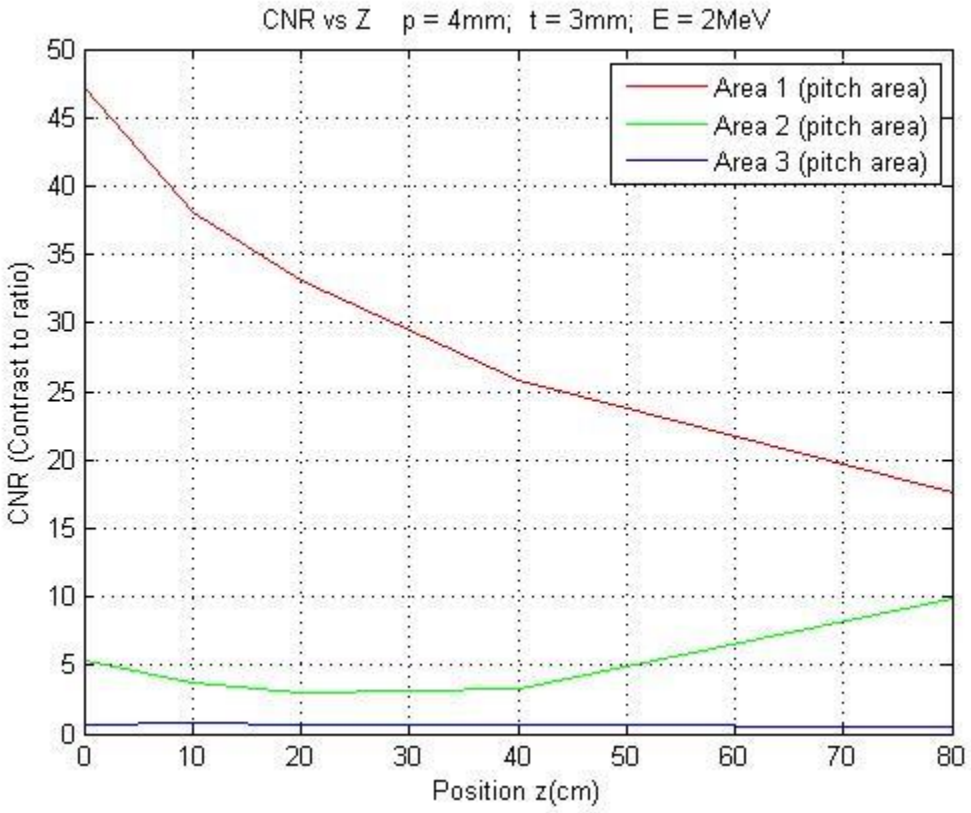

FIGURE 5.66 CNR VS POSITION (ALONG Z DIRECTION) FOR P=4 MM, T=3 MM E=2 MEV

Figure 5.66 has a spacing of 1 mm as Figure 5.61, which displays the same CNR for the third area, and so similar for the first area, and despite having a small amount, the second areas are similar, although with a smaller amount of CNR.

5.5.2 ANALYSIS FOR ENERGY WITH 5 MEV

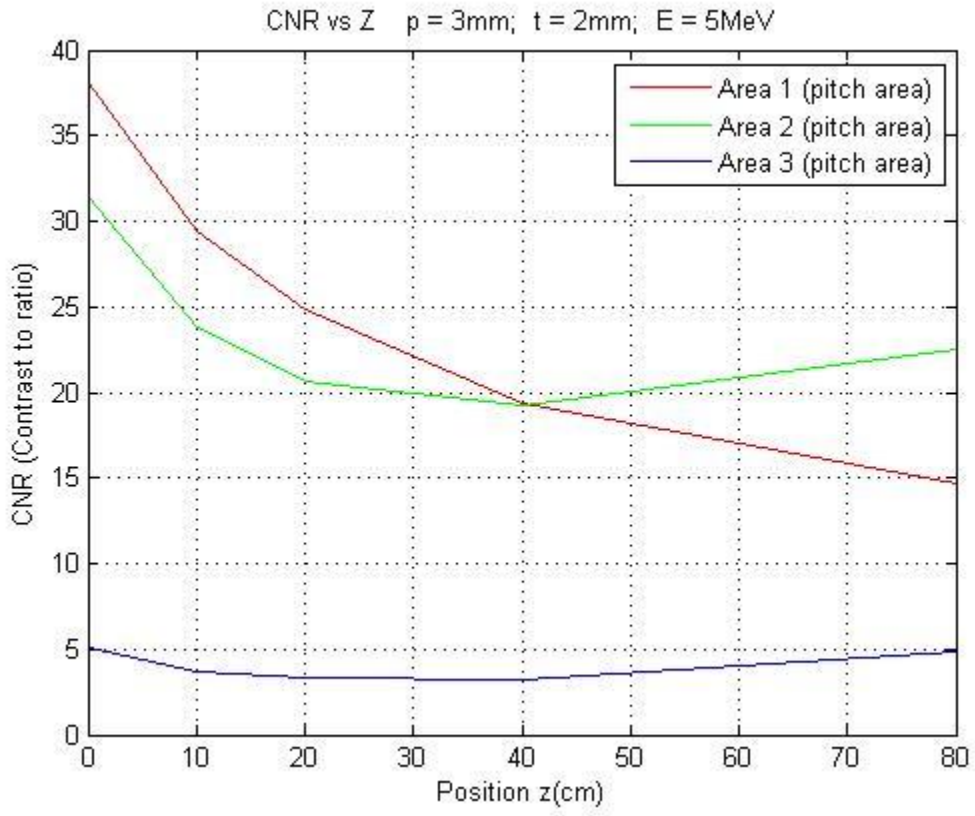

FIGURE 5.67 CNR VS POSITION (ALONG Z DIRECTION) FOR P=3 MM, T=2 MM E=5 MEV

Figure 5.67 has a new behavior, it can be seen just by comparing with Figure 5.61 that those are not equal. For some reason, there is a large quantity of signal in the second area. There is a non-small signal for the third area (compared to the same figure).

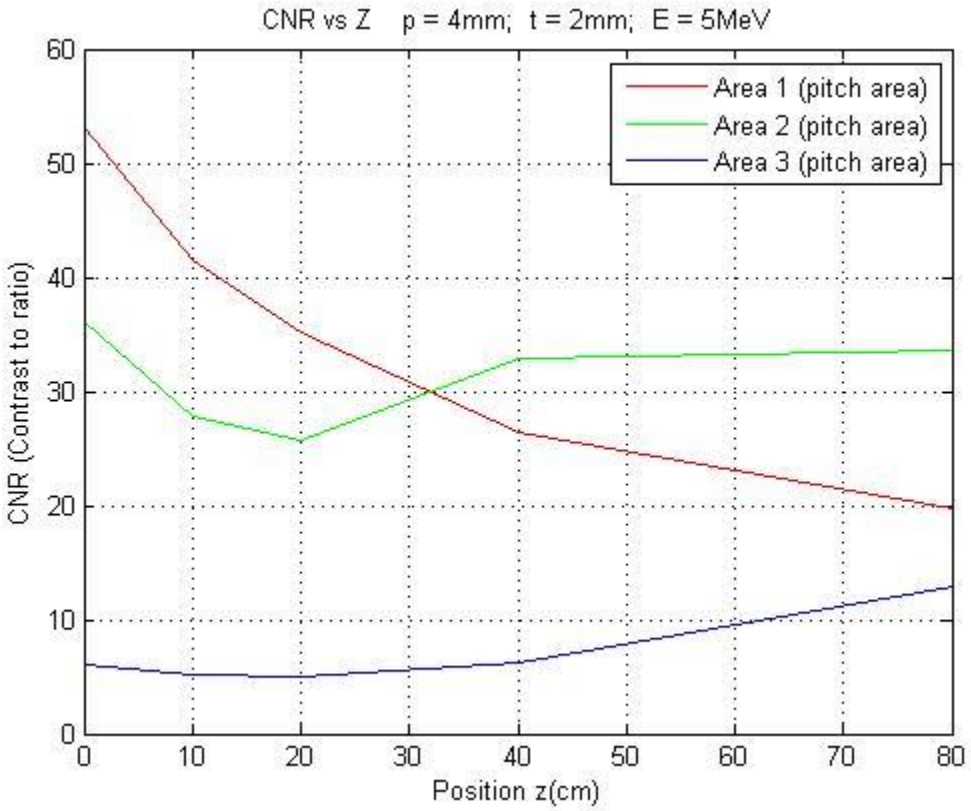

FIGURE 5.68 CNR VS POSITION (ALONG Z DIRECTION) FOR P=4 MM, T=2 MM E=5 MEV

Figure 5.68 looks more like Figure 5.62 (E=2 MeV), which displays a similar behavior but with different CNR for the second and third area (not so different from the first area).

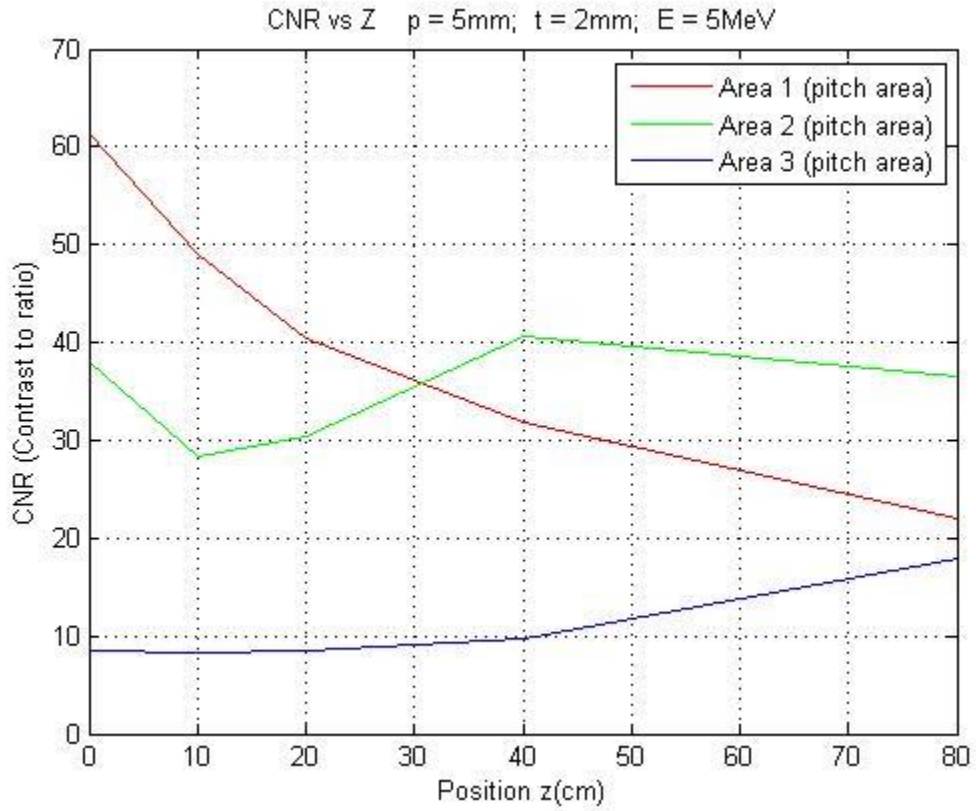

FIGURE 5.69 CNR VS POSITION (ALONG Z DIRECTION) FOR P=5 MM, T=2 MM E=5 MEV

Figure 5.69 has a resemblance to Figure 5.63, although with a phase shift for the second area and a slightly different increase for the third area. Being clear, those must have a higher height in CNR only for the energy, but apparently, it is not so for the first zone.

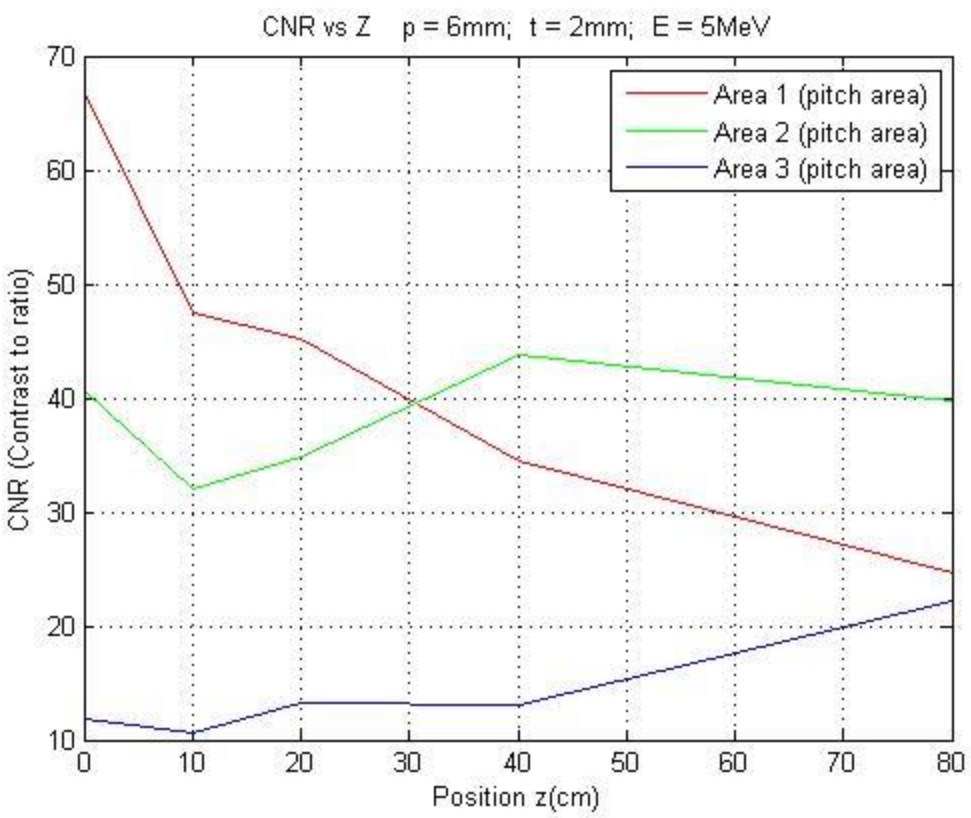

FIGURE 5.70 CNR VS POSITION (ALONG Z DIRECTION) FOR P=6 MM, T=2 MM E=5 MEV

Figure 5.70 has a different behavior for the first area between 20 and 40 cm, which is very interesting. For the third area, there is also a different patter for the CNR. This graph is interesting because it does not allow to pass so much signal in some way for the third region between 0 and 40 cm (compared to all the 5 MeV graphs).

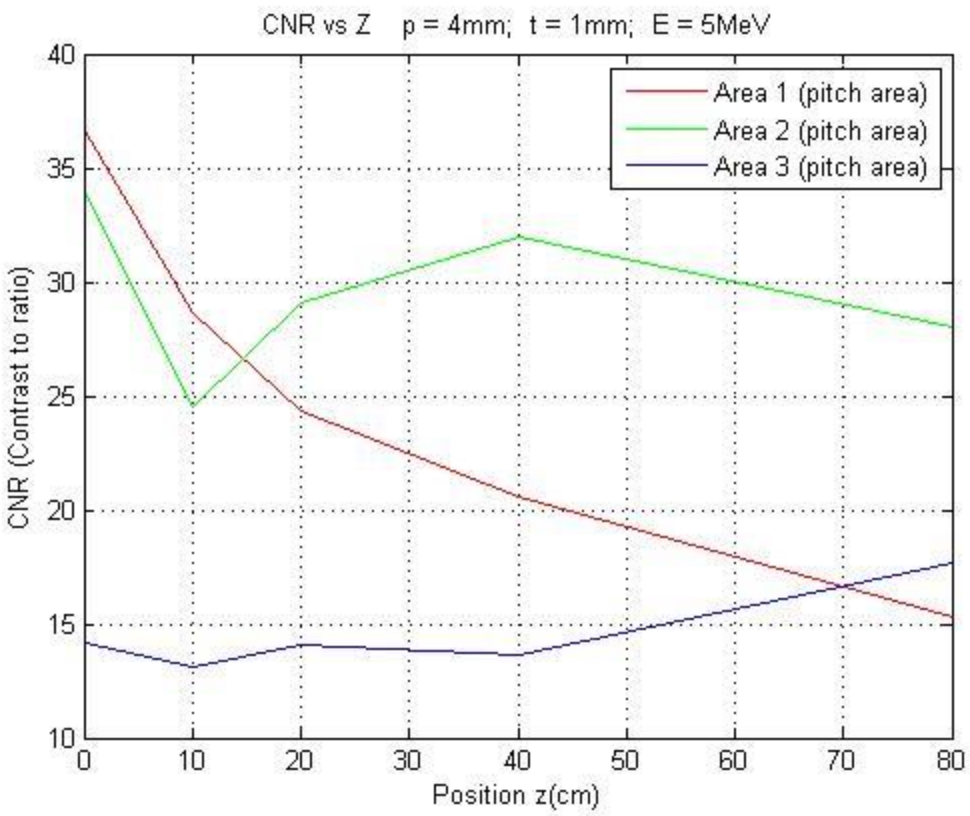

FIGURE 5.71 CNR VS POSITION (ALONG Z DIRECTION) FOR P=4 MM, T=1 MM E=5 MEV

Figure 5.71 represents a very good signal capture for the second region, leading us to a way to detect gamma particles with an energy of 5 MeV after 15-16 cm (given a set of signals for the three areas at least), it is also good for the third zone after 70 cm.

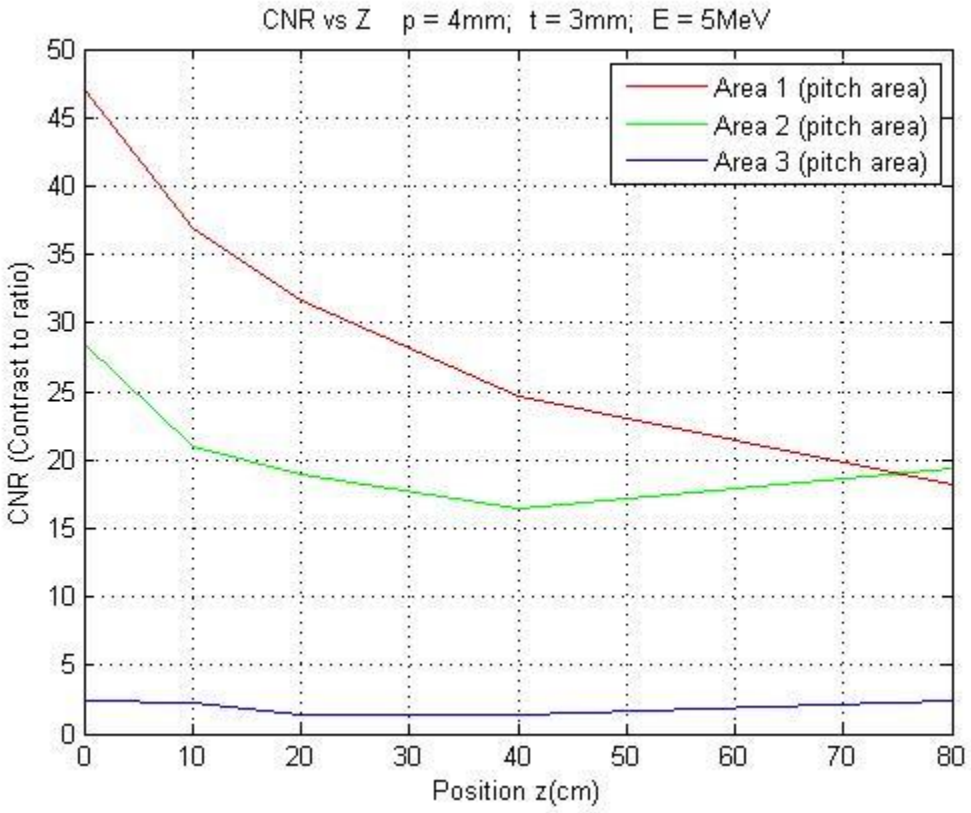

FIGURE 5.72 CNR VS POSITION (ALONG Z DIRECTION) FOR P=4 MM, T=3 MM E=5 MEV

Figure 5.72 even though it has 5 MeV energy, this does not allow to pass so much signal for the third zone and it has a slower signal in the second zone, intersecting at a long distance.

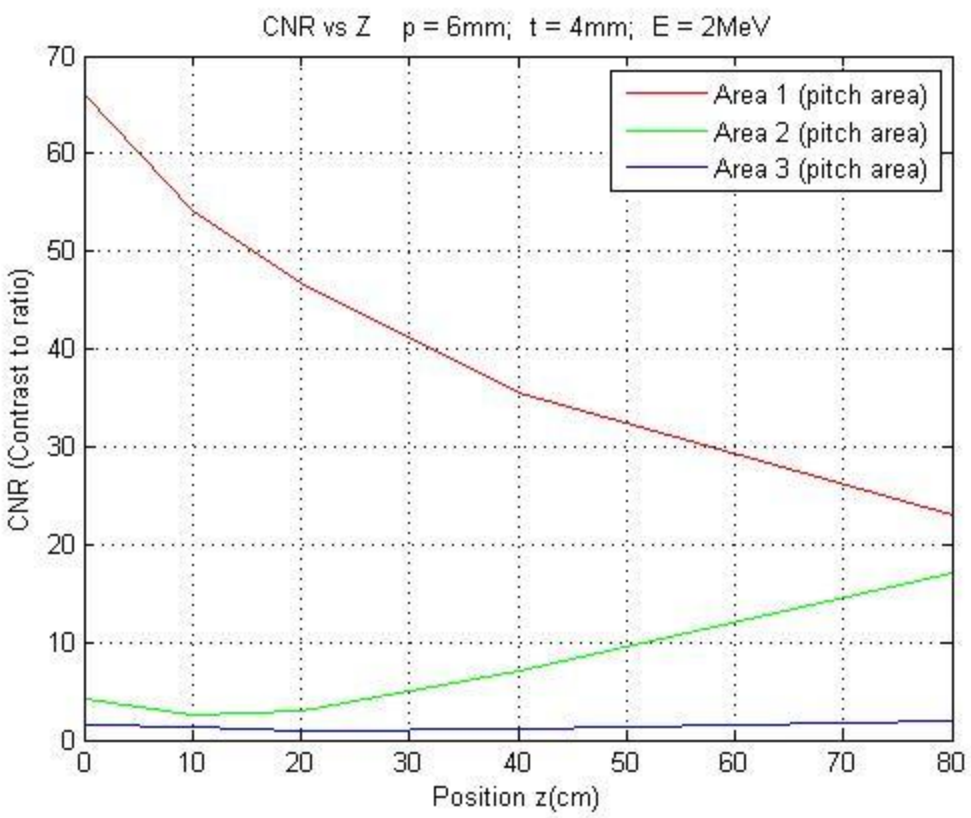

FIGURE 5.73 CNR VS POSITION (ALONG Z DIRECTION) FOR P=6 MM, T=4 MM E=2 MEV

Figure 5.73 is a special case to find some relationship for multiples of pitch and thickness, the previous one is a multiple of twice the pitch and thickness, being this way the parameters to compare P=3 mm and T=2 mm (Figure 5.61) for the same energy. The pattern is similar but very different in the amount of signal (CNR) because this configuration allows passing more signal, although the signal of the second area for Figure 5.73 is smaller than that of Figure 5.61, which is very strange. For the first area, as is expected, Figure 5.73 has more CNR than Figure 5.61 and a similar rate of change. For the third area shows a very similar display.

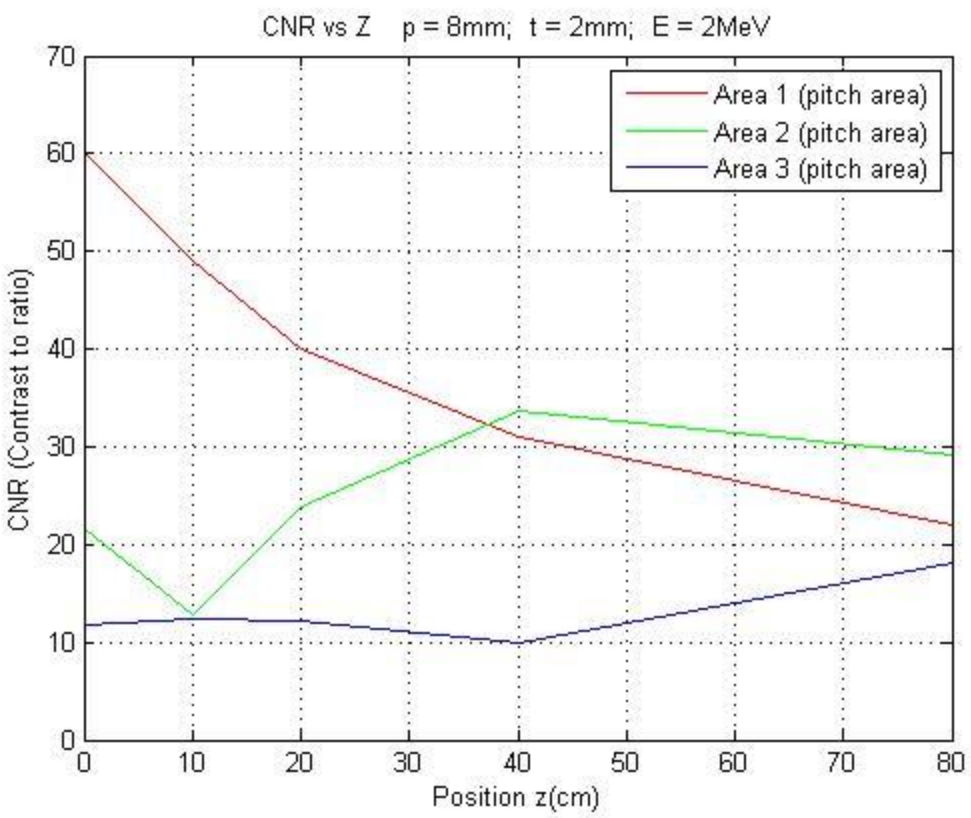

FIGURE 5.74 CNR VS POSITION (ALONG Z DIRECTION) FOR P=8 MM, T=2 MM E=2 MEV

Figure 5.74 is another special case of multiplicity two for P=4 mm and T=1 mm with the same energy (Figure 5.65). There are some similarities and some differences, such as the rate of change of the three zones of interest (similar), on the other hand, the differences are in the starting points of the graphs, also at the 10 cm point, which is same for Figure 5.74 and for Figure 5.65 is not.

CHAPTER 6: CONCLUSIONS

The main point of this thesis is to make a study for the field of medical physics, which mainly focuses on nuclear and atomic physics for diagnostics and treatments of cancer. As we know the cancer is the devourer of lives and therefore it is of great importance to make contributions to this field.

A promising method in which cancer is fought is proton therapy (the most commonly used is x-rays), protons have properties such as the Bragg's peak and less dispersion in the delivery of energy. When a nucleus-proton collision occurs, a Bragg peak is generated, and these produce gammas by the atomic interaction. For our study we need to give the location of the gamma source (where the proton interacted), so our job is to detect gamma rays to determine the location. This is important since during the radiotherapy it cannot be confirmed whether the tumor or healthy tissue is being destroyed or not, so our study tries to impact on radiotherapy *in vivo* to determine the location of the source *in vivo*. To achieve this task, we will contribute with a simulation to detect gammas with GEANT4 and analyze the data with ROOT. An important note is that a million radial gamma rays were used to give a better signal resolution, therefore, it would have to be scaled for a lower number of gamma rays.

The simulation is mainly the interaction of the gamma source with the collimator, for changes in the parameters pitch, thickness, and distance, for each case the signal was measured and analyzed for the first three regions.

The analysis for all the sets studied in this thesis showed that showed that the first zone decreases as a radial source except for the parameters (Figure 5.70) 6 mm pitch, 2 mm thickness

and 5 MeV energy between the distances of 10 cm to 40 cm. It can also be said that third region has a growing behavior as expected, except for the parameters (Figure 5.65 and Figure 5.7) P=4 mm, T=1 mm and E=2 MeV, and P=8 mm, T=2 mm and E=2 MeV, where both show a slightly weaker signal (given its decrease to nearby points) in 40 cm compared to the other graphs for 2 MeV.

The respective curves of each graph for the energy maintain a pattern, be phase-shift or larger increases, but so similar, saying roughly and the most interesting signal graphs happen 80 cm away, that is when you have a higher signal in the third region. Another important fact is that for some specific distances, there is a greater signal in the second region than in the first one, leading us to a way of locating the source, by inspecting a set of signals for several regions (more than three to know more about the source).

We tried to find an escalation factor for some parameters like P=4 mm, T=1mm with P=8 mm, T=2 mm, and P=3 mm, T=2 mm with P=6 mm, T= 4 mm, which showed a similar pattern although with some differences such as not keeping the same crossing points where the graphs show the same amount of signal for two different zones.

There is still much to be done in this study, such as finding a way to predict the crossing points of the graphs (where the same amount of signal is captured for certain regions) and find an escalation to predict the signal increments or decrements.

REFERENCES

[AAPM, 2018] American Association of Physics in Medicine. Retrieved on 2018-1-31 from https://www.aapm.org/publicgeneral/.

[Berman, 2015] Berman AT, James SS, Rengar R. Proton Beam Therapy for Non-Small Cell Lung Cancer: Current Clinical Evidence and Future Directions. Cancers (Besel) 2015; 7(3): 1178-90. doi: 103390/cancers/70308331.

[Campbell, W. G. 1990. Form and Style in Thesis Writing, a Manual of Style. Chicago: The University of Chicago Press.]

[Camphausen, 2008] Camphausen, K. A.; Lawrence, R. C. (2008). "Principles of Radiation Therapy". In Pazdur, R.; Wagman, L. D.; Camphausen, K. A.; Hoskins, W. J. (eds.) Cancer Management: A Multidisciplinary Approach. 11th ed.

[Carrier, 2004] J.-F. Carrier, L. Archambault, L. Beaulieu and R. Roy (2004). “Validation of GEANT4, an object-oriented Monte Carlo toolkit, for simulations in medical physics”.

[Chiari, 2013] Chiari, M., Fundamentals of the Particle Induced Gamma-ray Emission (PIGE) technique, experimental procedures and examples of PIGE analysis, Joint ICTP-IAEA Workshop on Nuclear Data for Analytical Applications. http://indico.ictp.it/event/a12218/session/23/contribution/14/material/0/0.pdf.

[Fix, 2013] Macro Monte Carlo for dose calculation of proton beams, Michael K Fix, Phys. Med. Biol. 58 (2013) 2027.

[FON, 2018] Fiber Optical Networking. Retrieved on 2018-2-9 from http://www.fiber-optical-networking.com/getting-know-fiber-collimator.html.

[Geant4, 2018] Geant4 official website, Retrieved on 2018-2-1 from http://geant4.cern.ch/support/introductionToGeant4.shtml.

[Guibelalde, 2012] Guibelalde E., Christofides S., Caruana C. J., Evans S. van der Putten W. (2012). Guidelines on the Medical Physics Expert' a project funded by the European Commission.

[Holmes, 2017] Physics seminar at UTEP, 2017, Jason Holmes, Arizona State, “Next generation detectors for proton therapy quality assurance”.

[Knopf, 2013] *In vivo* proton range verification: a review, Antje-Christin Knopf and Antony Lomax, Phys. Med. Biol. 58 (2013) R131.

[Levin, 2005] Levin, W. P.; Kooy, H.; Loeffler, J. S.; DeLaney, T. F. (2005). "Proton Beam Therapy", British Journal of Cancer 93, 849–854.

[Mayo, 2018] Mayo Foundation for Medical Education and Research (MFMER). Retrieved on 2018-1-29 from https://www.mayoclinic.org/departments-centers/mayo-clinic-cancer-center.

[Metz, 2006] Metz, James (2006-07-31). "Differences Between Protons and X-rays". Abramson Cancer Center of the University of Pennsylvania. Retrieved on 2008-02-04 from http://www.oncolink.org/treatment/article.cfm?c=9&s=70&id=210.

[NCI, 2018] National Cancer Institute. Retrieved on 2018-1-31 from https://www.cancer.gov/about-cancer/understanding/statistics.

[MDACC, 2018] MD Anderson Cancer Center. Retrieved on 2018-1-31 from https://www.mdanderson.org/patients-family/diagnosis-treatment/care-centers-clinics/proton-therapy-center/what-is-proton-therapy/history-of-proton-therapy.html.

[Newhauser, 2015] The physics of proton therapy, Wayne D Newhauser, and Rui Zhang, Phys. Med. Biol. 60 (2015) R155–R209.

[PhysMed,2018] Basics physics of nuclear medicine/ interaction of radiation with matter. Retrieved on 2018-5-10 from

[PTCOG, 2013] "Particle therapy facilities in operation". Particle Therapy Co-Operative Group. 2013-08-27. Retrieved on 2014-09-01 from http://www.ptcog.ch/index.php/facilities-in-operation.

https://en.wikibooks.org/wiki/Basic_Physics_of_Nuclear_Medicine/Interaction_of_Radiation_with_Matter

[ROOT, 2018] ROOT Data Analysis Framework. Retrieved on 2018-2-1 from https://root.cern.ch/.

[ROOTUG,2018] ROOT Data Analysis Framework User’s Guide. Retrieved on 2018-2-1 from https://root.cern.ch/root/htmldoc/guides/users-guide/ROOTUsersGuide.html#introduction.

[Turabian, K. L. 1987. A Manual for Writers of Term Papers, Theses, and Dissertations. 5th ed. Chicago: The University of Chicago Press.]

[Wilkins, 2006] “The Essential Physics of Medical Imaging”, Second ed., Philadelphia: Lippincott Williams & Wilkins, 2006, p. 261.

[Wilson, 1946] "Radiological Use of Fast Protons", R. R. Wilson, Radiology, 47:487-491 (1946).

VITA

My name is Selim Romero, the education that I have is Master of Physics in simulations at University of Texas at El Paso, August 2016 – present. Thesis title: “GEANT4 STUDY OF A GAMMA RAY COLLIMATOR FOR PROTON THERAPY.” And Bachelor of physics (2015), Autonomous University of Ciudad Juarez, Juarez City, Chihuahua, Mexico. My academic employment was as graduate Teaching Assistant, Department of physics, University of Texas at El Paso, August 2016 – present. Responsibilities included: Assist professors with the preparation and presentation of undergraduate courses, proctoring and tutoring.

I attended to a presentation at professional meeting known as Joint Fall 2017 Meeting of the Texas Section of the APS, Texas Section of the AAPT, and Zone 13 of the Society of Physics Students, The University of Texas Dallas, Richardson, Texas, 21 October 2017.

Contact Information: selimiles@live.com

This thesis/dissertation was typed by Selim Romero.